Modelling Symphony motion

Towards a better understanding of 2D motion of the Symphony

M.J.G. Boonman

Delft university of Technology

TU Delft Delft University of Technology

TEAMWORK

Challenge the future

Delft university of Technology

MODELLING SYMPHONY MOTION

TOWARDS A BETTER UNDERSTANDING OF 2D MOTION OF THE SYMPHONY

by
M.J.G. Boonman

in partial fulfillment for the degree of Master of Science
Sustainable Energy Technology

Faculty of Electrical Engineering, Mathematics and Computer Science

Student number:	4246608
Project duration:	September 1, 2018 – July 12, 2019
Supervisors:	dr. ir. Henk Polinder dr. ir. Bauke Vriesema ing. Fred Gardner
Thesis committee:	dr. ir. Henk Polinder (chair, TU Delft) prof. dr. Arno Smets (TU Delft) dr. ir. Peter Wellens (TU Delft) dr. ir. Bauke Vriesema (Teamwork Technology)

This thesis is to be kept confidential until July 12, 2021

An electronic version of this thesis is available at http://repository.tudelft.nl/.
July 4, 2019

TU Delft

TEAMWORK

PREFACE

The energy transition seems to be raging through our economy and our society. It only seems fitting that the Dutch should try to get the sea involved. I was lucky enough to be able contribute to research in ocean wave energy. I was also lucky enough to have the opportunity to work at a very clever, though complicated machine. The last nine months have thus been characterised by learning, having the illusion of understanding, asking stupid questions, rediscovery, realising I was wrong, asking again, and then, finally, understanding.

The past seven years have been a journey from freshman to engineer. This journey has been long, interesting and sometimes harsh. However, I don't regret a bit, as I can confidently say that I learned very much, both as an engineer and as a person.

Especially during the harsh parts I wouldn't have come out the other side without some people to whom I owe thanks. For this thesis in particular, I owe great thanks to Henk Polinder, who was very patient in guiding me in the process that ultimately yielded this thesis, Fred Gardner, who provided the framework in which I was able fall and crawl back up a better engineer and Bauke Vriesema who helped me countless times in understanding and improving the time domain model. I can't even begin to describe how much this man knows about Symphony. I also want to thank Arno Smets and Peter Wellens for taking the time to read and judge my work.

I also want to thank Antonio Jarquin Laguna for providing me with guidance in multiple cases, and to George Lavidas for being open to discussion about ocean wave energy any time. The same thanks go to Jian Tan, who took the time to provide me with very valueable feedback. The same goes for any graduates on the Symphony before me, who provided me with reports and guidance.

As any man in this world I owe big thanks to my mother, who dragged me through high school when I saw it a a necessary evil, and my father, who taught me the fine art of doing what you deem good, even if it's against better judgement.The same amount of thanks I owe to my sisters who have saved me more often than they may realise in the past seven years.

I also want to take the opportunity for a big shout-out to PH57, which has been my (sometimes) loving home for almost five of the last seven years. Besides these guys, I owe thanks and apologies to anyone who had to put up with some idiotic behaviour, bad moods, worse humour, and my terrible taste in music while working. This includes, but is not limited to, every rower at DDS who had to put up with my sense of humour after a day of work, the entire population of the Marine Engineering hallway, the guys of Hornbach (*"Je kan niet van een project spreken als je er niet voor naar de Hornbach bent geweest!"*), and in fact anyone with whom I had the pleasure of being in a boat with the past seven years, the BUVVOV and supporters, and all fellow graduates with whom I shared numerous angry, frustrated and sad cups of coffee. You know who you are.

M.J.G. Boonman
Delft, July 4, 2019

Gutta cavat lapidem, non vi sed saepe cadendo

SUMMARY

Ocean wave energy is one of the possible energy sources of the future. One possible way of harnessing ocean wave energy is by means of the Symphony wave power device. This thesis describes an addition to the existing time domain modelling structure which provides the possibility to assess body motions of the Symphony in operational and extreme conditions. Because the Symphony has a cylindrical shape the direction of incoming waves does not matter and hence the real 3D situation can be simplified to motion in the 2D plane.

The addition to the model has been based on rigid body dynamics and Newton's laws of motion. The interaction between the water and the Symphony has been derived based on Morison formulation and linear wave theory. The resulting equations of motion are implemented in the exiting time domain model and couplings with the operational model are made.

Based on data for two possible installation locations the operational conditions and extreme conditions are assessed. From these calculations a clear overview of the expected mooring reaction forces is obtained. From this it is concluded that several conventional mooring technologies are compatible with the Symphony. The calculations also provide insight in the expected differences in energy production between a rigidly restrained Symphony and a Symphony restrained with a single mooring line. These differences are in fact so small that they fall within the uncertainty of the energy calculations. In conclusion this thesis gives confidence in the current direction of development and did not identify large problems for the Symphony operation when the Symphony conducts body motions on the 2D plane.

CONTENTS

List of Figures

List of Tables

List of Symbols

Physical constants

Symbol	definition	value	unit
g	gravitational acceleration	9.81	$\frac{m}{s^2}$
ρ	water density	1010	$\frac{kg}{m^3}$

Symphony properties

Symbol	definition	value[1]	unit
A_{side}	side area of the Symphony	$f(z)$	m^2
AE	cross-sectional stiffness of the mooring line	[-][2]	N
C_d	drag coefficient of the Symphony	1.2 [1]	[−]
D_b	diameter of the base	1.250	m
D_{fl}	diameter of the floater	1.750	m
$dclr$	distance between still water level and top of the floater in top position	3	m
k_m	mooring line stiffness	$\frac{AE}{L_m}$	N/m
l_b	length of the base	10.9	m
l_{fl}	length of the floater	7.6	m
l_m	length of the mooring line	[-][3]	m
l_{min}	minimum length of the Symphony	11.2	m
l_{max}	maximum length of the Symphony	15.2	m
m_b	mass of the base	8000	kg
m_{fl}	mass of the floater	7500	kg
m_{sym}	total mass of the symphony	17500	kg
m_{water}	mass of water in the membranes	2000	kg

Wave properties

Symbol	definition	unit
A	amplitude	m
H_s	significant wave height	m
k	wave number	$\frac{1}{m}$
p	pressure	Pa
T_e	energy period	s
u	horizontal component of the orbital velocity	$\frac{m}{s}$
η	surface elevation	m
Φ	velocity potential	$\frac{rad*m^2}{s}$
ψ	phase shift	rad
ω	frequency	$\frac{rad}{s}$

[1] If the values is listed as $f(z)$ the value of this property is a function of the floater position, see appendix A

[2] Value depends on material choice for the mooring line, affecting the elasticity modulus, and the cross section of the mooring line, affecting the cross-sectional area

[3] Value depending on water depth. L_m is calculated as $L_m = h - dclr - l_{max}$

Other quantities

Symbol	definition	unit
a	acceleration	$\frac{m}{s^2}$
$\frac{dp}{dx}$	pressure gradient	$\frac{Pa}{m}$
F_{drag}	drag force	N
F_{FK}	Froude-Krilov force	N
h	water depth	m
I	moment of inertia	$kg * m^2$
L_p	pendulum length	m
M	moment	$N * m$
m	mass	kg
N_{kc}	Keulegan-Carpenter number [2]	$[-]$
r	distance (radius)	m
S	span force	N
v	velocity	$\frac{m}{s}$
x_{fl}	x-position of the fairlead of the Symphony	m
y_{fl}	y-position of the fairlead of the Symphony	m
z	local position of the floater with respect to its equilibrium position	m
θ	angle of the Symphony with vertical	$^\circ$
ϕ	angle of the central mooring line with vertical	$^\circ$
ω_n	natural frequency	$\frac{rad}{s}$

Abbreviations

EOM	Equation of motion
MIP	Mean index power
MRE	Mean Relative Error
PTO	Power Take Off
ROW	Remotely operated Vehicle
WAB	Wave Activated Body
WEC	Wave Energy Converter

1

INTRODUCTION

The major part of global energy use is currently generated from fossil fuels, and the global energy demand is still growing [3]. The use of fossil fuel comes at two major costs:

- the burning of fossil fuels releases carbon dioxide into the atmosphere, causing a potentially devastating shift in earth's climate [4].
- fossil fuels are utilised at a higher rate than they are naturally replenished, and thus they will run out eventually [5].

These two drawbacks have been motivating mankind to find alternative energy sources increasingly. Even before society was aware of the effects of climate change a rise in the price for oil (due to scarcity and/or geopolitical conflict [6]) has been an impulse to invest in the development of alternative energy sources. However, nowadays climate change is the main motivator for the development of renewable energy sources [7].
Ocean wave energy is a possible source of renewable energy. Oceans cover more than two third of the face of the earth and are in constant motion. This motion is associated with large amounts of energy, making the oceans large reservoirs of energy as well as water [8]. In the search for alternative energy sources many have considered ways to extract some of the energy contained in the wave motion [9]. It is important to note here that when this thesis refers to a "wave", this refers to a wind-generated wave and not a tidal wave. Tidal energy is an interesting topic but falls outside of the scope of this thesis.
The idea of ocean wave energy is not new: from the late 18th century mankind has had the idea to extract this energy. French mathematician Pierre-Simon Girard had the idea to have a large floater on the water, connected to a hinge on the shore. The motion of the rod which connected the floater to the hinge could be used to compress a working fluid, which would then be able to drive all sorts of machinery [10].
Since then various wave energy conversion concepts have been conceived and developed [9]. There are various devices that are capable of tapping energy from waves, usually these are referred to as Wave Energy Converters or WECs. WECs can be classified into different categories [11]. Various comparison studies have been done on the potential of the different types of WECs [12, 13]. One interesting type of WEC is the Wave Activated Body (WAB) type, which extracts ocean wave energy by having a mass follow the motion of a the wave and damping that motion by means of some Power Take Off (PTO). Usually a restoring force or spring force is also involved, preventing the moving body from getting too far from it's equilibrium position. A promising type of WAB is the submerged pressure differential WAB [12]. The case study done by van der Jagt focusses on the Symphony Wave

Power Device. This thesis will focus on the Symphony.

1.1. THE SYMPHONY WAVE POWER DEVICE

The Symphony is a project byTeamwork Technology. The Symphony is aimed to be deployed in coastal waters. Currently locations off the coast of Leixões, Portugal and Den Helder, the Netherlands are under investigation.

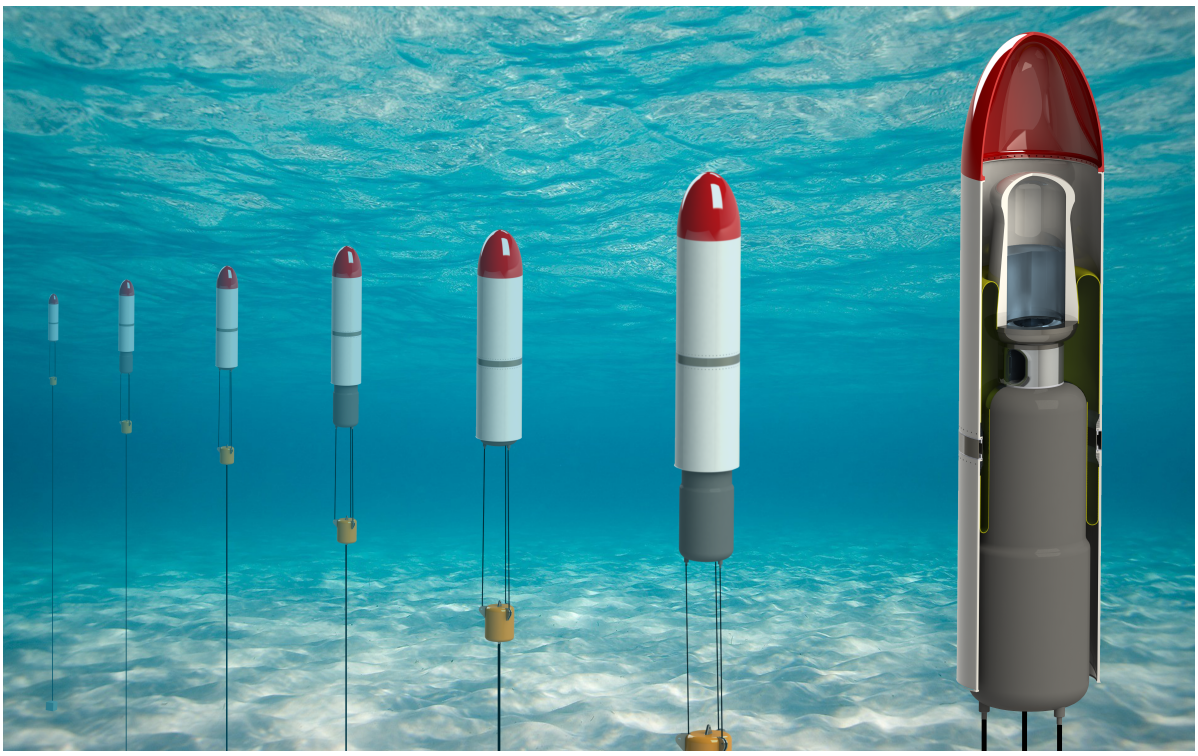

Figure 1.1: visualisation of multiple Symphony devices [14]

The Symphony is excitated by pressure variations in time due to passing waves. This phenomenon is referred to as the wave-induced pressure. The Symphony itself is naturally buoyant and fully submerged. Hence, it floats under the waterline, restricted by some mooring arrangement. The operation of the Symphony is explained in chapter 2.

As stated, research shows that the Symphony is a promising type of wave energy converter [12]. However, current modelling mainly focuses on the internal process of the Symphony. The device is modelled under the assumption that the base is stationary. Secondly, only motions in the direction of the centre line of the Symphony are modelled. This means that a fair estimate of the Symphony operation can be made, but that motions in other directions are completely ignored in the operational model. This thesis aims to better assess the occurrence and effect of horizontal motion of the Symphony in operation.

Several publications state that the performance of the WEC should also be considered when designing WEC mooring [15, 16]. This suggests that mooring design of a WEC can influence the WEC performance.
Another study already suggests a way to design an optimal mooring system for a submerged point absorber, accounting for performance as well as for the more classical mooring requirements of survivability and station keeping [17]. Muliawan et. al. [18] analyse the effects of mooring systems

on the energy capture of a specific WEC using time domain simulation. This study also suggests differences in energy production due to variation in mooring systems.

1.2. RESEARCH OBJECTIVE

Based on the research cited above it is to be expected that the performance of the Symphony will be affected by horizontal motions. Three effects are chosen to assess in this thesis. The most important performance factor is in this case energy production, as that is the main function of the Symphony. Therefore, the effect of incorporating horizontal motion in the existing simulation will be assessed. Secondly, in order to deploy the Symphony, a clear idea of the required reaction forces by the foundation is needed. Earlier research already gave an insight on the required reaction force for the one-dimensional case [19], This thesis intends to extend that for the two-dimensional case. This research will give an insight into the severity of the risk posed by this phenomenon for the Symphony.

This will be achieved by answering the following research question:

What is the effect of horizontal motion of the Symphony on the performance and mooring loads of the Symphony?

This question is answered by answering the following questions:

1. What are the relevant excitation forces on the Symphony in horizontal direction?
2. What motions will follow from this horizontal excitation?
3. What effects will these prior unconsidered horizontal motions have on the
   - energy extraction
   - mooring reaction forces

   of the Symphony?

1.3. METHOD

To achieve the research goal and answer these research questions a model of the Symphony is derived. This model is derived using linear wave theory and rigid body dynamics. This motion model is combined with the existing operational model to obtain a model that takes into account horizontal motion of the Symphony and assesses the internal operational process. The model will be referred to as the derived model. This derived model will be able to output the mooring reaction forces a a result of the elongation of a single mooring line and an assumed stiffness. These models are compared using the same wave-seeds in both the existing operational model, which will be used as a reference, and the derived model which takes into account the horizontal motions of the Symphony. From the difference in the results between these models conclusions can be drawn regarding the effect of taking into account horizontal motion of the Symphony.

1.4. REPORT STRUCTURE

Firstly, chapter 2 provides background for the research. Previous work, underlying theory and practical relevance of this work is adressed. Secondly a model of the system will be derived in chapter

3. This model will be implemented with the existing operational model of the Symphony to come to the new model of the Symphony. This process, and some steps to gain confidence in the derived model, are described in chapter 4. The results of running the derived model under various circumstances will be presented and compared in chapter 5. Based on the results presented in chapter 5 different possible mooring technologies are discussed in chapter 6. Finally, chapter 7 draws final conclusions from the results and gives recommendations with respect to Symphony design and further research.

2

RESEARCH BACKGROUND

This chapter provides the background of the research. First the frame of reference is introduced in section 2.1. Several relevant terms associated with the Symphony are explained in section 2.2. The different modelling cases are described in section 2.3. The working principle of the Symphony is explained in section 2.4. Section 2.5 discusses previous work on the Symphony operation and body motion. In order to derive a model, some assumptions and approximations are done and justified. This is explained in section 2.6. Based on these assumptions and approximations the use of linear wave theory is allowed to characterise waves. This is described in section 2.7. From this theory the external forces acting on the Symphony are derived. The choice of modelling tool is justified in section 2.8. Section 2.9 positions this thesis with respect to other work.

2.1. FRAME OF REFERENCE

The frame or reference is chosen to be two dimensional. In this two dimensional frame of reference the horizontal axis is called the x-axis, the vertical axis is labelled y. ϕ and θ denote the angle of the single mooring line of the Symphony and the angle of the Symphony itself. Both angles are measured positive from vertical in the clockwise direction. Adding to these coordinates, there is one local coordinate: z. This coordinate denotes the local displacement of the Symphony floater from its midposition. Figure 2.1 depicts the frame of reference. From the description above it is clear that the floater and the base undergo the same translation and rotation, and that the only relative motion between floater and base is a result of floater displacement along the local z-axis.

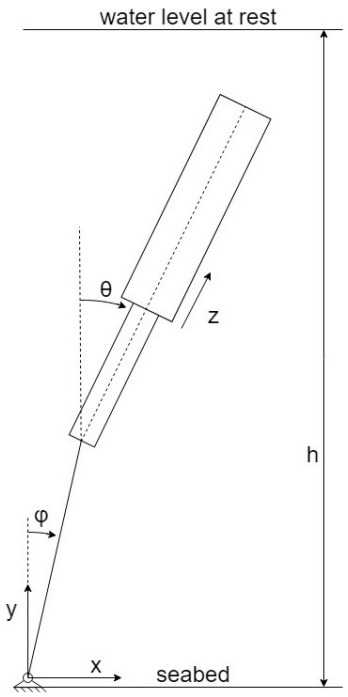

Figure 2.1: Sketch of the frame of reference

2.1.1. WAVES

In order to understand the working principle of the Symphony it is important to make some definitions clear about waves. The mathematical description of waves is explained in section 2.7. However, three definitions are important:

- A wave's crest; the highest point of a wave
- A wave's trough; the lowest point of a wave
- The mean water level; the waterlevel if the water were at rest

Figure 2.2 sketches this.

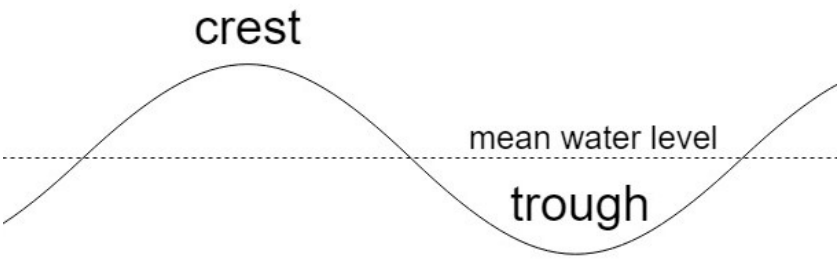

Figure 2.2: Sketch of the meaning of a wave crest, trough and the mean water level

2.1.2. SEA STATES

Real waves in real water are usually irregular. Irregular waves can be defined by defining a *sea state*. The sea state consists of two numbers: a wave height and a period. This thesis uses significant wave height Hs the energy period Te of the sea state. Using Hs and Te and a spectrum the irregular wave can be approximated using several regular waves, all with their own amplitude and frequency. These amplitudes and frequencies are determined using a spectrum. This thesis uses the JONSWAP spectrum for the Den Helder location and the Bretschneider spectrum for the Leixões location. Adding these regular components gives an irregular periodic signal. For more information on sea states and wave spectra the reader is kindly referred to [20].

2.2. THE SYMPHONY

In order to understand the Symphony working principle and its motions it is important to clarify some definitions. This section clarifies some part names, definitions and specific terms.

BREAKDOWN

Currently the Symphony design is such that the floater can make a four meter stroke, from z = -2 to z = 2. If the floater position would exceed these boundaries, the Symphony could suffer extreme of even fatal damage. Hence, the Symphony is said to break down when this occurs. The model is programmed in such a way that when the floater position exceeds this boundary the model is terminated at that time step and a breakdown message is returned.

CUT OUT WAVE HEIGHT

The cut out wave height is the highest wave height at which the Symphony does not break down. It is to be expected that the rated power occurs at a sea state with the cut out wave height. The cut out wave height can be different for different wave periods.

SURVIVAL MODE

For sea states higher than the operational sea state the Symphony will not generate energy. In order to protect the operational parts from large excursions and impacts the Symphony is shut down instead, and the floater is locked in a certain position. The model allows to define a survival position z-survival of the floater. For the outputs generated in this report z-survival = 0. [1]

2.3. CASE DESCRIPTION

The model derived in this thesis is applied to two installation cases mentioned in chapter 1. These cases are described in this section.

2.3.1. LEIXÕES

The first location is based on a previous motion analysis off the coast of Leixões, Portugal. Based on previous work the water depth is assumed to be 100m [21].

CHARACTERISTIC SEA STATES

Based on previous work [19] the wave spectrum at Leixões is assumed to be a Bretschneider spectrum. For the Leixões location the full scatter diagram given in table D.1 is used to determine 5 characteristic sea states. This is done by clustering several groups of sea states close to the diagonal in the scatter diagram together. This is visualised in table D.2. The resulting characteristic sea states and their occurrences are given in table 2.1. Together these sea states account for 90.2% of the waves. Based on previous work done by Leijten the maximum operational sea state (cut out sea state) is expected to be around Hs = 5m [19].

Sea State	$H_s[m]$	$T_e[s]$	Occurrence [%]
1	1.0	6.0	34.3
2	2.25	9.0	38.1
3	3.5	10.0	11.8
4	4.75	12.0	5.0
5	7.5	13.0	1.1

Table 2.1: Characteristic sea states for the Leixões location

SURVIVAL CONDITIONS

The survival sea state for the Leixões location is determined at Te = 18s and Hs = 15m. The survival sea state at a location is the highest sea state that can be reasonally expected at that location [21]. The highest current for survival is estimated at 1 m/s. However, steady currents in coastal waters

[1] At the moment of finalising this thesis the design of the Symphony is not finalised yet. Ultimately, a z-survival of -2 is expected. z-survival = 0 is assumed to ensure enough buoyancy using the current dimensions.

usually don't have large velocities perpendicular to the coast, but usually run parallel to the coast. Because the coast of Leixões is at the open ocean the survival wave is expected perpendicular to the coast. Hence, in the 2D approach of this thesis, the current does not affect the survival situation.

2.3.2. DEN HELDER

The second location is based on intentions of deploying the Symphony in Dutch territorial waters close to Den Helder. The location of the site is depicted in figure 2.3. The local water depth at the site is estimated to be 35 metres. The wave spectrum for the North Sea is assumed to be a JONSWAP spectrum [22].

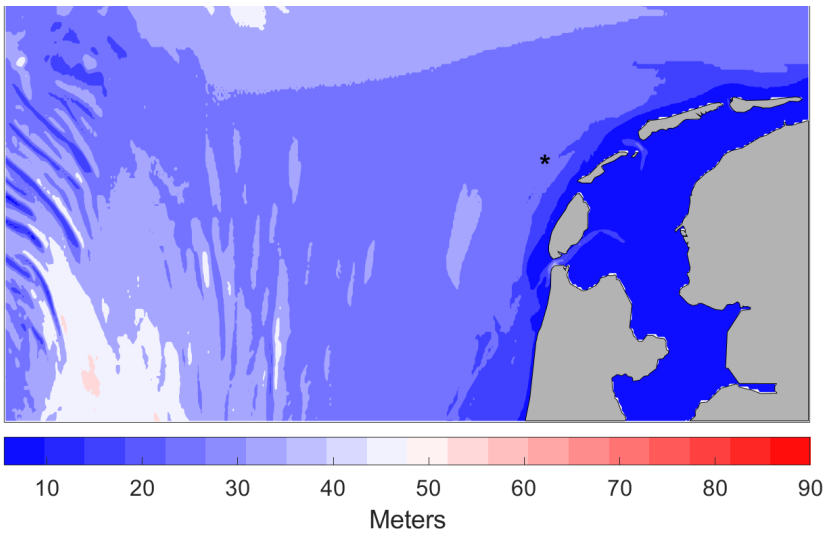

Figure 2.3: Location of the Den Helder site. Survival sea state is valid at the location of the black star. The colour scale gives the water depth [23]

CHARACTERISTIC SEA STATES

For the Den Helder location the characteristic sea states are taken from literature [24]. These characteristic sea states account for 99.7% of the waves. The characteristic sea states for the Den Helder location are given in table 2.2.

Sea State	$H_s[m]$	$T_e[s]$	Occurrence [%]
1	0.5	4.72	40.7
2	1.5	5.58	39.4
3	2.5	6.44	14.1
4	3.5	7.29	4.3
5	4.5	8.13	1.2

Table 2.2: Characteristic sea states for the Den Helder location

The cut out wave height is again expected to be around at Hs = 5m.

SURVIVAL CONDITIONS

For the Den Helder site a survival sea state has been chosen based on work by Lavidas [25]. The parameters of the survival sea state are Hs = 8.7m and Te = 12.6s. The current for survival is estimated at 50 cm/s [26]. Because of the specific situation in the north sea the survival wave and the

current could very well come from the same direction [27]. Therefore, for the Den Helder case, the survival case is ran for a steady current at 0 m/s, -0.5 m/s and 0.5 m/s to assess the survival case for the neutral tidal condition and the worst and best case tidal condition.

2.4. WORKING PRINCIPLE OF THE SYMPHONY

To be able to achieve the research goal the working principle of the Symphony must first be understood. Figure 2.4 gives a schematic representation of the longitudinal cross section of the Symphony. The concept is based on the changing pressure of water under the surface of a wave. When a wave crest passes, the pressure in the water under the crest rises. Similarly, the pressure falls under a wave trough. because of the assumption that the diameter of the Symphony is small compared to the wavelength this can be interpreted to cause a uniform pressure oscillation at the location of the top of the Symphony. Because the the top of the floater is perceived as an equivalent disk this pressure oscillation can be perceived as an harmonic excitation force on the floater of the Symphony. This force is perpendicular to the equivalent disk and thus always acts in the direction of the centreline of the Symphony. Apart from this external excitation force there are also internal forces that act on the floater. The first force is related to the floater position and is a result of a pressure rise of the air in the spring chamber and in the floater itself and pushed the floater up when it is pushed down. This can thus be seen as a spring force. The second internal force is related to the floater velocity and is a result of the resistance of the generator and the turbine. By cleverly designing the Symphony it is ensured that in the quasi-static situation the resulting force will always push the floater to it's midposition. In other words, the floater will oscillate around the midposition and energy is removed from the motion by the velocity-dependant (and thus damping) internal force component related to the generator and turbine. This process is described step-by-step below:

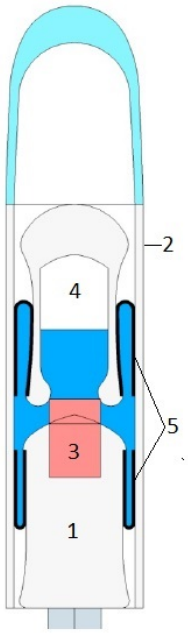

Figure 2.4: Schematic representation of the Symphony parts [2]

Let's assume a wave crest passes. The pressure on the equivalent disk rises, so a downward force acts on the floater (2). The floater starts to move downwards, rolling the structural membranes (5) downwards. Because the gap between the base (1) and the inner wall of the floater is smaller than the gap between the outside of the spring chamber (4) and the inner wall of the floater the volume enclosed by the membranes decreases. This causes the pressure in the membranes to rise, driving a water flow through the turbine (3) into the spring chamber. The turbine drives a generator, generating electricity. This flow causes the water level in the spring chamber to rise. The pressure of the air above the water in the spring chamber rises with the water level (the air is compressed in a smaller volume). This provides a restoring force; the air will push back against the water, acting as a spring. If the crest has passed and the trough is above the Symphony the pressure on the top of the floater will fall. This drop in downward force combined with the built up pressure in the spring chamber causes an upwards resulting force on the floater, accelerating it in upward direction. Upon this upward motion, water is pushed through the turbine again, driving the turbine and the generator and generating electricity. These steps are visualised in figure 2.5. This mass-spring-damper system is cleverly designed to have a natural frequency matching the wave frequency, in order to be able to extract as much energy as possible. More information on the exact operation of the Symphony and the tuning of the natural frequency can be found in previous work [19, 28].

[2] base (1), floater (2), turbine (3), spring chamber (4), and structural membranes (5)

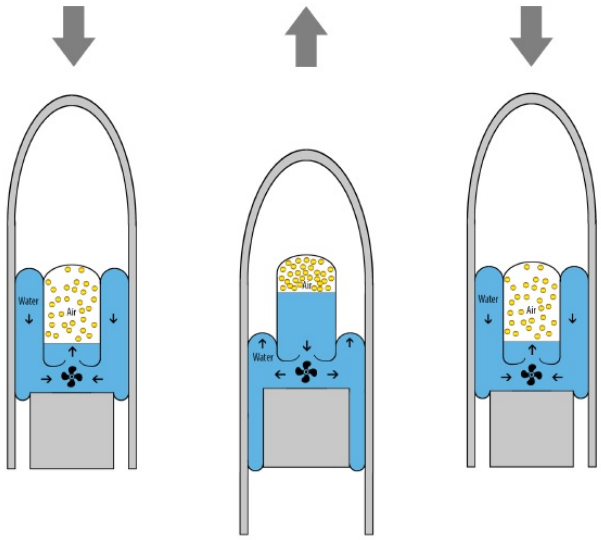

Figure 2.5: Schematic visualisation of the Symphony operation [14]

2.5. PREVIOUS WORK ON THE SYMPHONY

Because the development history of the Symphony already spans multiple years it is important to look at previous work. The Symphony specifically has been subject to several studies. These studies provide valuable insights for this thesis.

2.5.1. MOTION ANALYSIS

One study in particular looks at similar effects as this study and is therefore important to study thoroughly. This study has been completed in 2016 at InnoSea [21].The study was done in the frame of WP2 of the WETFEET project and takes the Symphony to be a single cylinder and analyses the motion of this cylinder using potential flow theory and Morison formulation [29]. In this analysis a three dimensional model is meshed and time domain simulations are conducted.
This study gives several interesting outputs and some reason for further research.
Firstly the relative motion of the two bodies is neglected. This means that only the behaviour of an equivalent, inert body is assessed. From the introduction of this thesis we know that the Symphony changes volume under the influence of changing pressure in the water around it and the reaction of the PTO-turbine assembly. This volume changing will be influenced by the horizontal motion, and the other way around.

2.5.2. HYDROMECHANICAL ANALYSIS

In an effort to estimate the magnitude of horizontal effects some calculations using boundary element method software (WAMIT) with respect to horizontal hydromechanical forces have already been done. These calculations yielded surge loads in the order of several kilonewtons per meter of wave amplitude. These loads vary with frequency and Symphony submersion depth.
It must be noted that in these calculations the Symphony was represented by a single cylinder.

Figure 2.6 shows a significant area of interest in the frequency interval from 0.5 rad/s to 1.8 rad/s, where surge loads per metre wave height exceed 3 kN/m. This corresponds with waves between T = 12 s and T = 3.5 s with the peak at 1 rad/s or T = $2*\pi$ s ($\approx$ 6.28 s) and approximately 6.5 kN/m.

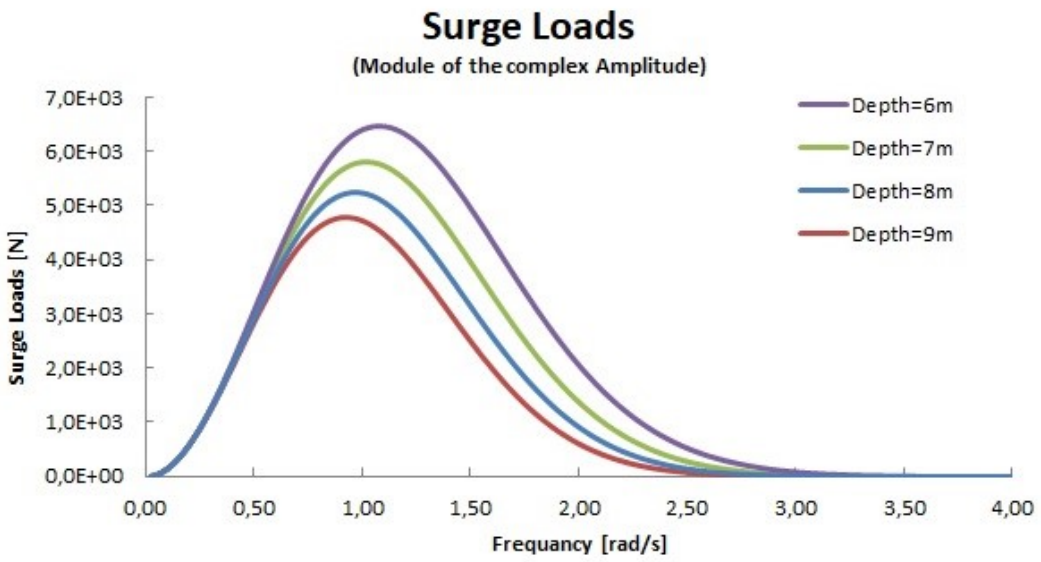

Figure 2.6: Surge loads on the Symphony at different instalment depths and exciting frequencies. Wave amplitude had been set to 1 metre

If we calculate the Keulegan-Carpenter number [2] for this case using a horizontal flow velocity amplitude of 0.55 m/s (assuming deep water an a submersion depth of 6 metres), a period of 6 seconds and a characteristic length of 1.5 metres (the diameter of the Symphony) we obtain equation 2.1

$$N_{kc} = \frac{uT}{L} = \frac{0.55 * 6}{1.5} = 2.2 \tag{2.1}$$

Where u, T and L denote the flow velocity amplitude, oscillating period of the flow (and the wave) and the characteristic length of the cylinder, respectively. The Keulegan-Carpenter number is used as a measure to indicate whether inertia forces or drag forces dominate the motion of an object. Literature suggests a Keulegan-Carpenter number of 8 to be the upper limit of the inertia-dominated region [30]. For a preliminary analysis it is thus justified to neglect drag forces. Based on the calculation above it is to be expected that surge loads on the restrained Symphony in survival mode are close to the values presented in figure 2.6.

2.6. ASSUMPTIONS AND APPROXIMATIONS

This thesis uses the following assumptions:

- The Symphony is small compared to the wave
- the Symphony is always fully submerged
- viscosity is ignored
- flow is assumed to be irrotational
- the fluid is incompressible
- the fluid is homogenous

Because of these assumptions the use of the Froude-Krilov assumption and linear wave theory is allowed.

2.6.1. FROUDE KRILOV APPROXIMATION

The Froude Krilov approximation states that if a body is sufficiently small compared to the length of the incident wave the influence of the body on the wave can be neglected. In mathematical terms: if $\frac{l}{\lambda} << 1$ then the diffraction potential and the radiated wave potential can be ignored. When $\frac{l}{\lambda} << 1$ is true is of course debateable; what is "sufficiently small"? Different references give different answers to this question. MIT [31] suggests $\frac{2\pi * l}{\lambda} = 1$ as the upper boundary of the validity of the Froude-Krilov approximation; or $\frac{l}{\lambda} < \frac{1}{2\pi}$. In the case of the Symphony, which operates in waves of a dominant period of around 10s [19] and has a characteristic length l (diameter) close to 1.5 m this approximation can be made, as a deep water wave with a period of 10 seconds has a length of 156 m and $\frac{1.5}{156} < \frac{1}{2\pi}$. If the diameter of the Symphony would be increased and reach one sixth of the wavelength the Froude Krilov approximation will lose it's validity and so will the derived model. This corresponds with a diameter of $\lambda 2\pi$ which, in the case of a 156 m wave, corresponds to a diameter of approximately 25 metres.

2.6.2. MOORING ARRANGEMENT

To be able to assess the behaviour of the Symphony under wave loading a first assumption about the mooring arrangement must be made. Initially the mooring is assumed to consist of a single line that always has tension (no slacking) and is connected to a single, fixed point on the seabed (the anchor). Assuming a considerable tension in the line, it is a fair first assumption to assume the line to be "straight", in other words: there are no significant bends in the line. This is in accordance with the representation in figure 2.1.

2.6.3. DRAG FORCES

In order to be able to account for drag forces a simplified approach is used. In line with Morison formulation, the drag force is calculated as $F_d = -\frac{1}{2} C_d \rho v|v|$. Here v is the velocity in the direction of interest and C_d denotes the drag coefficient for that direction. ρ is the density of the medium, in the case of this thesis water unless indicated differently.

2.7. WAVE CHARACTERISATION

In order to clearly explain the working principle of the Symphony it is useful to clearly describe the way a wave is characterised and described in this thesis.

This thesis uses linear wave theory or Airy wave theory [20] to characterise waves. Irregular waves are simulated by taking the superposition of several, harmonic wave components. This section gives relevant expression which are obtained from linear wave theory, that will later be used to calculate the excitation forces the Symphony experiences. All expressions below are derived from Holthuijsen [20].

When a wave passes the water under the wave experiences an ongoing change in pressure. This thesis limits itself to the following time- and position dependant variables:

- the wave-induced pressure p_{dyn}
- the wave-induced horizontal pressure gradient $\frac{dp}{dx}$
- the wave elevation η
- the horizontal component of the orbital velocity u

The vertical component of the orbital velocity is neglected.

The velocity potential is given by

$$\Phi(x,y,t) = \frac{\omega A}{k} * \frac{cosh(k*(y+h))}{sinh(kh)} * cos(\omega t - kx + \psi) \tag{2.2}$$

where A is the amplitude of the wave, ω is the frequency of the wave in rad/s, ψ is the phase angle of the wave in rad, k is the wave number in $\frac{rad}{m}$, h is the water depth in meters and $\frac{cosh(k*(y+h)}{sinh(k*h)}$ is a dimensionless number which is often referred to as the "depth-effect". This number effectively provides information on how much the effect of the wave will decrease with the position nearing the seabed. This thesis will refer to this number as f_d or the depth effect. As seen from the mathematical expression this is a function of position y and water depth h as well as the wave number k. For large h (deep water) this number approaches e^{ky}.

From the definition of the velocity potential in (2.2) the following expressions follow for the wave elevation:

$$\eta(x,t) = A * sin(kx - \omega t + \psi) \tag{2.3}$$

The wave-induces pressure and the associated pressure gradient are obtained by solving Bernoulli's equation:

$$p = -\rho * \left(\frac{1}{2}(\nabla\Phi)^2 + \frac{\partial\Phi}{\partial t} + g * h\right) \tag{2.4}$$

From which the first term is non-linear and the last term is static. Because we are interested in the dynamic effect and deriving a linear model, these terms are omitted and (2.5) yields:

$$p(x,y,t) = -\rho\frac{\partial\Phi}{\partial t} = \frac{\rho * A * \omega^2}{k} * \frac{cosh(k*(y+h))}{sinh(kh)} * sin(\omega t - kx + \psi) \tag{2.5}$$

Because $\omega^2 = kg * tanh(kh)$ this equation develops to

$$p(x,y,t) = \rho * A * g * \frac{tanh(kh) * cosh(k*(y+h))}{sinh(kh)} * sin(\omega t - kx + \psi) \tag{2.6}$$

which, when using the goniometric identity $\frac{tanh(x)}{sinh(x)} = \frac{1}{cosh(x)}$ yields equation 2.7

$$p(x,y,t) = \rho * A * g * \frac{cosh(k*(y+h))}{cosh(k*h)} * sin(\omega t - kx + \psi) \tag{2.7}$$

Deriving the pressure oscillation with respect to x yields

$$\frac{dp}{dx}(x,y,t) = -\rho * A * \omega^2 * \frac{cosh(k*(y+h))}{sinh(k*h)} * cos(\omega t - kx + \psi) \tag{2.8}$$

Deriving the velocity potential with respect to x yields the expression for the horizontal component of the orbital velocity of water particles u:

$$u(x,y,t) = A * \omega * \frac{cosh(k*(y+h))}{sinh(k*h)} * sin(\omega t - kx + \psi) \tag{2.9}$$

Using these equations the external forces on the Symphony can be calculated.

2.8. CHOICE OF METHOD

Section 1.3 already presented the chosen method to answer the research question. This section explains the choice of method for this project. First of all, because the operation of the Symphony is described by a set of non linear differential equations, a time domain model must be used [28]. Two time domain simulation options are considered to simulate the model derived in chapter 3. The first option is using the time domain model used by Teamwork Technology. It has been subject to several Msc. theses and is improved by multiple graduate interns in that process [19, 28, 32, 33]. The model has been monitored throughout the years by senior engineer dr. ir. Vriesema.
The second option is the WEC-Sim package developed by the National Renewable Energy Laboratory (NREL) and Sandia National Laboratories [34]. This package has been used by van der Jagt [12] for his comparison study. WEC-Sim is supported by multiple publications.
Both models operate in a MATLAB/Simulink environment. The in house model consists of a Simulink model that is run from a set of MATLAB scripts and functions. WEC-Sim uses a Simulink environment simulating rigid body dynamics and is also operated from the MATLAB environment.

The descriptions above give confidence in the performance and validity of both modelling options. The choice for one of these options can hence be made on more practical grounds: What is the most straight forward option to implement? What has the most value for follow-up research?
At this point in the process it is important to point out that the most complicated part of the Symphony is the PTO arrangement. The PTO arrangement makes up the bulk of the existing model. Using WEC-Sim would imply that, apart from the actual answering of the research question in this thesis, the entire model has to be translated from the current form into WEC-Sim. In consultation with management at Teamwork Technology and earlier graduates on the subject it has been deemed unrealistic to do this properly together with the actual research. This has lead to the choice to use the in house model of the Symphony operation.
However, this comes at a price. the WEC-sim environment offers some nice options to calculate hydrodynamic forces. These options are not present in the in house model. Hence, in implementing the derived model the hydromechanical forces have to be derived separately. This is done using linear wave theory, as can be seen from chapter 3.

2.9. POSITION IN THE RESEARCH FIELD

This thesis of course does not stand alone. The introduction has already referred to some work that suggests that performance and mooring should be assessed together. This thesis applies these

more general statements to the Symphony with an assumed mooring arrangement. The assumed single line mooring system is combined with the existing model built by previous work [19, 28, 32, 32], thus extending the modelling environment for the Symphony specifically. This thesis uses the theory described in this chapter together with Newton's laws of motion to make this extension of the modelling environment of the Symphony.

2.10. CONCLUSION

This chapter has described the frame of reference that is used for the model derived in this thesis. The wave characterisation used in the model has been described, and the nature of the associated excitation forces were explained from linear wave theory. Several assumptions and approximations and associated boundaries to the validity of the model were presented and justified. The chosen modelling method is presented and justified. Lastly, this chapter has explained the position of this thesis with respect to other literature and work.

3

PHYSICAL MODELS

In order to assess the motion of the Symphony without conducting experiments a physical model has to be derived. This physical model will be derived in this chapter. The model will be derived step by step, starting with a very simple model, adding detail with every iteration. The starting point will be the existing model. Firstly, in section 3.1 the external forces are expressed based on the theory presented in chapter 2. Section 3.2 shortly describes the existing model which will be incorporated in the final model. The first model, having only one degree of freedom, is described in section 3.3. Based on this model the final model is derived in section 3.5.

3.1. EXTERNAL FORCES ON THE SYMPHONY

Because this thesis focuses on the body motion of the Symphony this section will limit itself to the relevant excitation forces being the horizontal drag force, the horizontal pressure force and the associated moments.

The Symphony is also constrained by its mooring arrangement, which exerts a mooring force on the Symphony. Lastly, the Symphony is subject to gravity buoyancy in the vertical direction.

3.1.1. DRAG FORCE

Horizontal drag force is calculated using the relative velocity of the water with respect to the Symphony as

$$F_{d,x} = \frac{1}{2} * \rho * (u - v_S)^2 * C_d \tag{3.1}$$

where v_S is the horizontal translational velocity of the Symphony with respect to the frame of reference.

3.1.2. PRESSURE FORCE

Pressure force or Froude-Krilov force is calculated as

$$\vec{F}_{FK} = -\int p\vec{n}dS \tag{3.2}$$

The equation above expresses the Froude-Krilov force to be the integral over the surface of interest of the pressure multiplied by the normal vector of the surface. For a object fully submerged in water which is at rest the vertical component simplifies to

$$\vec{F}_{FK} = \int p\vec{n}dS = \rho * g * \nabla = F_b \tag{3.3}$$

The last expression in (3.3) is also known as Archimedes' law. ∇ denotes the volume of the submerged body, $\vec{F}_b$ denotes the buoyancy force acting on the object. Archimedes' law is usually used in the vertical direction. However, the pressure in water that is at rest is equal to $-\rho g y$ at a certain height y. Therefor we can write the pressure gradient $\frac{dp}{dy}$ as $-\rho g$. Hence, (3.3) can be rewritten as

$$F_y = F_b = \rho * g * V = -V * \frac{dp}{dy} \tag{3.4}$$

This last expression tells us that if a body is in a fluid where a pressure gradient is present the body as a whole will experience a force equal to the pressure gradient times its own volume, in the opposite direction of the pressure gradient. In other words; the object is pushed from high to low pressure. If we draw up this equation in another dimension we get

$$F_x = -\frac{dp}{dx} * \nabla \tag{3.5}$$

From (2.8) a pressure gradient at a given time and a given coordinate is known. If the pressure gradient is assumed to be constant over the volume of the Symphony this horizontal adaptation of Archimedes' law can be used to compute the horizontal wave-induced pressure force on the Symphony.

(3.5) is written in a way that the pressure gradient is constant in space. Because the pressure gradient is dependent of the velocity potential it is a function of space. Taking this space dependency into account, but assuming long waves (hence the pressure gradient is constant in x-direction) and an upright position of the object yields

$$F_x = -\int_0^l \frac{dp}{dx}(l)dl * A \tag{3.6}$$

Where A is the cross sectional area of the object and l is the position along the length of the object. From this representation a simplification can be made for the pressure force, representing it as a single force acting in a single position.

In the case of the Symphony the point of action along the Symphony length has to be corrected for the local floater position z. This is done by shifting the point of action of the force with $\frac{1}{2} * z$.

The pressure force is assumed to act in the centre of the side area of the Symphony. This is because the force is calculated as a pressure integrated over a surface, and the side area of the Symphony is the area perpendicular to the direction of the pressure force.

The depth effect of the wave force components is taken at one third of the equilibrium length below the top of the floater in equilibrium position, and is assumed to be constant.

Of course there is also an excitation in the vertical direction. Firstly, because the floater has no continuous wetted surface, a correction in hydrostatic force must be made. Let's assume the Symphony to be in a vertical position; see figure 1.1. Clearly, the base experiences a net upward hydrostatic force, and the floater experiences a net downward hydrostatic force. For the excitation of the floater we are primarily interested in the floater forces. To calculate the correct hydro static force three

forces have to be added: the force on the bottom of the floater itself, the force on the outer half of the bottom of the lower membrane and the force on the top of the floater. Because the Symphony is symmetric about its z axis the first two can be said to work in the upward (towards positive z) direction and the last one can be said to work in downward (towards negative z) direction. All three forces are calculated by integrating the pressure over the surfaces they work on. Because of aforementioned symmetry this can be simplified to multiplying the pressure with the horizontal projection of the surface. For the top of the floater the hydrostatic pressure at a predefined pressure point will be taken to act over an equivalent disk at that height.

The wave excitation of the floater in z direction is calculated in a similar way. However, extra steps are involved. Because an irregular wave is modeled by different wave components with different amplitudes and frequencies the wave force for all wave components are calculated separately, with their own depth effect and phase angle and then all force components are added. The same procedure can be followed to calculate the force on the bottom of the base.

3.1.3. MOORING FORCES

The mooring force consists of a static and a dynamic part. The static part is calculated by calculating the distance between the anchor and the centre of the bottom of the base. This distance, the momentary mooring line length, is divided by the unstretched mooring line length. This elongation is multiplied by the static mooring line stiffness. The dynamic part is calculated by taking the time derivative of the mooring line elongation and multiplying by an artificial dynamic mooring line stiffness. This artificial damping ensures that energy is extracted from the oscillation of the mooring line length. Without this damping the mooring line itself would be excitated in its axial elongation, but it would not be damped in this mode. This would pose a possible threat to the model stability. Both forces can only pull; that is, they can only act in the negative x- and y direction.

3.2. EXISTING MODEL

The existing model considers the Symphony as a single degree of freedom system. The base is hereby fixed to the frame of reference. Figure 3.1 gives a visual representation of the model. It is important to note that coordinate z is measured from the equilibrium position of the floater. Secondly, the drawing might suggest that the Symphony is founded on the seabed. In reality, this is not true. The Symphony is assumed to float at that depth under the sea surface, independent of the water depth. From this picture and the explanation above it can be concluded that this existing model assumes the Symphony does not experience any motion other than the floater moving up and down along the z axis.

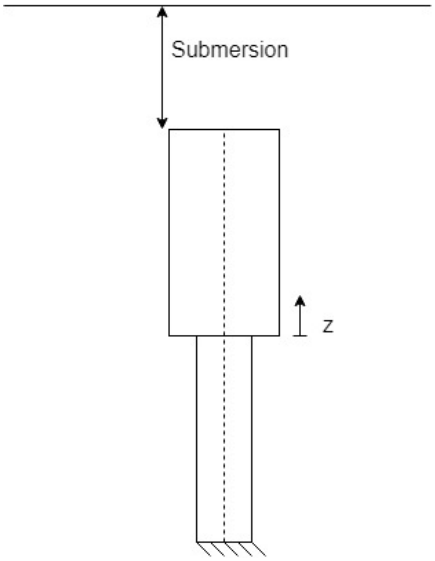

Figure 3.1: Schematic representation of the existing model

This motion is modelled in quite some detail. For this description it suffices to say that the Symphony can be seen as a mass-spring-damper system, which is excited by an excitation force which is based on linear wave theory. This excitation force is computed based on the wave-induced pressure at the horizontal surfaces of the floater (see (2.7). The same calculation is done at the positions of the bottom of the floater and the bottom of the membrane with the corresponding areas. For a

more detailed description of this model the reader is referred to previous descriptions [19, 33].

This existing model brings about the major part of this research, loosely formulated in the following question: What happens horizontally?

3.3. SINGLE DEGREE OF FREEDOM MODEL

The first models presented in this chapter are one-dimensional. This means that the Symphony only has one degree of freedom. The first model of the Symphony considers the Symphony as a rigid cylinder with mass m, height H and diameter D connected rigidly to a massless, stiff, slender rod which is in connected to a hinge on the seabed. The centre of mass and centre of buoyancy of the SWPD are assumed to coincide on the centreline of the device, a distance L_p from the anchor. The degree of freedom can be perceived as the angle θ the device makes with vertical.

Following from the degree of freedom the system has angular velocity $\dot{\theta}$ and angular acceleration $\ddot{\theta}$. The rotational inertia I is given by $I = m * L_p^2$. This system is depicted in figure 3.2.

The equation of motion of the shown system is given by (3.7).

$$I * \ddot{\theta} = M_{net} \tag{3.7}$$

in which

$$M_{net} = M_{exc} + M_{drag} + M_{res} \tag{3.8}$$

which yields:

$$\ddot{\theta} = \frac{M_{exc} + M_{drag} + M_{res}}{I} \tag{3.9}$$

If we state that the excitation moment is equal to the horizontal wave induced force on the body corrected for angle θ and multiplied by radius L_p. The excitation moment can then be calculated using (3.5) and using $M = F * L_p$. This yields (3.10).

$$M_{exc} = \frac{dp}{dx} * \nabla * L_p * cos(\theta) \tag{3.10}$$

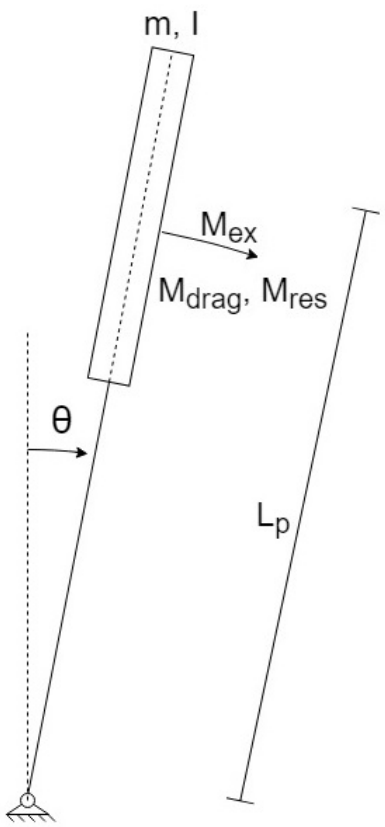

Figure 3.2: Schematic representation of the single degree of freedom

The drag moment M_{drag} is calculated assuming small angles so we can say that

$$M_{drag} = F_{drag} * L_p \tag{3.11}$$

and

$$F_{drag} = \frac{1}{2}\rho C_d A(u - v) * |u - v| \tag{3.12}$$

and

$$v = L_p * \dot{\theta} \tag{3.13}$$

Combining equations 3.11, 3.12 and 3.13 and rearranging yields for the drag moment:

$$M_{drag} = \frac{1}{2} L_p \rho C_d A (u - \dot{\theta} * L_p) |u - \dot{\theta} * L_p| \tag{3.14}$$

The restoring moment is the result of the net buoyancy of the SWPD (difference between buoyancy and weight) working vertical out of the vertical line that passes through the hinge. This yields the following restoring moment:

$$M_{res} = (\rho * \nabla - m) * g * L_p * sin(\theta) \tag{3.15}$$

3.4. DISCUSSION OF THE SINGLE DEGREE OF FREEDOM MODEL

The model described in section 3.3 provides a useful insight in the dynamics of the Symphony body motions. Using this representation of the Symphony an easy estimate of the natural frequency of the system can be made by using the relation for the undamped natural frequency of a single pendulum. For a hanging pendulum the undamped natural frequency is given by

$$\omega_n = \sqrt{\frac{g}{L_p}} = \sqrt{\frac{\frac{F_{down}}{m}}{L_p}} \tag{3.16}$$

The Symphony is essentially an upside-down hanging pendulum. Hence, the undamped natural frequency can be expressed as

$$\omega_n = \sqrt{\frac{\frac{\rho g \nabla - mg}{m}}{L_p}} = \sqrt{\frac{\frac{F_{b,net}}{m}}{L_p}} \tag{3.17}$$

This last equation can be used to gain confidence in the derived model by solving the undamped natural frequency analytically for the used parameters and comparing the two obtained natural frequency with an undamped free vibration simulated by the numerical model, see section 4.4.

3.5. MULTI DEGREE OF FREEDOM MODEL

As stated earlier, the Symphony and its mooring are more complicated than projected in the models above. Therefore a multi degree of freedom model has been derived. In explaining the multi degree of freedom model it is important to consider how the model will be implemented later. The existing operational model is solved in the time-domain. Because the model predicting the Symphony body motions has to run together with this operational model it will also be solved in the time domain. Thus, it is useful to be able to define the Symphony position for each time step. Because the Symphony is modelled as a 2D shape with finite dimensions in a 2D plane it is possible to define the position of the Symphony for each time step using four coordinates: the x- and y-position of the fairlead, denoted by x_{fl} and y_{fl} , respectively, the angle if the Symphony with vertical (θ) and of course the local floater position z. This is depicted in figure 3.3. For clarity, the fairlead is indicated by the red dot.

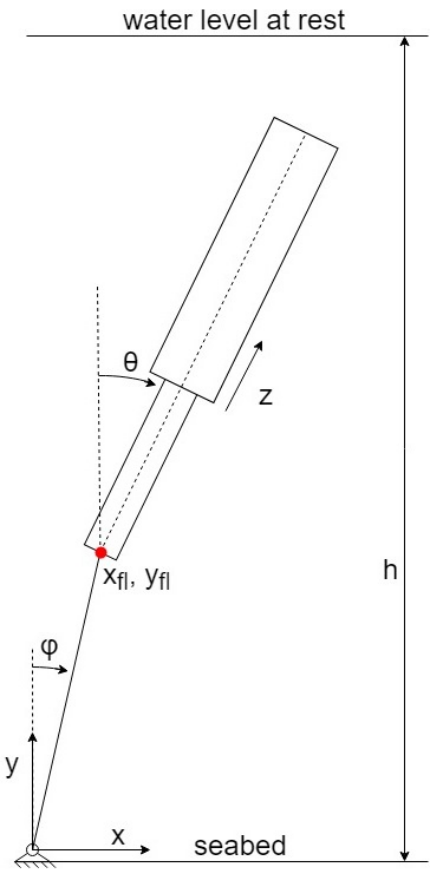

Figure 3.3: Schematic representation of the multi degree of freedom model

In the time domain model, each of the four coordinates has to be determined in order to be able to move on to the next time step. In addition to the existing operational model governing the relative floater motion the model that takes care of the Symphony body motion has to determine three motions:

- the horizontal translation of the Symphony x
- the vertical translation of the Symphony y
- the rotation of the Symphony about its centre of mass θ

Combining these three motions will yield a new situation for the next timestep. This is done by calculating the resulting forces in x- and y-direction and the moment about the centre of mass and calculating the three accelerations independently. Then the body acceleration is integrated twice, determining the new location of body. Integrating the angular acceleration twice allows the calculation of the new angle θ and the fairlead position.

The equations for each of these motions are given below:

$$\ddot{x}_{body} = \frac{\Sigma(F_x)}{m_{sym}} \tag{3.18}$$

$$\ddot{y}_{body} = \frac{\Sigma(F_y)}{m_{sym}} \tag{3.19}$$

$$\ddot{\theta} = \frac{\Sigma(M)}{I_{sym}} \tag{3.20}$$

3.5.1. HORIZONTAL FORCES

$\Sigma(F_x)$ is calculated by the following equation:

$$\Sigma(F_x) = F_{FK} + F_{drag,x} + F_{span,x} \tag{3.21}$$

in which:

$$F_{FK} = \frac{dp}{dx} * \nabla(z) \tag{3.22}$$

acting in the centre of buoyancy of the Symphony,

$$F_{drag,x} = \frac{1}{2} * \rho * C_d * |u - \dot{x}|u - \dot{x} * A_{side}(z) * sin(\theta) \tag{3.23}$$

acting in the centroid of the sidearea of the Symphony and

$$F_{span,x} = -S * sin(\phi) \tag{3.24}$$

Acting in the fairlead. The vertical forces are shown in figure 3.4.

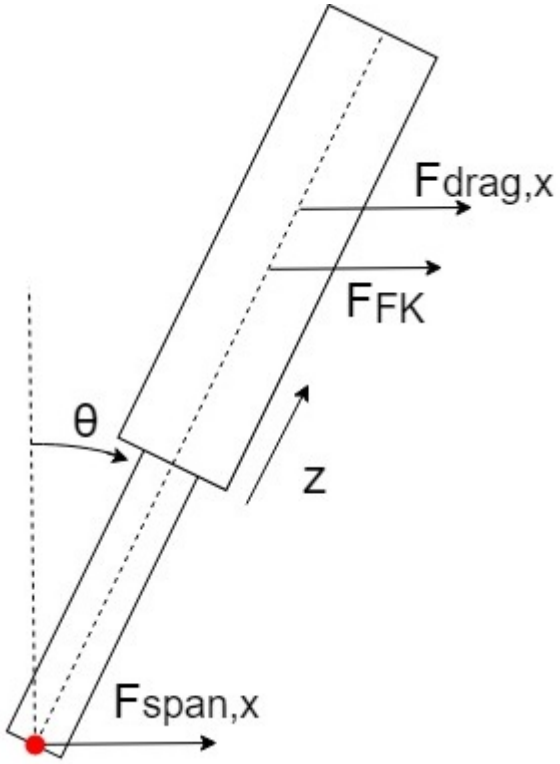

Figure 3.4: Horizontal forces acting on the Symphony

3.5.2. VERTICAL FORCES

$\Sigma(F_y)$ is calculated by the following equation:

$$\Sigma(F_y) = F_{b,net} + F_{drag,y} + F_{span,y} \tag{3.25}$$

in which:

$$F_{b,net} = \rho * g * \nabla(z) - m_{sym} * g \tag{3.26}$$

acting in the centre of buoyancy of the Symphony,

$$F_{drag,y} = -\frac{1}{2} * \rho * C_d * |\dot{y}|\dot{y} * A_{side}(z) * sin(\theta) \tag{3.27}$$

acting in the centroid of the side area of the Symphony and

$$F_{span,y} = -S * cos(\phi) \tag{3.28}$$

acting in the fairlead.

The vertical forces are shown in figure 3.5.

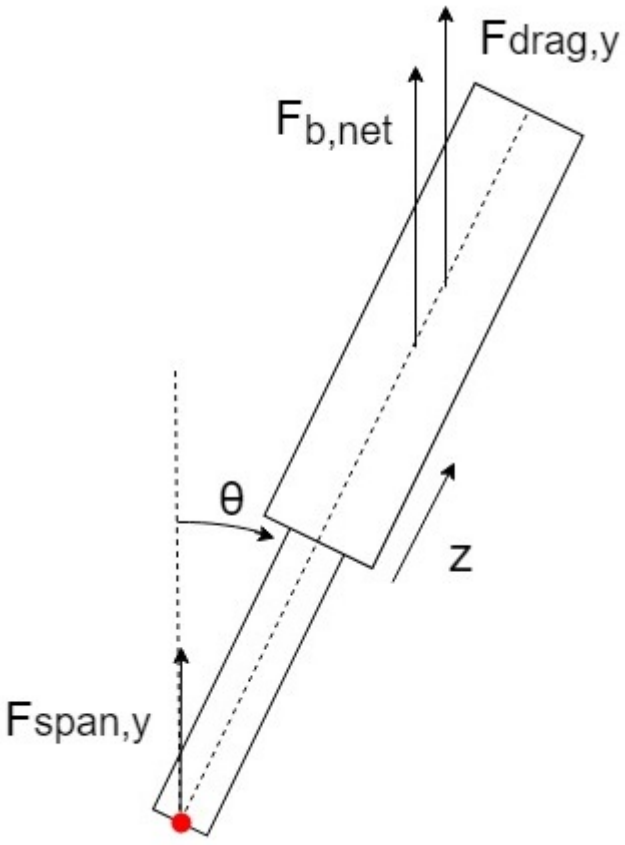

Figure 3.5: Vertical forces acting on the Symphony

Line tension S is calculated by

$$S = l - l_{mooring_0} * k_m + \frac{dl}{dt} * k_{m,dyn} \tag{3.29}$$

Here, again, values lower than zero of each of the terms are neglected.

The buoyancy force is calculated as:

$$F_b = \nabla(z) * \rho * g \tag{3.30}$$

3.5.3. OPERATIONAL FORCES AND SPAN FORCE CORRECTION

In the model description above one issue is not yet addressed; the working forces of the Symphony. These working forces are already described in section 2.4. This section explains how these forces are handled in the model. From Newton's third law of motion we can state that any upward (in the positive z-direction) force on the floater is associated with a force of the same magnitude in the opposite direction. The same holds for a downward force on the floater. Consequently, if we assume that ϕ and θ are always close to each other (see appendix B for an example), we can approximate the following: All positive resulting force on the floater (base pushes the floater up) is associated with a deduction of the span force of the same magnitude. Correspondingly, any pulling force by the floater on the base leads to an additional mooring line span force.

Secondly, the wave force that acts at the top of the floater also acts at the bottom of the base. This force, the wave-induced pressure integrated over the surface of the bottom of the base, is be added to the mooring span force.

3.5.4. MOMENTS

The net moment about the centre of mass $\Sigma(M)$ is calculated as

$$\Sigma(M) = M_{F_{FK}} + M_{F_b} + M_{drag} + M_{F_{span}} + M_\theta \tag{3.31}$$

all separate moments are calculated multiplying the force by the distance between their line of action and the centre of mass:

$$M_{F_{FK}} = F_{FK} * r_{CoB}(z) - r_{CoM}(z) \tag{3.32}$$

$$M_{F_b} = F_b * (r_{CoB}(z) - r_{CoM}(z)) * sin(\theta) \tag{3.33}$$

$$M_{F_{drag}} = F_{drag,x} * (r_{CoA}(z) - r_{CoM}(z)) * cos(\theta) - F_{drag,y} * (r_{CoA}(z) - r_{CoM}(z)) * sin(\theta) \tag{3.34}$$

$$M_{F_{span}} = F_{span,y} * r_{CoM} * sin(\theta) - F_{span,x} * r_{CoM} * cos(\theta) \tag{3.35}$$

Subscripts CoM, CoB and CoA denote the centre of mass, centre of buoyancy and distance to the centroid of the side area. All radii r are measured along the centreline of the Symphony from the fairlead. These radii are a function of floater displacement z. The inertia of the Symphony, the

sidearea of the Symphony and the displacement of the Symphony are also functions of z. These functions of z are further described in appendix A.

In order to make an effort to simulate the damping effect on the pitch motion of the Symphony resulting from the rotation about the centre of mass an extra damping moment is added to the total moment. This moment is calculated as follows:

Let's imagine that the Symphony rotates about it's centre of gravity. The local translational velocity of every horizontal slice of the Symphony is then calculated as $\dot{\theta} * R$ with R the absolute distance between the slice and the slice at the location of the centre of gravity. The local force per length can be calculated as $\frac{1}{2}\rho(\dot{\theta} * R)^2 C_d D$ where D is the local diameter. The local moment per length associated with this force is then calculated as $\frac{1}{2}\rho(\dot{\theta} * R)^2 C_d D * R$. The total moment by this drag force is then calculated by integrating from the centre of mass in upward direction and in downward direction to the top and bottom end of the Symphony. Hence,

$$M_{top} = \int_{CoM}^{top} \frac{1}{2}\rho(\dot{\theta} * R)^2 C_d D * R dR \tag{3.36}$$

$$M_{bottom} = \int_{CoM}^{bottom} \frac{1}{2}\rho(\dot{\theta} * R)^2 C_d D * R dR \tag{3.37}$$

For the top part the local diameter is always the floater diameter because the bottom of the floater is always below the centre of mass. For the bottom part the diameter shifts from the floater diameter to the base diameter at the position of the bottom of the floater.

Hence (3.36) develops to

$$M_{top} = \frac{1}{2}\rho\dot{\theta}^2 C_d D_{fl} \int_{CoM}^{top} R^3 dR \tag{3.38}$$

and (3.37) is split into the part above the bottom of the floater but below the centre of gravity and the part below the bottom of the floater:

$$M_{bot} = \frac{1}{2}\rho\dot{\theta}^2 C_d D_{fl} \int_{CoM}^{bfl} R^3 dR + \frac{1}{2}\rho\dot{\theta}^2 C_d D_b \int_{bfl}^{bottom} R^3 dR \tag{3.39}$$

where bfl denotes the bottom of the floater.
Combining and forcing the correct sign gives

$$M_\theta = -\frac{|\dot{\theta}|}{\dot{\theta}} * (|M_{top}| + |M_{bottom}|) \tag{3.40}$$

3.6. CONCLUSION

Several models of the Symphony have been derived. The simple model derived in section 3.3 can be used to estimate the undamped natural frequency of the system. When final model presented in section 3.5 is implemented, simulated natural frequencies can be compared to analytic results of the simplified model. If these values are close that gives confidence in the results of the model. The final model described in section 3.5 is implemented in chapter 4.

4

MODEL IMPLEMENTATION

In chapter 3 a model describing the 2D body motion of the Symphony has been derived. As stated in chapter 2 a lot of modelling has already been done in prior research related to the Symphony. Therefore the derived model can be added to the existing modelling structure to be able to assess the effects of the horizontal motions of the Symphony. This means the derived model will be implemented in the existing Matlab/Simulink structure.

In order to explain the implementation of the body motion part of the model firstly the existing model structure will be explained briefly. Then the body motion model with the appropriate couplings with the existing model will be explained.

4.1. EXISTING SIMULINK MODEL

The existing model is based on solving the differential equation which governs the motion of the floater relative to the base numerically. This equation is one-dimensional and is based on Newton's second law of motion: $F = m * a$ which yields $a = \frac{F}{m}$ for the acceleration. The velocity is then calculated by integrating the acceleration and integrating once more yields the position. The time domain model does this numerically, which means that every timestep all forces are calculated and divided by the moving mass. The resulting acceleration is assumed constant over the timestep and integrated twice to obtain the velocity and position. The new position, velocity and acceleration in turn are inputs for the forces for the next timestep. The observant reader might notice that this implies an algebraic loop in the model, which is in fact true. This loop was identified during the the research and a method to eliminate the loop has been proposed. However, for some cases the algebraic loop is needed to be able to calculate the correct values with the model. In these cases Simulink solves the loop iteratively. The block diagram of the existing Simulink model is given in figure 4.1.

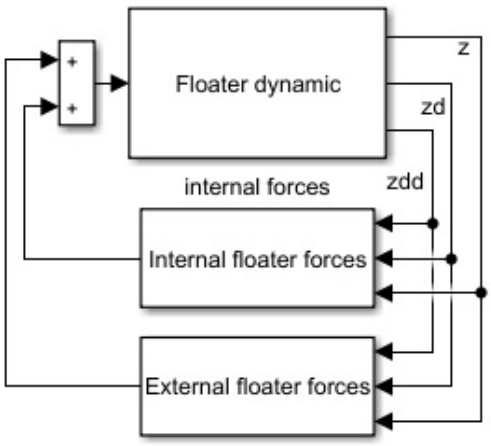

Figure 4.1: Block diagram of the existing Simulink model [1]

4.2. BODY MOTION MODEL

Based on section 3.5 the body motion model has been implemented in Simulink.
The schematic of this model is depicted in figure 4.2 [2]. The diagram clearly shows that for each degree of freedom the velocity is calculated from the equation of motion (EOM). Then the total translation and rotation is solved in the motion combination block and the new situation is input for the next time step. Using this new situation the new forces and moments are determined as a function of the state of the Symphony and time.

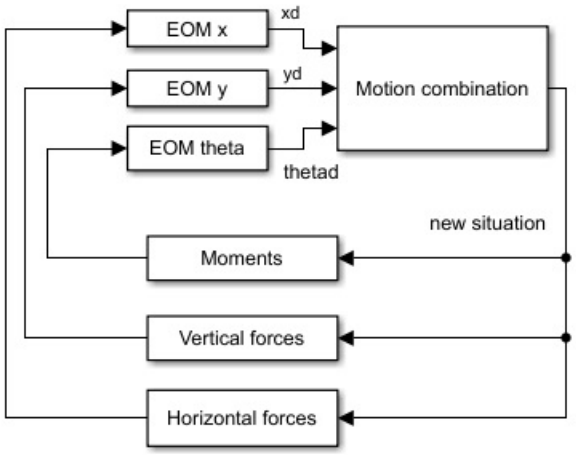

Figure 4.2: Block diagram of the derived body motion model

4.3. COUPLED MODEL

With both models working separately the models can be coupled. This coupling is done by exchanging information between the models every time step. The exchanged information consists of the floater position and the resulting force on the floater from the operational model to the body motion model and the x-position of the top of the floater, the angle of the Symphony and the y position of the fairlead from the body motion model to the operational model. In the operational model, the external forces on the floater are influenced by the height of the Symphony (affecting the hydrostatic pressures on the different parts) and the x position of the Symphony, affecting the momentary wave-induced pressure at the position of the floater. Because the dominating wave force acting on the Symphony is the wave force in the top of the floater the used x position is that of the top of the floater. The height of the different parts is calculated using the height of the fairlead above the seabed and correcting for the local floater position z and the angle of the Symphony θ.

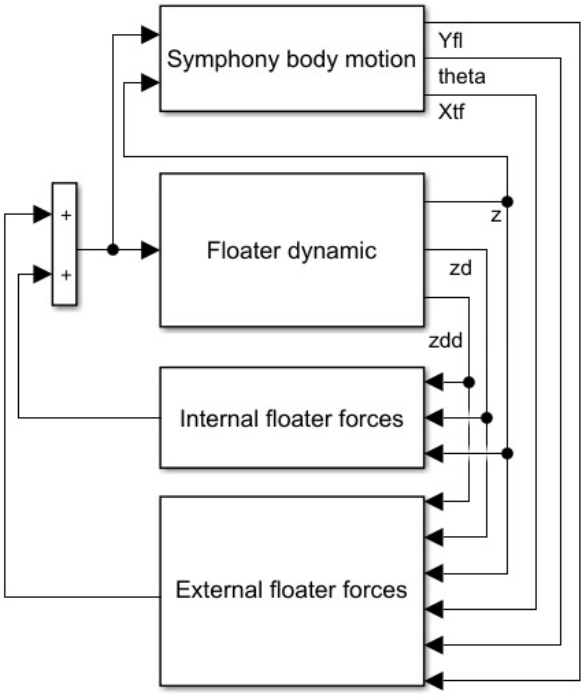

Figure 4.3: Block diagram of the derived Simulink model [2]

[2] Please note that this is a schematic and not the actual Simulink model. Single lines may represent multiple variables.

4.4. TESTING THE MODEL

In order to confirm that the implemented model gives reliable outputs it has to be tested in some way. For practical reasons experiments to validate this model are not an option. Hence, the next best way to gain confidence in this model is to test it against existing modelling and to compare it with simple cases that can be estimated analytically.

4.4.1. SIMULATION TIME STEP

The time step is initially inherited from the previous iterations of the operational Symphony models, which is 0.01s. Looking at figures 4.5 and 4.6 0.01s seems to be sufficiently small for the motion simulation of the Symphony. However, one very stiff element, the mooring line, is introduced. When doing a time domain simulation it is sensible to have a time step that is much smaller than the natural period of the system. In this case the worst case scenario (highest natural frequency) is the Den Helder case. The axial natural frequency of the system is approximated by $\omega_n = \sqrt{\frac{k_m}{m}} = \sqrt{\frac{11.9*10^6}{20*10^3}} = 24.4\frac{rad}{s} = 3.9Hz$ which corresponds to a natural period of $T_n = \frac{1}{f} = \frac{1}{3.9} = 0.26s$ which is 26 time steps. Hence, the time step is small enough with respect to this natural frequency. Therefore the time step of 0.01s which was inherited from previous iterations can be maintained. Running the model at this time step confirms that it is stable and that the relevant motions indeed oscillate slow enough to be facilitated by the 0.01s time step, see figure 4.4.

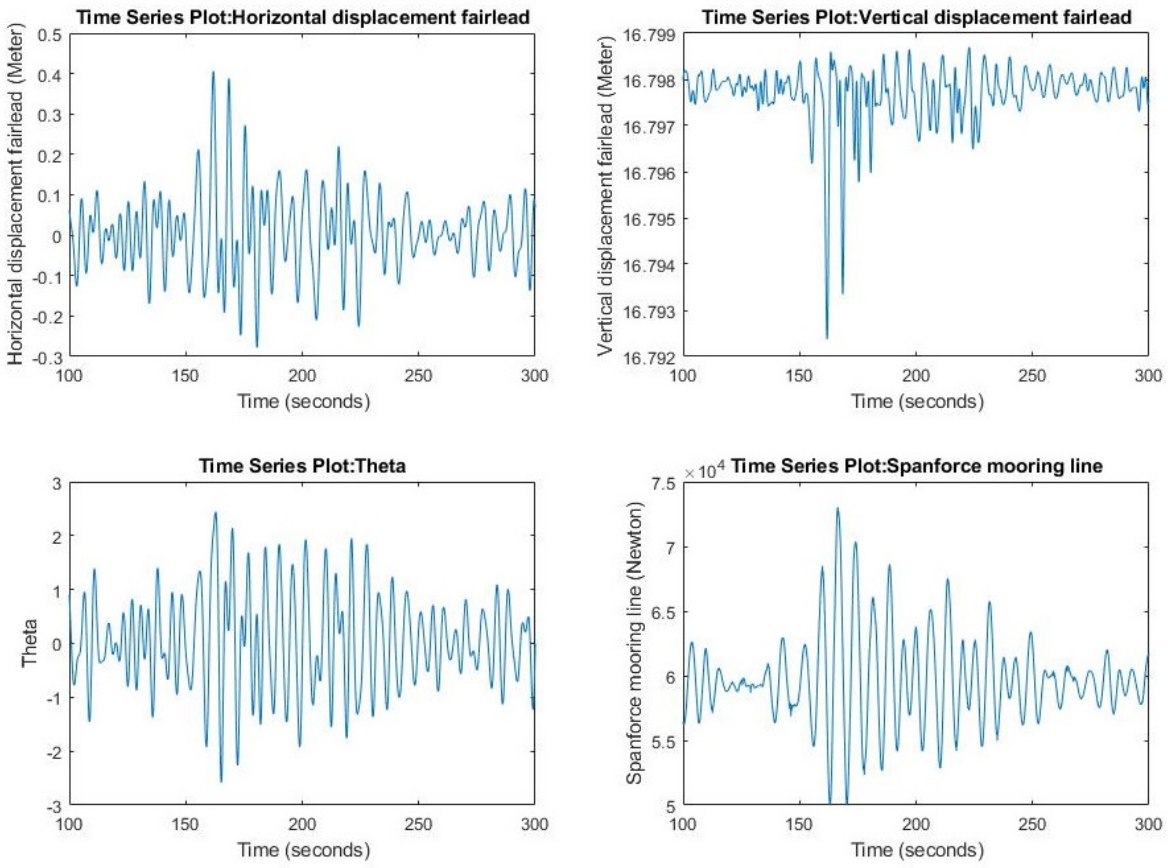

Figure 4.4: Time trace of normalised Symphony motions. Den Helder location, Hs = 1.5m, Te = 5.5s. Angle θ in degrees

4.4.2. SIMULATION RUN TIME

In order to produce reliable outputs the model has to be run several times, and with a sufficiently long duration. In line with previous research [21] a run time of 1300 seconds discarding the first 100 seconds to avoid influence of transient effects as a result of starting the model seems to be reasonable. However, in order to verify that this is also valid for this model a short study is undertaken. The output power of the Symphony is selected as normative output. The model is run 10 times for one sea state using several run times. The power output of every run is compared to the mean of all runs with that simulation time. The resulting mean relative errors are given in table 4.1. This mean relative error (MRE) is defined as the mean of the relative difference between the outputs of the 10 individual runs and the mean of those ten outputs. For n runs this is calculated as

$$MRE = \frac{\sum_{i=1}^{i=n} |\frac{output_n}{meanoutput} - 1|}{n}$$

The full results of the runs conducted to determine a reliable run time are listed in appendix C. From table 4.1 1900 seconds it can concluded that until 1900 seconds the performance seems to increase significantly. Hence, a duration longer than 1900 seconds is not required. This is in line with the suggestion in literature that between 15 and 30 minutes (900 and 1800 seconds) is a reasonable length for a sea state [20].

Mean relative error

Run time (s)	*Leixões*
200	20%
400	8%
700	5%
1300	5%
1900	2%
2500	2%
Run time (s)	*Den Helder*
200	20%
400	7%
700	5%
1300	5%
1900	2%
2500	2%

Table 4.1: Mean relative error of Symphony power for different run times at both locations. The first 100 seconds of the results are always discarded

4.4.3. TESTING AGAINST THE EXISTING MODEL

With consistency and stability of the model assured it is important to compare the results of the implemented model with those of the existing model in order to assure that no errors in the integration between the models are made. To do this comparison the new Simulink model has been fitted with a set of switches which restrain the x, y and θ degrees of freedom. For this comparison the characteristic sea states given in tables 2.1 and 2.2 are used. For every sea state a wave seed is generated ten times. This wave seed is used to run the new Simulink model and the existing Simulink model. Then the results are compared. This comparison yields identical results for all runs. Hence, the model still simulates the Symphony operation correctly.

4.4.4. DECAY SIMULATION

As stated in section 3.4 confidence in the model can be gained by comparing results of an undamped free oscillation of the body motion model to the analytical solution of that oscillation for the single degree of freedom model. Because this thesis has two location which are of particular interest this will done for both locations. The locations are described in more detail in section 2.3. For this comparison it suffices to know that the water depths are 35 and 100 metres, respectively. This yields pendulum lengths $L_{p,35} = 35 - dclr - L_{sym,max} + r_{CoM,eq} = 24.5m$ and $L_{p,100} = 35 - dclr - L_{sym,max} + r_{CoM,eq} = 89.5m$ The estimates for the natural frequency for these water depths with the Symphony locked in its equilibrium position ($z = 0$) are calculated below

$$\omega_{n,35m} = \sqrt{\frac{\frac{F_{b,net,eq}}{m_{sym}}}{L_{p,35}}} = \sqrt{\frac{\frac{59000}{17500}}{24.5}} = 0.371\frac{rad}{s} = 0.059Hz$$

This corresponds with a natural period of $\frac{1}{0.059} = 16.9s$. Figure 4.5 gives the time trace for the horizontal oscillation of the symphony body according to the implemented numerical model. From the figure the natural period can be estimated around $17.5s$. For the Leixões location the same calcula-

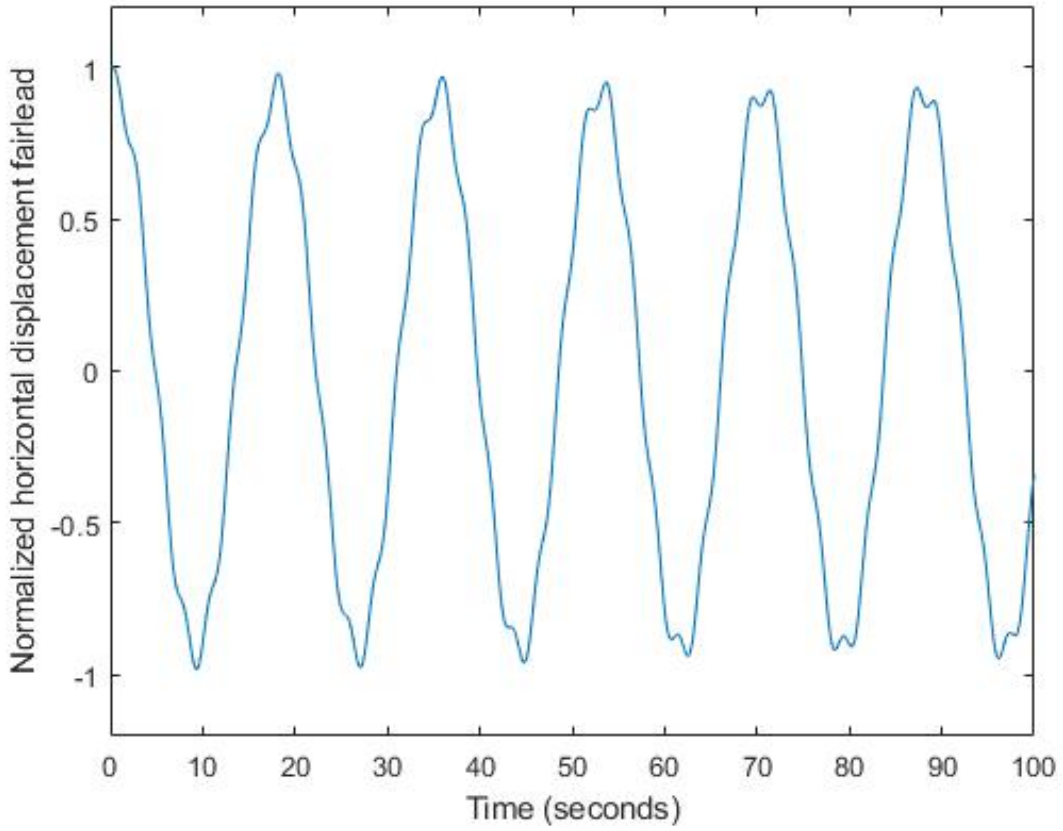

Figure 4.5: timetrace of the free horizontal oscillation of the symphony in survival mode in $35m$ water depth [3]

tion applies:

$$\omega_{n,100m} = \sqrt{\frac{\frac{F_{b,net,eq}}{m_{sym}}}{L_{p,100}}} = \sqrt{\frac{\frac{59000}{17500}}{89.5}} = 0.194\frac{rad}{s} = 0.031Hz$$

This corresponds with a natural period of $\frac{1}{0.031} = 32.3s$. Figure 4.6 gives the time trace for the horizontal oscillation of the symphony body according to the implemented numerical model.From the figure the natural period can be estimated at $32s$.

As can be seen above the modelled values of the natural frequencies are close to the results obtained by running the simulation. This gives confidence in the validity of the body motion model.

4.5. COMPARING SURGE LOADS

Section 2.5.2 presents model results for surge loads on the restrained Symphony in survival mode. The time trace for this situation ran in the implemented model is given in figure 4.7. From the figure

[3] The small ripple on the large oscillation is due to the rotation in the θ degree of freedom

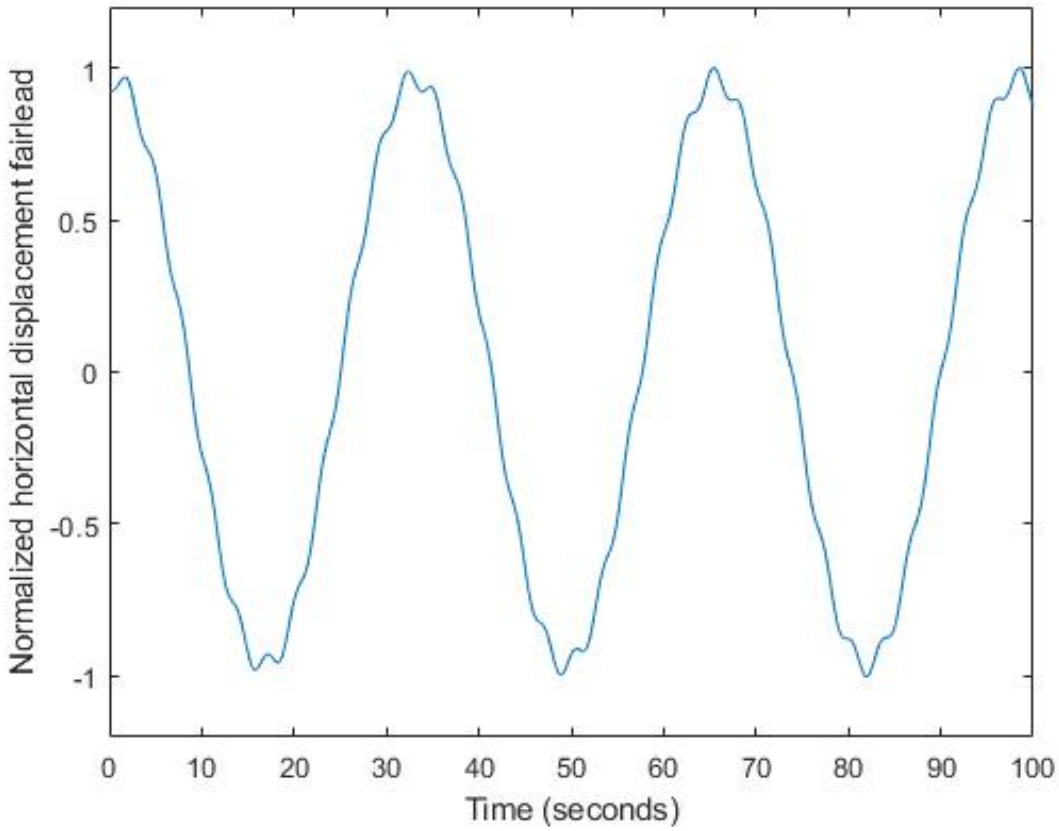

Figure 4.6: time trace of the free horizontal oscillation of the symphony in survival mode in 100m water depth [3]

it can be seen that the surge load amplitude is 5 kN at a submersion of 6 meters and a monochromatic wave of 1 meter amplitude and 5 seconds period. This is close to the values presented in 2.5.2.

4.6. CONCLUSION

The implementation of the model in the Matlab/Simulink environment has been described. Simple simulations have been compared to analytic solutions of simple cases in order to gain confidence in the model. Also one simulated case has been compared to results in previous work. In the presented comparisons the results by the implemented model match the analytical results good enough to gain confidence in the correctness of the model. Hence, this model can be used to estimate horizontal Symphony motion in the 2D plane and associated mooring reaction forces.

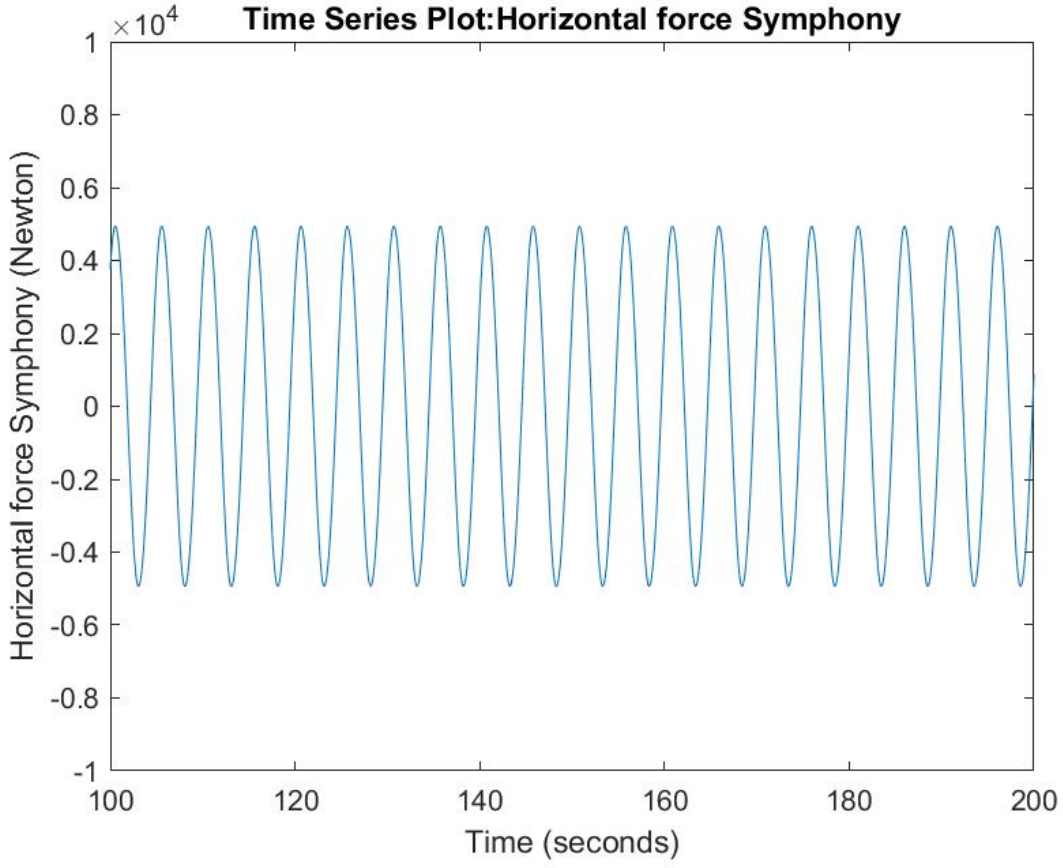

Figure 4.7: time trace of surge loads on the restrained Symphony. Wave period is 5 seconds, amplitude 1 meter

5

RESULTS

This chapter presents the model results. Firstly, the input parameters that are not yet discussed are explained. Then the results for both cases and both locations are presented and discussed.

5.1. MODEL INPUT PARAMETERS

For running the model several inputs have to be chosen. The characteristic sea states are given in section 2.3. In addition to the sea states the mooring line properties have to be estimated. Preliminary runs show expected maximal reaction forces close to 100 kN. It is appropriate to wield a safety factor of 3 for these kind of loads so for a priliminary estimate the line should be designed to have a break load of at least 300 kN. Assuming the line to fail when the yield stress is reached and a yield stress of 300 MPa this yields an equivalent cross sectional area of $\frac{0.3MN}{300MPa} = 1000mm^2$ [1]. If the line material is assumed to have a Youngs' modulus of 200 GPa then the line stiffness is equal to $k = \frac{AE}{L}$ which for the Leixões case equals 2.44 kN/mm and for the Den Helder case 11.90 kN/mm.

5.2. OUTPUT VALUES

The values of interest are the following:

- mean output power
- maximum horizontal mooring reaction force ($F_{x,max}$)
- maximum vertical mooring reaction force ($F_{y,max}$)
- magnitude of the expected worst case reaction force (F_{wc})
- angle of the expected worst case reaction force (α_{wc})

Of these values, the mean output power does not apply to the survival case because the Symphony does not produce any power when in survival mode.

For the operational case a series of sea states from zero to the cut out sea state will be simulated to provide a useful set of numbers to be used in choosing the operational envelope of the Symphony. For the survival case only the survival sea state will be simulated as the survival case cannot be chosen but is a property of the deployment location.

[1] Material properties are chosen based on common values [35]

Sea state	Power (W)	$F_{x,max}$ (N)	$F_{y,max}$ (kN)	F_{wc} (kN)	α_{wc} (degrees)
1	108	370	71.6	61.3	0.37
2	1486	1189	77.9	62.7	1.07
3	2865	1936	77.6	75.0	1.83
4	0	0	0	0	0
5	0	0	0	0	0
Cut out	9073	3501	92	78.1	2.21

Table 5.1: Results for the characteristic sea states at the Leixões location

For all of the outputs the model has been run three times with the same sea state, but a unique wave seed. For the power the mean of the three runs is taken, for the reaction forces the maximum of the three runs is taken.

5.3. RESULTS

The results are presented in the following sections. Only the results of the survival case and the characteristic sea states are presented in this section. For the full output matrices please see appendices E and F.

5.3.1. LEIXÕES

This section presents the results for the characteristic sea states and the survival case (Te =18s, Hs = 15m) for the Leixões location.

SURVIVAL CASE

Table 5.2 gives the maximum loads for the survival case. In order to properly visualise these loads polar a plot iss produced. This plot gives the time trace of the force *vector*. Every point on the line gives the magnitude of the force at a certain point in time and the corresponding angle op the force at that point in time. This way it is easily identified where the bulk of the loads are. one polar plot from the simulations done to assess the Leixões survival case is given in figure 5.1.

Output	value
$F_{x,max}$	10.7 kN
$F_{y,max}$	63.7 kN
F_{wc}	57.6 kN
α_{wc}	10.7°

Table 5.2: Outputs for the Leixões survival case

OPERATIONAL CASE

The results for the characteristic sea states are given in table 5.1. The zeros for the fourth and fifth sea state denote a Symphony breakdown. From the full power diagram in table F.1 the cut out sea state for Leixões had been determined at Hs = 7.5m and Te = 5.5s[2]. This sea state has been added to the results to determine the maximal operational loads.

Using these outputs, the rated power for the Symphony at this location[3] and the occurencies of the characteristic sea states (table 2.1) a capacity factor of the Symphony for this location can be computed. This is done by calculating the energy the Symphony is expected to generate in a year and dividing by the theoretical maximum annual power production defined by the rated power times

[2]Based on the force and power diagram given in appendix E Hs = 7.5, Te = 5.5 is chosen as the cut out sea state. This is to ensure the estimates to be conservative

[3]The rated power for a location is defined as the highest output power in the scatter diagram for that location

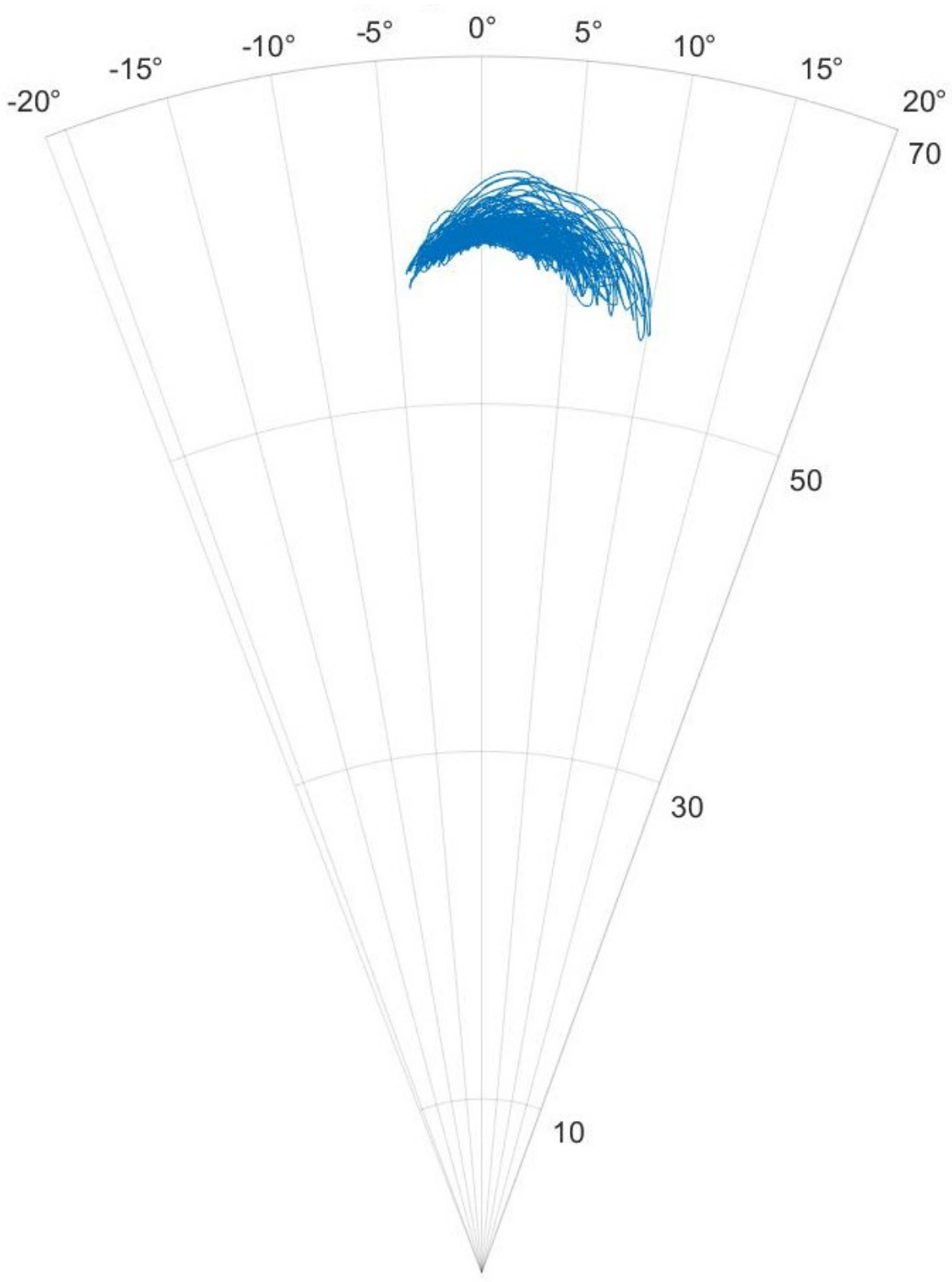

Figure 5.1: Polar plot of the required mooring reaction forces for the Leixões survival case

the length of a year. If the rated power is taken as 9073W[4] for Leixões location this yields a capacity factor of

$$C_p = \frac{8766 * (0.344 * 108 + 0.381 * 1486 + 0.118 * 2865)}{8766 * 9073} = 0.1083 = 10.38\%$$

MOTIONS

The model also determines the motions of the Symphony. Table5.3 gives the maximum horizontal excursion of the fairlead for the characteristic sea states and the survival conditions in Leixões. Time traces of the motions are given in appendix H.

	Maximum Symphony horizontal excursion (m)
Characteristic sea state 1	0.55
Characteristic sea state 2	1.89
Characteristic sea state 3	3.07
Characteristic sea state 4	no data
Characteristic sea state 5	no data
Survival case	17.7m

Table 5.3: Horizontal excursion of the Symphony fairlead for characteristic sea states and survival conditions for the Leixões location. Cells with no data are above cut out seastate

COMPARISON OF THE MOVING AND THE RESTRAINED SYMPHONY

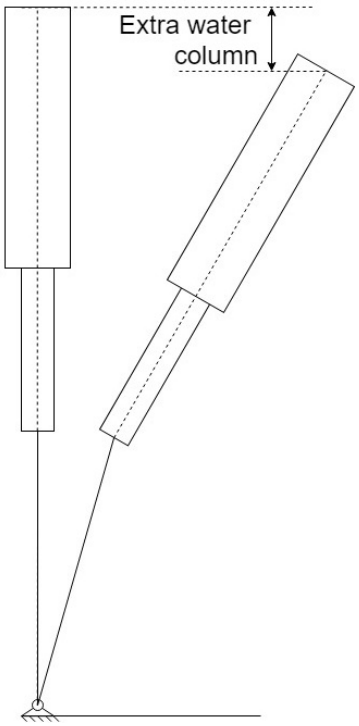

Figure 5.2: Extra water column due to Symphony motion

To compare the energy yield of the restrained Symphony and the moving Symphony several model runs have been conducted. The expectancy is that a difference in energy yield between the moving

[4] the 9073 watt belonging to sea state Hs = 7.5m and Te = 5.5s is selected rather than the 10953 watt belonging to Hs = 9.5m and Te = 4.5s because the latter is an isolated value in the power matrix and therefore highly unlikely

	Mean index power (%)		
Sea state	Moving	Restrained	Restrained with extra water column
1	100	97.27	99.27
2	100	100.52	100.78
3	100	99.36	100.41
4	100	no value	no value
5	100	no value	no value

Table 5.4: Mean index power for different sea states fir the Leixões location

Symphony and the restrained Symphony can be explained by the vertical displacement of the top of the floater, effectively adding an extra "wave" to the excitation forces, expressed as an extra water column.
For all characteristic sea states a ten wave seeds are generated. For every wave seed the Symphony model is run. From the results of the first run the time trace of the vertical displacement of the top of the floater with respect to the restrained situation is calculated. See figure 5.2. Then the model for the restrained Symphony is ran, with this extra water column height added to the water column responsible for the hydro static forces on the floater.
Table 5.4 gives the results for the characteristic sea states for the Leixões location. The index power is defined as the mean power resulting from the restrained model divided by the power resulting from the moving model *with the same wave seed*. Table 5.4 Gives the mean index power (MIP) for the characteristic sea states for Leixões.
From the results it can be concluded that the difference in energy yield is very small. It is in the same order of magnitude as the error that was accepted in the process of justifying the time step. Hence, the only real conclusion that can be drawn from these simulation is that incorporating the horizontal motion in the Symphony modelling does not matter a great deal for the energy production. For the lowest sea state the extra water column indeed seems to correct the difference between the moving and restrained Symphony, however, in the other sea states this relation does not seem to hold. The differences are too small compared to the inconsistencies of the model output to draw any real conclusion other that that the energy production is not greatly affected.

MAXIMUM EXPECTED LOADS

From the two previous sections the maximum expected loads for the mooring can be identified. It is interesting to see that the vertical maximum expected required mooring forces are in fact reached in operational conditions and not in survival conditions. This might feel counter intuitive, but can be explained. As already mentioned by Leijten [19] the floater pulls the base upward in operation. In survival condition, this extra (mainly vertical) force is not present. Hence, the maximum required vertical reaction forces are significantly lower in the survival case than in the operational case. The maximum expected loads are listed in table 5.5.

Load	occurs in	magnitude	angle with respect to vertical
Maximum horizontal	survival condition	10.7 kN	90 degrees
Maximum vertical	operational condition[5]	95.4 kN	0 degrees
Expected worst case	survival condition	57.6 kN	10.7 degrees

Table 5.5: Maximum expected loads for the Leixões location

[5]Maximum values from table E.3 is taken

5.3.2. DEN HELDER

The results for the Den Helder case are presented below.

SURVIVAL CASE

Table 5.6 gives the maximum loads for the Den Helder survival case. Again, polar plots have been made to visualise the loads. The polar plots from the simulations done to assess the Leixões survival case are given in figure 5.3.

	Current velocity		
Quantity	0 m/s	0.5 m/s	-0.5 m/s
$F_{x,max}$	30.7 kN	53.0	15.0 kN
$F_{y,max}$	72.9 kN	88.0	73.3 kN
F_{wc}	80.9 kN	97.6	60.0 kN
α_{wc}	30.6°	32.9	21.7°

Table 5.6: Outputs for the Den Helder survival case

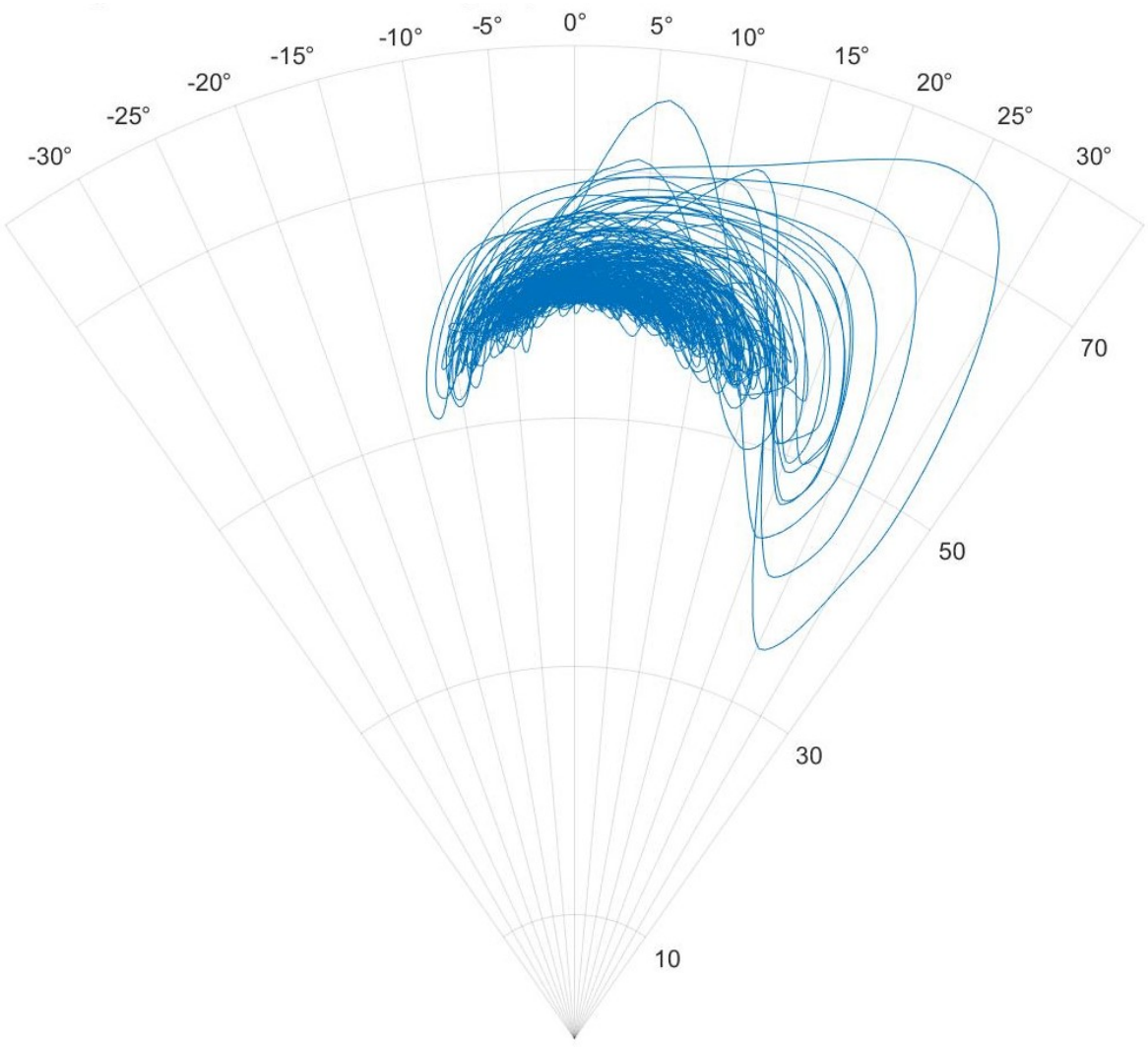

Figure 5.3: Polar plot of the required mooring reaction forces for the Den Helder survival case

OPERATIONAL CASE

The results for the characteristic sea states are
given in table 5.7. Again, zeros are present at a sea state which is apparently above the cut out sea state as the model predicts a breakdown of the symphony at that sea state. Again, the cut out sea state is determined at Hs = 4.5m and Te = 8s[6] and ran to complete the results.

Sea state	Power (W)	$F_{x,max}$ (N)	$F_{y,max}$ (kN)	F_{wc} (kN)	α_{wc} (degrees)
1	11	315	61.9	60.0	0.32
2	207	1717	76.6	63.6	1.43
3	2043	3517	79.6	50.4	4.37
4	3767	7093	80.0	59.2	7.30
5	0	0	0	0	0
Cut out	5071	7848	80.4	68.0	7.85

Table 5.7: Results for the characteristic sea states at the Den Helder location

Using the same procedure as in section 5.3.1 and taking a rated power of 5964W[7] the capacity factor for the Den Helder location can be calculated as

$$C_p = \frac{(0.407 * 11 + 0.394 * 207 + 0.141 * 2043 + 0.043 * 3767)}{5964} = 0.0899 = 8.99\%$$

MOTIONS

The model also determines the motions of the Symphony. Table 5.8 gives the maximum horizontal excursion of the fairlead for the characteristic sea states and the survival conditions in Den Helder. Time traces of the motions are given in appendix I.

	Maximum Symphony horizontal excursion (m)
Characteristic sea state 1	0.09
Characteristic sea state 2	0.52
Characteristic sea state 3	1.27
Characteristic sea state 4	2.03
Characteristic sea state 5	no data
Survival case no current	7.5
Survival case positive current	10.3
Survival case negative current	5.8

Table 5.8: Horizontal excursion of the Symphony fairlead for characteristic sea states and survival conditions for the Den Helder location. Cells with no data denote Symphony breakdown; so this sea state is above cut out

COMPARISON OF THE MOVING AND THE RESTRAINED SYMPHONY

Again, the moving and restrained Symphony are compared. Mean index powers are given in table 5.9. From the results it is again clearly seen that the difference in energy yield is quite small. Again, we can concluded that the incorporation of the Symphony body motions in the operational model does not have a large impact on the energy yield by the Symphony.

[6]The cut out sea state for Den Helder is outside the chosen range of the power diagram. It has been determined by running some small power matrices around the expected cut out sea state. Time traces for the cut out sea state are given in figures F.2 and F.1

[7]based on table G.1

	Mean index power (%)		
Sea state	Moving	Restrained	Restrained with extra water column
1	100	99.27	99.92
2	100	97.68	98.34
3	100	102.82	101.83
4	100	102.90	102.00
5	100	100.47	100.1

Table 5.9: Mean index power for different sea states for the Den Helder location[8]

MAXIMUM EXPECTED LOADS

From the two previous sections the maximum expected loads for the mooring can be identified. It is interesting to see that the maximum expected vertical reaction forces required bot the mooring are in fact reached in operational conditions and not in survival conditions. This might feel counter intuitive, but it can be explained. As already mentioned by Leijten [19] the floater pulls the base upward in operation. In survival condition, this extra (mainly vertical) force is not present. Hence, the maximum required vertical reaction forces are significantly lower in the survival case than in the operational case. The maximum expected loads are listed in table 5.10.

Load	occurs in	magnitude	angle with respect to vertical
Maximum horizontal	survival condition	30.7 kN	90 degrees
Maximum vertical	operational condition	92.5 kN	0 degrees
Expected worst case	survival condition	80.9 kN	30.6 degrees

Table 5.10: Maximum expected loads for the Den Helder location

5.4. CONCLUSION

From the model results it can be concluded that the maximum vertical mooring forces for both cases occur in operational conditions. The calculated maximum vertical mooring forces are close to the forces proposed by Leijten [19]. The difference with Leijtens results can be attributed to the fact that the wave force on the base is now also accounted for. These forces were neglected in his previous work.
From the results it can also be seen that the maximum vertical forces for different water depths are close to each other. This was to be expected, because the time domain model designs the Symphony spring characteristic so that a certain maximum is not exceeded [19].
The maximum horizontal and maximum inclined loads occur in survival conditions for both cases. This is explained by the larger horizontal excursions in survival mode. Because the horizontal excursion is larger, the mooring line angle ϕ becomes larger, making for a larger horizontal component in the mooring reaction force. Particularly in shallower waters (Den Helder case) the horizontal component becomes large. This is due to two effects of shallow water: (1) the mooring line is shorten, making the angle ϕ larger at a certain horizontal excursion ($x = l * sin(\phi)$) and (2) the depth effect described in section 2.7 is larger at a certain depth below the sea level than in deeper waters, making the horizontal excitation larger and with that the horizontal excursions.

[8] Running the fifth sea state the Symphony model detected a Symphony break down in three instances. MIP is calculated using the other six values

6

MOORING DESIGN DISCUSSION

Based on the resulting mooring reaction forces presented in chapter 5 a short investigation of the possible mooring solutions has been conducted [36, 37]. Several possible mooring solutions are presented and discussed. The different possibilities are compared and a recommendation for the two considered locations is done.

6.1. SUITABLE MOORING TECHNOLOGIES

This section presents several suitable technologies that can be used to facilitate the mooring line of the Symphony. Based on these descriptions possible mooring solutions are described in section 6.3.

6.1.1. DEADWEIGHT ANCHOR

A deadweight anchor is used to withstand large vertical loads: the deadweight can withstand vertical loads equal to the submerged weight of the anchor. However, a deadweight anchor's only resistance against horizontal forces is based on friction between the soil surface and the deadweight. This friction force is calculated by some friction factor multiplied by the contact area between the deadweight and the soil surface and the pressure between the surface and the deadweight. Typically these friction factors are in the order of 10%. This poses possible problems in the case of large inclined loadings, where the pressure between the soil surface and the deadweight is less than the submerged weight and a considerable horizontal load is applied. Secondly, a force vector that is out of line with the gravity (a load that has a horizontal component) is asociated with a moment around one of the corners of the deadweight. This poses possible problems when large horizontal or inclined loads are applied. The moment associated with the loading force vector could be larger than the restoring moment which is equal to the half width of the deadweight multiplied by its submerged weight when the deadweight is still flat. If this occurs the deadweight can start rotating and might be tipped over. Thirdly, a deadweights mass and therefore its submerged weight is determined by its relative density (the difference between the material density and the water density) and its volume. The dominant component of the horizontal loads on the Symphony are a result of the wave induced pressure gradient. This force scales linearly with the objects' volume (see equation 3.5. In shallow water the pressure gradient oscillation still has a considerable amplitude which could provoke a negative design spiral: large horizontal loads lead to a large required volume, which would lead to bigger horizontal loads et cetera. This is especially problematic in shallow (coastal) waters. A very heavy gravity anchor has a considerable volume. Concrete has an underwater weight

in the order of 25 kN/m3. A gravity anchor of considerable underwater weight would have a considerable volume as well. Especially in shallow water this will pose problems, because the horizontal pressure gradient at the seabed-level is still considerable. When a gravity anchor of considerable weight an thus volume will be used, the horizontal force on the anchor will be considerable as well. This would call for an even heavier anchor, which would in turn have a larger volume, meaning the horizontal force will be larger et cetera. Hence a gravity anchor is not adviseable in shallow water.

6.1.2. DRIVEN PILE

A driven pile mooring resists vertical loadings thanks to the submerged weight of the pile itself and the friction between the pile and the soil. The resistance against horizontal loading originates from the resistance of the pile and the soil against deformation. Especially in cohesive soils driven piles can resist large loadings. Literature points out that tension pile foundations and suctions anchors are the principle method of installation for existing offshore structures and thus are a good option to consider for offshore energy producers as well. Looking at other research

6.1.3. DRAG ANCHOR SINGLE POINT MOORING (DASP)

Drag anchors are dragged into the soil and can withstand serious horizontal loads. However, a drag anchor has little to no resistance to vertical loads. In order to translate the vertical loads to horizontal loads three anchors can be dragged to a central point, usually in 120 degree angles, where the lines are connected. A vertical load to this central point will lift the point and the three lines will lift up from the soil which will rotate the force vector in the line (which is always in line with the line) and they will all have a vertical component. The drag anchors need to have a very large horizontal capacity compared to the vertical loads on the mooring point because of the large angle between the anchor line and vertical.

6.1.4. SUCTION PILE

A suction pile is a (usually circular) hollow steel pile with a closed top end and and open bottom end. In order to install a suction pile it is lowered onto the seabed and water is drained from the pile using an Remotely Operated Vehicle (ROV). When the water is drained from the inside of the pile a large resulting force due to the hydrostatic pressure on the top of the pile pushes the pile in. Suction piles can withstand loads due to the friction between the soil and the suction anchor and the resistance of the soil and the pile itself against deformation. Because the working of a suction pile is based on the water column on top of the pile suction piles are particularly fit for use in deep waters.

6.1.5. GRAVITY INSTALLED ANCHOR (GIA)

A GIA is dropped from a considerable height above the seabed and penetrates the soil due to the velocity it gained during the drop. This type of mooring is easily installed and can withstand both horizontal and vertical loads in a similar way as the other two pile type moorings. However, it can only be used in soft soils and a considerable water depth is needed to build up sufficient velocity which could render it incompatible for shallow, coastal waters.

6.1.6. VERTICAL LIFT ANCHOR (VLA)

Vertical lift anchors are similar to drag anchors. However, during installation the anchor is rotated in such a way that is can withstand both vertical and horizontal loads. These anchors are suitable for deep sea moorings. However, they are not particularly fit to handle loads that change in direction. As the horizontal loads on the Symphony changes direction with the wave frequency, this might pose a problem for this mooring type.

6.1.7. SUCTION EMBEDDED ANCHOR (SEA)

The last mooring possibility that will be discussed is the suction embedded anchor. This type of anchor is pushed in the ground by a follower in a similar way a suction pile is installed. However, if the suction embedded anchor is at the desired depth, the follower is removed and the anchor itself is brought into the vertical loading mode. This type of mooring is suitable for cohesive soils and can't be used in sandy soils.

6.2. COMPARISON OF THE MOORING OPTIONS

Based on the presented mooring possibilities and consultation with several industrial players for both locations the mooring options are shortly discussed below. Table 6.1 gives the applicability to different situation of different mooring types

	deadweight	driven pile	DASP	suction pile	GIA	VLA	SEA
non-cohesive soils	+	+	+	+	x	x	x
cohesive soils	+	+	+	+	+	+	+
deep waters	+	+	+	+	+	+	+
shallow waters	-	+	+	+	+	+	+

Table 6.1: Applicability of different mooring types in different situation. + means good, - means not so good and x means not possible.[1]

6.3. POSSIBLE MOORING SOLUTIONS

With an idea of the required mooring reaction forces (as can be seen from the results presented in chapter 5 this varies per location) and the overview of suitable solutions in section 6.1 mooring solutions can be proposed. As mentioned in section 2.6 the mooring design was initially assumed as a single line and a gravity anchor. However, as seen in chapter 5 the horizontal loads are considerable. Gravity anchors are not capable of withstanding large horizontal loads, without being very heavy themselves [38]. Section 6.1 describes why a gravity anchor, at least in shallow waters, might not be the best option.

6.3.1. SINGLE TECHNOLOGY SOLUTIONS

From section 6.1 the following single technology mooring solutions can be suitable for the Symphony:

- Driven Pile

[1] No hard definition is given for deep and shallow water. However, it stands to reason to have this boundary at half the wave length [20].

- Suction Pile
- Gravity Installed Anchor
- Suction Embedded Anchor

These solutions are all restricted by the restrictions already noted in section 6.1.

6.3.2. MULTIPLE ANCHOR SINGLE POINT MOORING

If one wants to use a drag embedment anchor to provide a suitable mooring for the Symphony the large vertical loads need to be translated to horizontal loads in order to load the drag embedment anchor in the direction in which it can withstand large loads. This can be done by dragging several angles from different directions to a single point and connecting the lines near the seabed. This way a stable point near the seabed is created. The simplest case is three anchors under 120°with each other. This way the arrangement is symmetric over the lines coinciding with the three mooring chains (see figure 6.1). The maximum purely vertical load that can be withstood by this arrangement (still assuming symmetry) is calculated as $F_u = 3 * F_{max,chain} * sin(\gamma)$ with $F_{max,chain}$ the maximum allowable tension in one chain (limited by the maximum allowable pull force of the anchor and the break load of the chain) an γ the angle of the chain with horizontal. The maximum horizontal load is equal to $F_{max,chain}$.

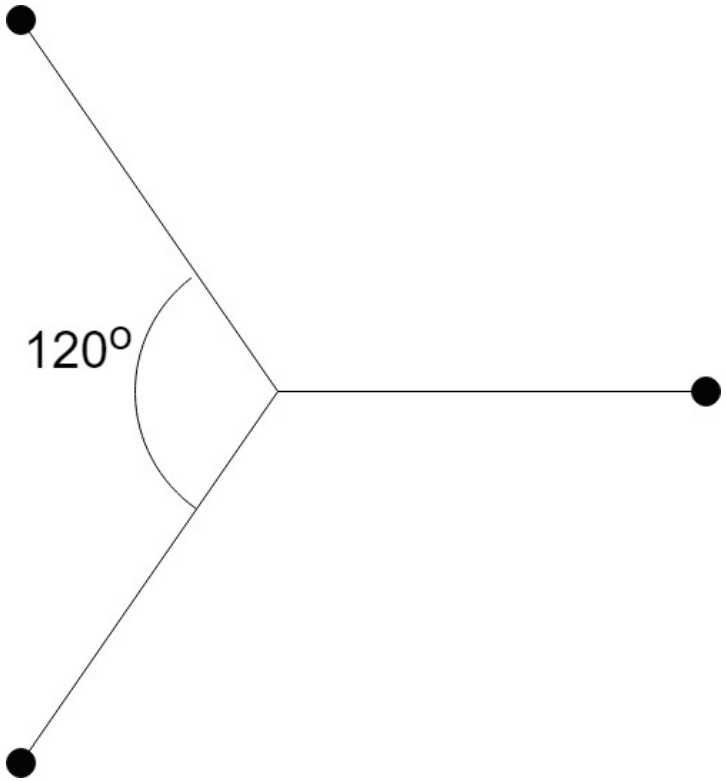

Figure 6.1: example of the spread of drag embedment anchors

6.3.3. DEAD WEIGHT INTEGRATED ANCHORS

Because the angle γ should usually be kept below 10°[36] the vertical load can be expected to dominate the required dimensions for this system In order to be able to design more efficiently the above described system can be combined with a dead weight of some kind. Especially a large, flat disk

with a high density (steel or concrete) can be useful to reduce the required vertical strength of the anchor system by "hanging" the dead weight from the Symphony mooring line. When the required vertical mooring force exceeds the submerged weight of the dead weight, it will want to lift from the sea bed. From that moment the anchors will have to contribute to the vertical mooring force. If the underwater weight of the deadweight is cleverly chosen at the maximum vertical mooring reaction force (close to 100kN, see chapter 5) the anchors will only have to withstand the horizontal forces resulting form Symphony motions. Assuming an underwater weight of 70kN/m^3 this would be a steel disk with a volume of 1.42 m^3. To give an idea of what such a disk could look like; such a disk could measure 0.10x2.12m (height x radius).

7

CONCLUSIONS AND RECOMMENDATIONS

Using the results presented in chapter 5 the research question can be answered.

7.1. SYMPHONY MOTION

The derived model is capable of predicting the motion of the Symphony in a given sea state. For the Leixões en Den Helder location the Symphony motion has been predicted using the derived model. Chapter 5 presents the results. For the operational cases in Leixões and Den Helder the maximum excursions are listed in table 7.1

Maximum horizontal excursion (m)	Leixões location	Den Helder location
Operational	3.07	2.03
Survival	17.7	10.3

Table 7.1: horizontal excursion of the Symphony fairlead for characteristic sea states and survival conditions

It is interesting to see that the excursion in Den Helder, despite the lower sea states, comes close to that in Leixões. However, this can be explained by the fact that the water at the Den Helder location is shallower, making the wave forces at the instalment depth are relatively higher than they are in Leixões. This is expressed in the depth effect explained in section 2.7.

7.2. EFFECT OF INCORPORATION BODY MOTION ON ENERGY PRODUCTION

As stated in sections 5.3.1 and 5.3.2 the effect on energy production is very limited. A effort has been made to explain what little difference that has been found. One possible explanation is that the extra water column on top of the Symphony is accountable for a difference in energy production. For the smallest sea states the simulation results seem to confirm this hypotheses. In larger sea states there is no real consistency in this pattern. From the results it can be concluded that the difference in energy production between the moving Symphony and the restrained Symphony are very small.

7.3. MOORING REACTION FORCES

On the mooring reaction forces this research has presented a useful model to estimate required mooring reaction forces for a Symphony wave power device in a certain region. Table 7.2 presents

these expected maximal loads the expected loads for the Symphony at the Leixões and Den Helder locations.

Quantity	***Leixões location***	***Den Helder location***
Maximum expected horizontal load	10.7 kN	30.7 kN
maximum expected vertical load	95.4 kN	92.5 kN
Worst case expected inclined load	57.6 kN	80.9 kN
Worst case expected inclined load angle	10.7°	30.6°

Table 7.2: Maximum expected loads for both cases

7.4. MOORING AND DESIGN RECOMMENDATIONS

Sections 6.1 and 6.3 give an overview of possible mooring design options for the Symphony. In the current stage of development it is neither sensible nor possible the make a general choice for the "right" mooring solution, as this will vary from location to location. Also cost of installation will play a role in this decision, which also varies with the design of the to be installed Symphony(s).
In the design of the Symphony it is important to have enough net buoyancy in the survival mode. If the Symphony has little net buoyancy it can be seen from the equations in section 3.5 that the restoring forces will be small, making the symphony make very large excursions.

7.5. RECOMMENDATIONS FOR FURTHER RESEARCH

As mentioned in section 7.2 there might be an effect on the optimal tuning of the Symphony when considering horizontal motion. In fact, energy production seems to decrease. This could be due to the fact that the Symphony moves with the wave, throwing the wave phase experienced by the Symphony a bit off of the expected phase. Therefore, the Symphony is not optimally tuned for the wave phase it experiences. However, the differences are too small to say anything conclusive about this hypothesis. Further research could shed more light on this.

A

SYMPHONY PROPERTIES DEPENDING ON THE FLOATER POSITION

This appendix explains the relation between several properties of the Symphony and the floater position. As far as positions are concerned, they are measured along the centreline of the Symphony, starting at the bottom of the base. Also see figure A.1.

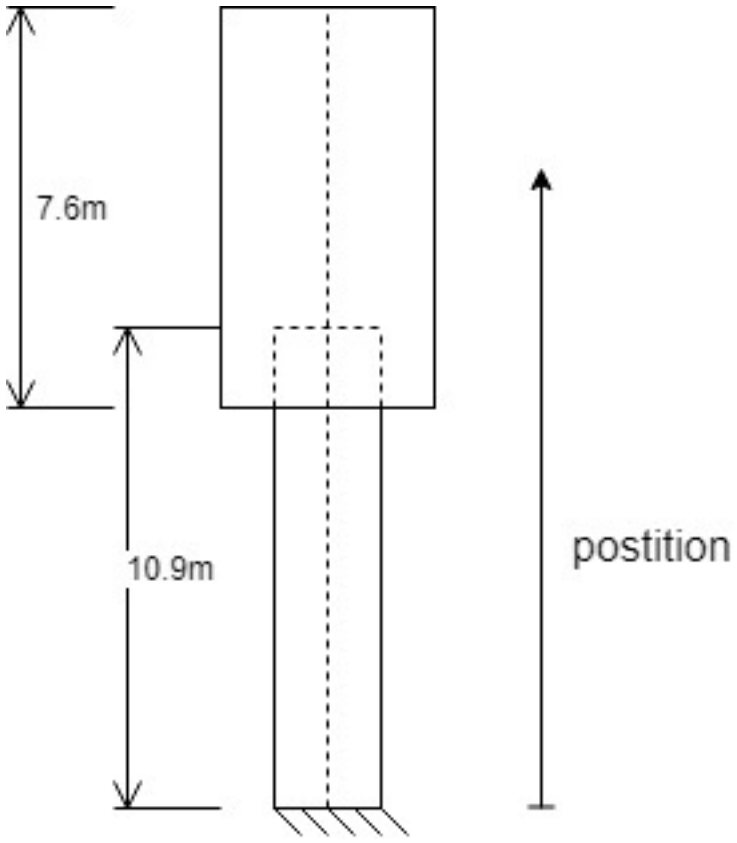

Figure A.1: Measurement of locations

A.1. CENTRE OF MASS

The centre of mass is determined by assuming the floater and base have their centre of mass halfway their length and the centre of mass of the water is at the top of the base. This last assumption is reasonable because the spring tank, which holds most op the water, is situated there.
All moments are calculated and added. This total moment is divided by the total mass, yielding the centre of mass of the total structure. The development of the centre of buoyancy when the floater moves is shown in figure A.2.

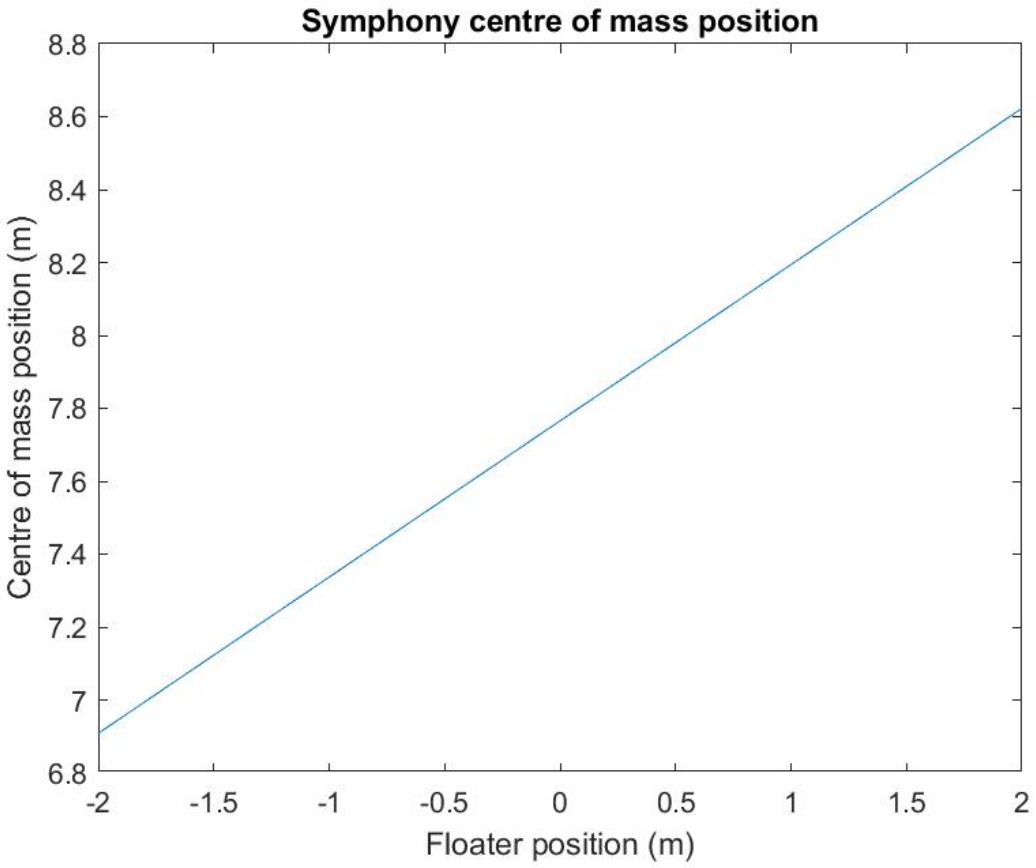

Figure A.2: Development of the centre of mass of the Symphony as a function of z

A.2. BUOYANCY

The buoyancy of the Symphony is found by calculating the volume enclosed by the floater and the volume enclosed by the part of the base that sticks out of the floater. This is determined by subtracting the overlapping length from the total base length and then multiplying by the base cross sectional area. The relation with the floater position is shown in figure A.3.

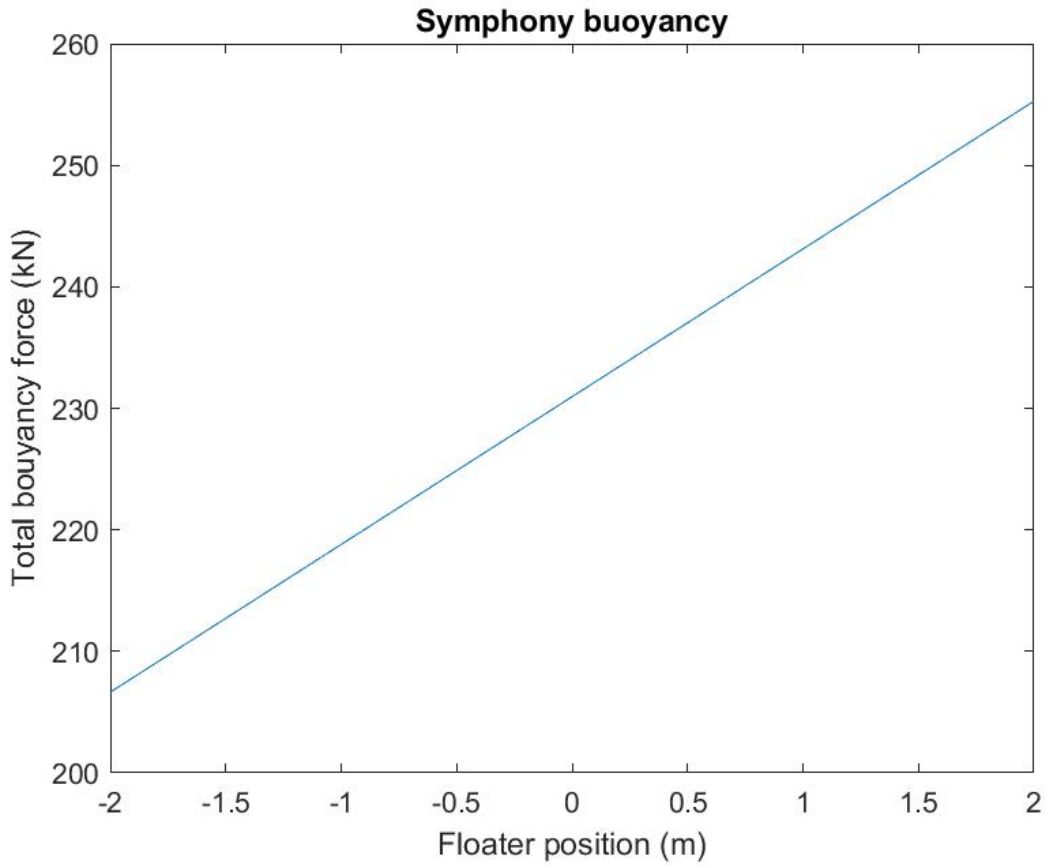

Figure A.3: Development of the buoyancy of the Symphony as a function of z

A.3. NET BUOYANCY

The net buoyancy is calculated by subtracting the total weight of the Symphony from the buoyancy. The dependency on the floater position is depicted in figure A.4.

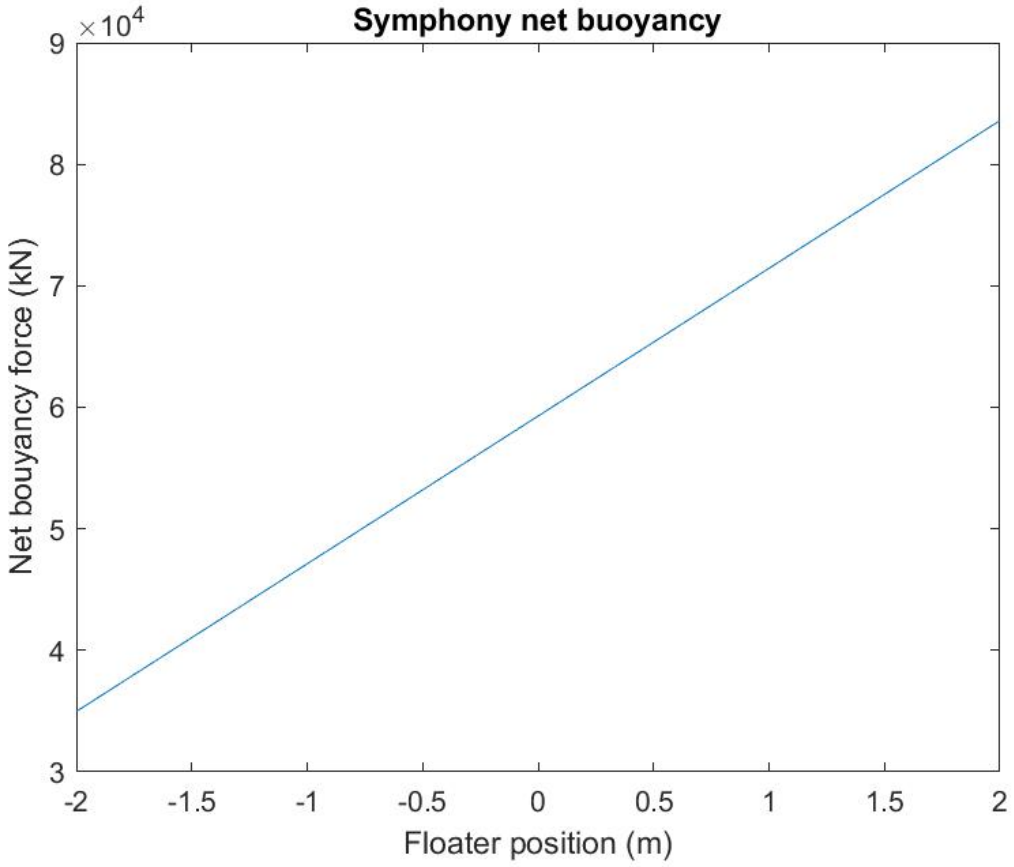

Figure A.4: Development of the net buoyancy of the Symphony as a function of z

A.4. CENTRE OF BUOYANCY

The centre of buoyancy is determined by finding the individual centres of volume of the base and the floater. Then, again, moments are calculated and divided by the total buoyancy, yielding the total centre of buoyancy. The dependance on the floater position is shown in figure A.5.

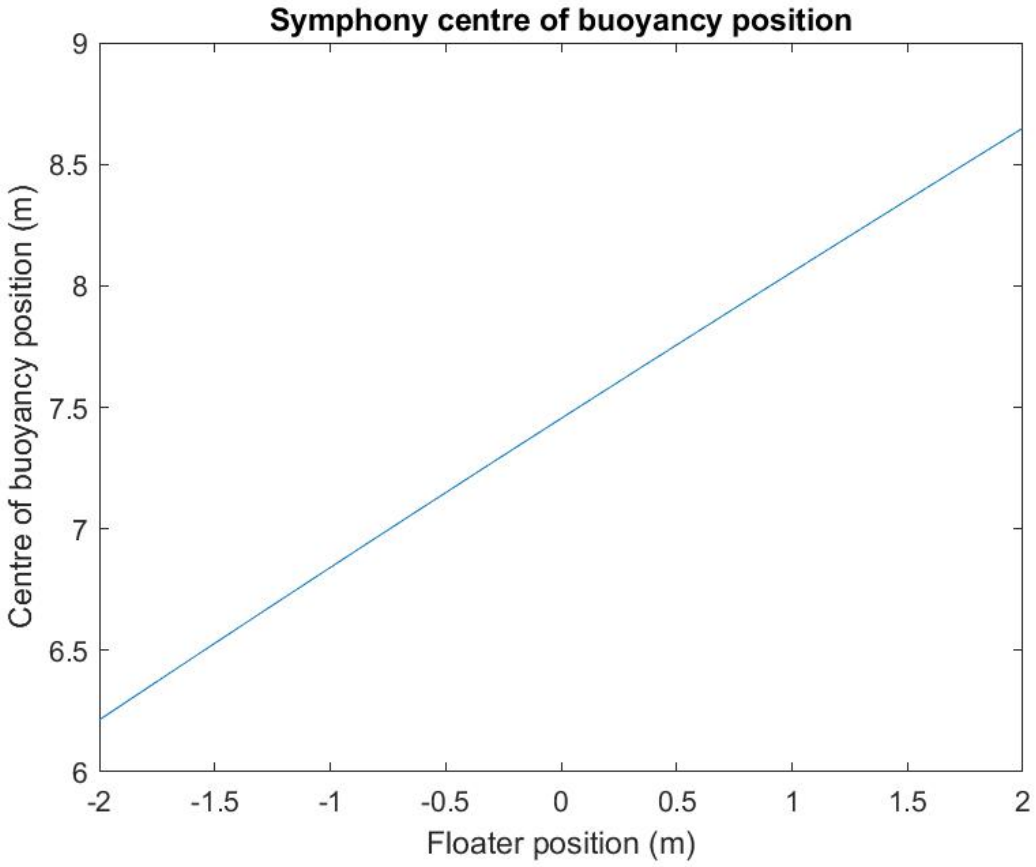

Figure A.5: Development of the centre of buoyancy of the Symphony as a function of z

A.5. SIDE AREA

The side area of the Symphony is found by taking the area of the side view of the floater and adding the length of the part of the base that is sticking out, multiplied by the base diameter. This relation with the floater position is shown in figure A.6

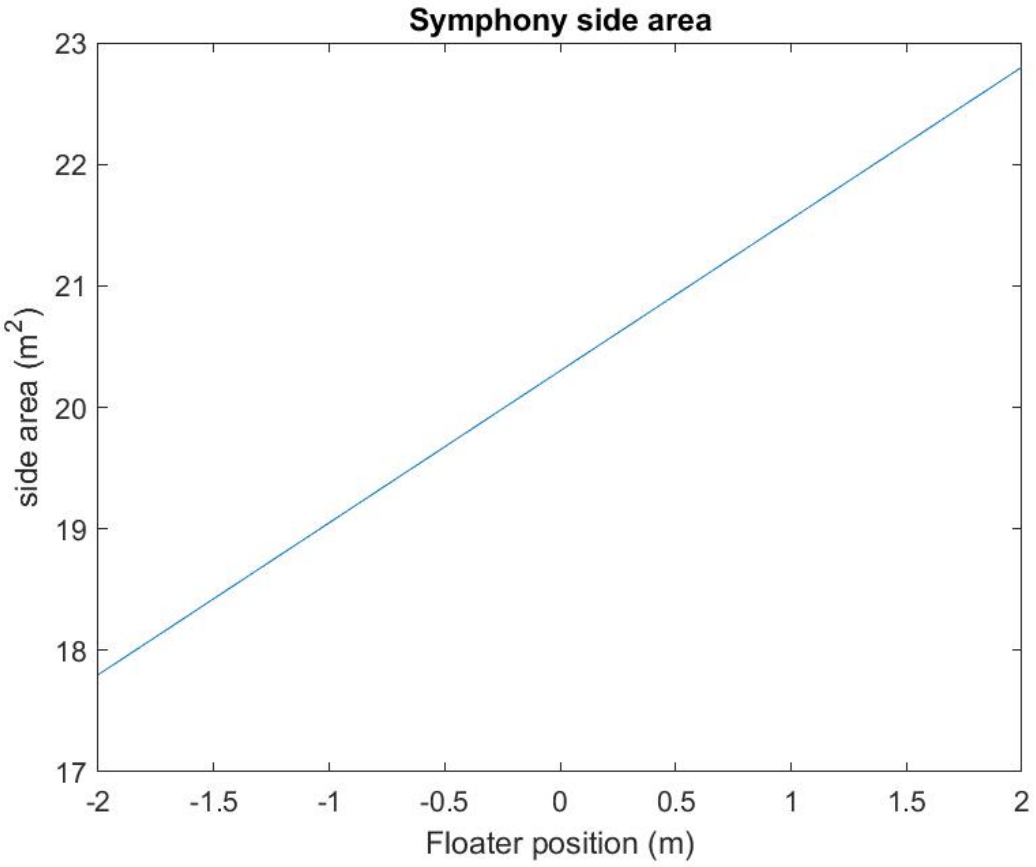

Figure A.6: Development of the side area of the Symphony as a function of z

A.6. CENTRE OF SIDEAREA

The location of the centre of side area (the assumed acting point of the drag force) is found by finding the centres of area of the sideviews of the floater and the part of the base that is sticking out of the floater and again, using a moment and the total side area, the

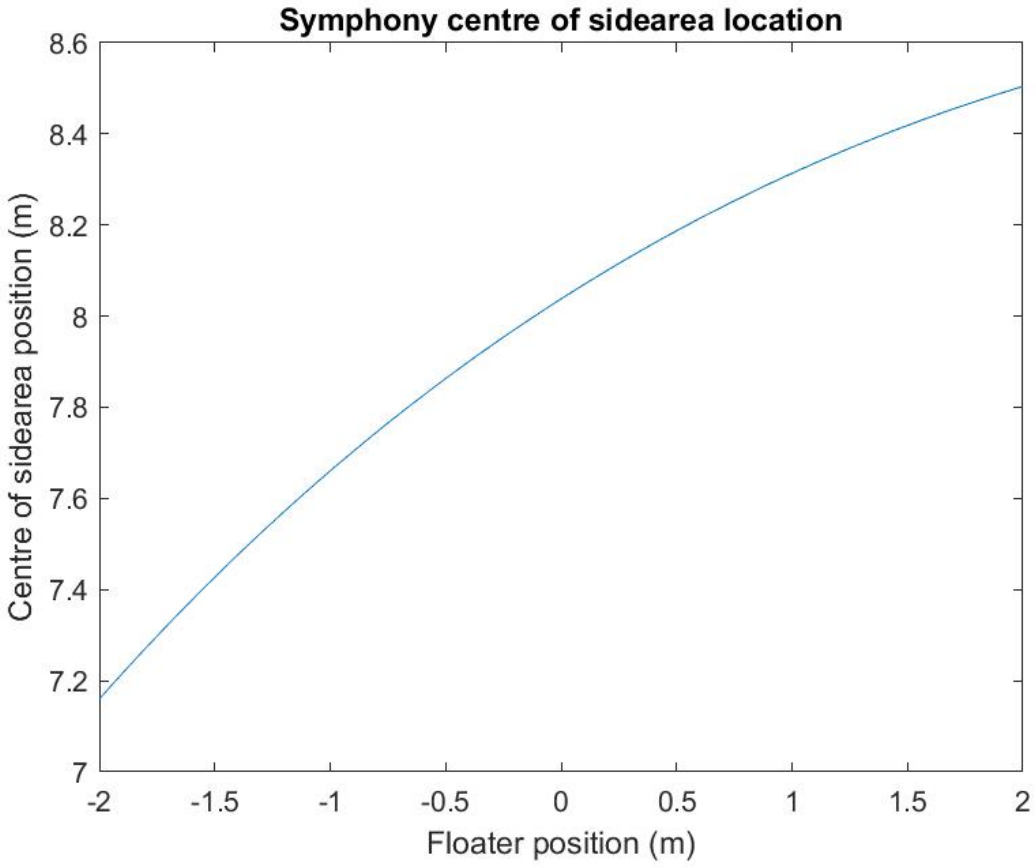

Figure A.7: Development of the centre of the side area of the Symphony as a function of z

A.7. INERTIA

The inertia is calculated by dividing both the Symphony base and floater in 20 equal slice. Each slice is assumed to account for the same amount of mass. The distance between every slice and the centre of mass is calculated. Then the moment of inertia of every slice is calculated by $I = m * r^2$. All individual moments of inertia are added to obtain the total moment of inertia. The development of the moment of inertia when the floater is moved is shown in figure A.8. The contribution of the water to the rotational inertial of the body is neglected.

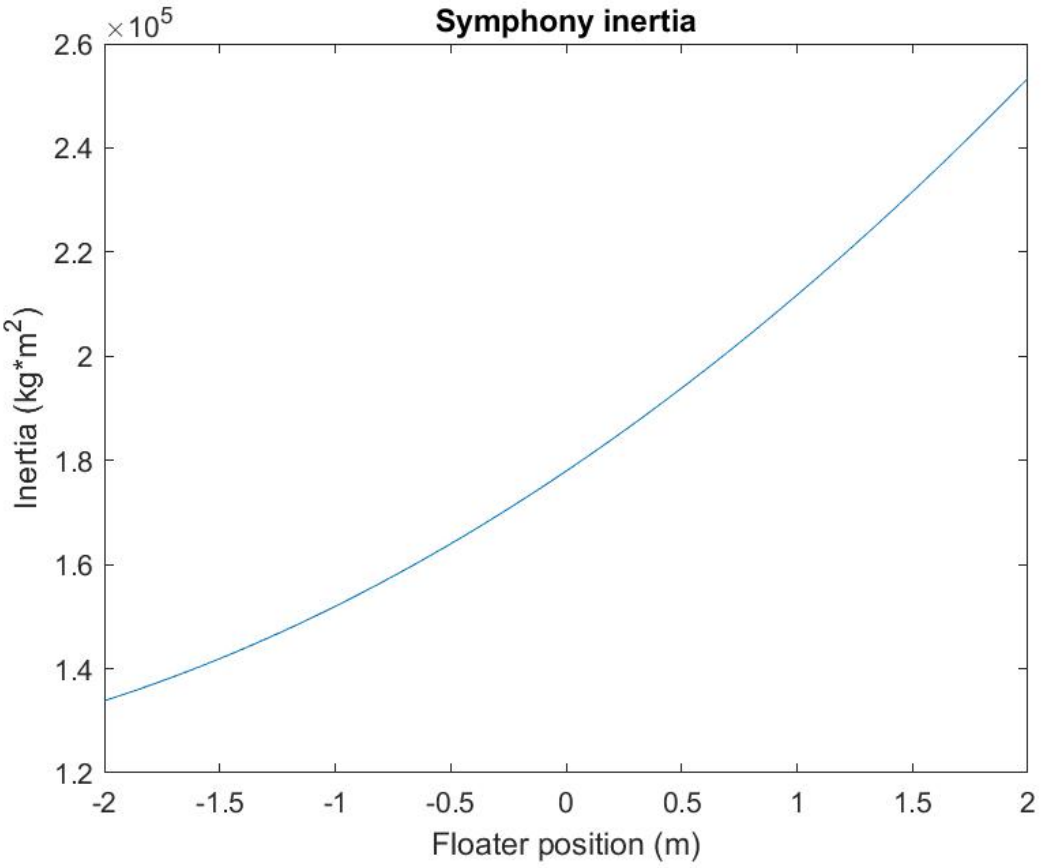

Figure A.8: Development of the inertia of the Symphony as a function of z

B

COMPARISON MOORING LINE AND SYMPHONY ANGLE

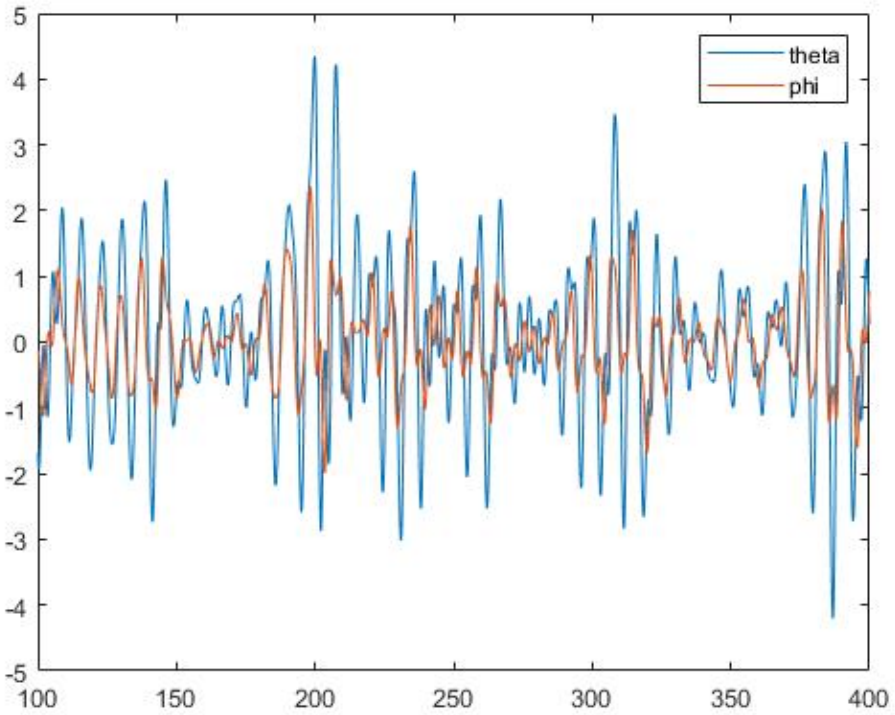

Figure B.1: Time trace of Symphony angle (theta) and mooring line angle (phi) with vertical. Angles in degrees. Den Helder, Hs = 1.5m, Te = 7s.

C

OUTPUTS USED TO DETERMINE MEAN RELATIVE ERROR

Runtime	***200 seconds***		***400 seconds***		***700 seconds***	
Instance	Power (W)	% mean	Power (W)	%of mean	Power (W)	% of mean
1	140	80%	178	88%	205	102%
2	140	80%	227	113%	205	102%
3	172	98%	199	99%	196	97%
4	145	83%	216	108%	226	112%
5	172	98%	179	89%	190	94%
6	280	160%	205	102%	212	105%
7	187	107%	219	109%	198	98%
8	150	86%	177	88%	213	106%
9	233	133%	208	104%	186	92%
10	132	75%	203	101%	185	92%
Mean	175	100%	201	100%	201	100%
MRE		20%		7%		5%
Runtime	***1300 seconds***		***1900 seconds seconds***		***2500 seconds***	
Instance	Power (W)	% mean	Power (W)	%of mean	Power (W)	% of mean
1	196	97%	192	97%	201	101%
2	193	95%	197	100%	202	102%
3	196	97%	201	102%	192	96%
4	214	106%	207	105%	193	97%
5	212	105%	200	101%	199	100%
6	229	113%	190	96%	212	106%
7	196	97%	202	102%	196	98%
8	193	96%	196	99%	203	102%
9	192	95%	191	97%	198	100%
10	197	98%	199	101%	197	99%
Mean	202	100%	197	100%	199	100%
MRE		5%		2%		2%

Table C.1: Outputs for multiple runs using different model runtimes. For MRE definition see section 4.4.2. All runs are done using the Den Helder location and a seastate of Hs = 1.5m, Te = 5.5s, first 100s of output are discarded

Runtime	***200 seconds***		***400 seconds***		***700 seconds***	
Instance	Power (W)	% mean	Power (W)	%of mean	Power (W)	% of mean
1	865	61%	1470	96%	1487	103%
2	2275	159%	1478	97%	1593	110%
3	1154	81%	1654	108%	1415	98%
4	1369	96%	1878	123%	1502	104%
5	1435	101%	1301	85%	1383	96%
6	1265	89%	1587	104%	1499	104%
7	1965	138%	1565	102%	1425	98%
8	1363	95%	1340	88%	1536	106%
9	1454	102%	1409	92%	1273	88%
10	1134	79%	1612	105%	1366	94%
Mean	1428	100%	1529	100%	1448	100%
MRE		20%		8%		5%
Runtime	***1300 seconds***		***1900 seconds***		***2500 seconds***	
Instance	Power (W)	% mean	Power (W)	%of mean	Power (W)	% of mean
1	1319	90%	1423	98%	1404	96%
2	1435	98%	1440	99%	1456	99%
3	1467	100%	1436	99%	1496	102%
4	1551	106%	1400	97%	1396	95%
5	1461	99%	1486	103%	1514	103%
6	1432	97%	1455	100%	1487	102%
7	1519	103%	1495	103%	1457	100%
8	1520	103%	1518	105%	1424	97%
9	1624	111%	1407	97%	1475	101%
10	1365	93%	1426	98%	1530	105%
Mean	1469	100%	1449	100%	1464	100%
MRE		5%		2%		2%

Table C.2: Outputs for multiple runs using different model runtimes. For MRE definition see section 4.4.2. All runs are done using the Leixoes location and a seastate of Hs = 2.25m, Te = 9.0s, first 100s of output are discarded

D

SCATTER DIAGRAM LEIXÕES LOCATION

Te\Hs	=< 0.5m	0.5- 1m	1- 1.5m	1.5- 2m	2- 2.5m	2.5- 3m	3- 3.5m	3.5- 4m	4- 4.5m	4.5- 5m	5-6m	6-7m	7-8m	8-9m	9-10m	10- 12m	P[Te]
=< 4 s																	
4 - 5 s		0,07%	0,03%														0,10%
5 - 6 s		2,41%	4,53%	1,73%	0,23%												8,90%
6 - 7 s		2,21%	10,14%	7,04%	2,57%	0,59%	0,03%										22,58%
7 - 8 s		0,33%	5,80%	7,22%	3,77%	2,01%	0,99%	0,18%	0,01%								20,31%
8 - 9 s		0,01%	2,03%	5,39%	4,28%	2,82%	1,74%	1,05%	0,53%	0,11%							17,96%
9 - 10 s			0,38%	2,29%	3,78%	2,52%	1,77%	1,43%	0,83%	0,60%	0,36%						13,96%
10 - 11 s			0,05%	0,34%	1,77%	1,88%	1,35%	1,12%	0,75%	0,70%	0,83%	0,17%	0,03%				8,99%
11 - 12 s			0,01%	0,12%	0,41%	0,71%	0,52%	0,70%	0,51%	0,55%	0,61%	0,34%	0,07%	0,01%			4,56%
12 - 13 s					0,05%	0,13%	0,23%	0,16%	0,22%	0,29%	0,33%	0,18%	0,13%	0,05%	0,03%		1,80%
13 - 14 s						0,01%	0,05%	0,06%	0,08%	0,10%	0,07%	0,06%	0,05%	0,09%	0,05%	0,01%	0,63%
14 - 15 s									0,01%	0,01%	0,03%	0,05%	0,02%	0,03%		0,01%	0,16%
15 - 16 s															0,01%		0,01%
16 - 17 s															0,01%		0,01%
17 - 18 s																	
P[Hs] (%)		5,03%	22,97%	24,13%	16,86%	10,67%	6,68%	4,70%	2,94%	2,36%	2,23%	0,80%	0,30%	0,18%	0,10%	0,02%	100%

Table D.1: Scatter diagram for the Leixões location [19]

Te\Hs	=< 0.5m	0.5- 1m	1- 1.5m	1.5- 2m	2- 2.5m	2.5- 3m	3- 3.5m	3.5- 4m	4- 4.5m	4.5- 5m	5-6m	6-7m	7-8m	8-9m	9-10m	10- 12m	P[Te]
=< 4 s																	0,0
4 - 5 s		0,07	0,03														0,1
5 - 6 s		2,41	4,53	1,73	0,23												8,9
6 - 7 s		2,21	10,14	7,04	2,57	0,59	0,03										22,6
7 - 8 s		0,33	5,8	7,22	3,77	2,01	0,99	0,18	0,01								20,3
8 - 9 s		0,01	2,03	5,39	4,28	2,82	1,74	1,05	0,53	0,11							18,0
9 - 10 s			0,38	2,29	3,78	2,52	1,77	1,43	0,83	0,6	0,36						14,0
10 - 11 s			0,05	0,34	1,77	1,88	1,35	1,12	0,75	0,7	0,83	0,17	0,03				9,0
11 - 12 s			0,01	0,12	0,41	0,71	0,52	0,7	0,51	0,55	0,61	0,34	0,07	0,01			4,6
12 - 13 s					0,05	0,13	0,23	0,16	0,22	0,29	0,33	0,18	0,13	0,05	0,03		1,8
13 - 14 s						0,01	0,05	0,06	0,08	0,1	0,07	0,06	0,05	0,09	0,05	0,01	0,6
14 - 15 s									0,01	0,01	0,03	0,05	0,02	0,03		0,01	0,2
15 - 16 s															0,01		0,0
16 - 17 s															0,01		0,0
P[Hs] (%)	0,0	5,0	23,0	24,1	16,9	10,7	6,7	4,7	2,9	2,4	2,2	0,8	0,3	0,2	0,1	0,0	100

Table D.2: Clustered scatter diagram for the Leixões location. The alternation blue and red areas give the clusters. The wave height and energy period are estimated based on the middle of every cluster, emphasised by the orange cells.

E

Full outputs Leixões

Te\Hs	0,75	1,25	1,75	2,25	2,75	3,25	3,75	4,25	4,75	5,5	6,5	7,5	8,5	9,5	11
4,5	28	94	185	322	610	1055	1539	2104	2729	3943	5514	7319		10953	
5,5	49	146	382	750	1357	2010	2872	3741	4445	5667	7417	9073			
6,5	67	226	641	1180	1923	2474	3312	4033	4797	6040					
7,5	83	328	863	1455	1995	2608	3262	3833	4501						
8,5	106	432	898	1502	2047	2616	3158	3837							
9,5	145	535	998	1475	2012	2617	3214								
10,5	171	551	1034	1530	2069	2624									
11,5	193	607	1109	1605	2094	2637	3171								
12,5	200	647	1069	1552	2051	2540	2992								
13,5	223	641	1082	1484	2053	2361									
14,5	226	604	1056	1497	1915	2294									
15,5	223	586	998	1428	1828	2289									
16,5	229	585	935	1367	1747										
17,5	227	556	922	1287	1731	2116									

Table E.1: Full power diagram for the Leixões location. Hs in meters, Te in seconds, power in watts. Sea state 9.5m, 4.5s is ignored because it is isolated from the rest of the diagram

Te\Hs	0,75	1,25	1,75	2,25	2,75	3,25	3,75	4,25	4,75	5,5	6,5	7,5	8,5	9,5	11
4,5	160	250	370	486	621	720	1108	1081	1258	1533	2192	2785		3564	
5,5	213	345	502	596	886	1107	1316	1576	1644	2122	3600	3501			
6,5	327	484	697	830	1086	1366	1573	1744	2310	2740					
7,5	373	665	837	1056	1378	1470	1911	2077	2819						
8,5	478	714	918	1061	1467	1633	1840	2387							
9,5	450	790	946	1097	1448	1904	2058								
10,5	421	810	996	1339	1641	1981									
11,5	468	771	977	1361	1553	1942	2261								
12,5	545	817	1122	1327	1681	1911	2319								
13,5	579	948	1123	1358	1808	2112									
14,5	584	1029	1183	1617	1844	1990									
15,5	599	958	1287	1482	2056	2217									
16,5	618	1026	1271	1707	1959										
17,5	731	1092	1328	1712	2200	2151									

Table E.2: Full maximal horizontal reaction force diagram for the Leixões location. Hs in meters, Te in seconds, forces in newton. Sea state 9.5m, 4.5s is ignored because it is isolated from the rest of the diagram

Te\Hs	0,75	1,25	1,75	2,25	2,75	3,25	3,75	4,25	4,75	5,5	6,5	7,5	8,5	9,5	11
4,5	63,75	68,23	73,02	79,18	81,47	81,65	83,34	85,46	85,12	87,48	89,67	95,17		100,36	
5,5	67,21	72,47	79,61	79,83	80,95	81,63	82,98	84,51	85,25	86,79	90,64	91,99			
6,5	70,14	77,96	79,02	79,24	80,02	81,11	80,99	81,85	81,88	84,67					
7,5	72,59	77,85	77,96	78,38	78,49	78,94	79,76	79,78	80,46						
8,5	75,88	77,03	77,40	78,12	78,25	78,89	78,69	79,27							
9,5	76,20	76,74	76,99	77,30	77,54	77,80	78,38								
10,5	75,65	76,06	76,20	76,24	76,46	76,89									
11,5	74,99	75,24	75,45	75,71	75,72	76,06	76,41								
12,5	74,34	74,56	74,86	74,90	75,38	75,91	75,83								
13,5	73,81	74,20	74,29	74,68	75,04	75,18									
14,5	73,36	73,91	74,07	74,49	74,67	74,78									
15,5	72,99	73,53	73,81	74,16	74,44	74,64									
16,5	72,54	73,20	73,79	74,08	74,16										
17,5	72,13	73,34	73,71	74,06	74,26	74,56									

Table E.3: Full maximal vertical reaction force diagram for the Leixões location. Hs in meters, Te in seconds, forces in kilo newton. Sea state 9.5m, 4.5s is ignored because it is isolated from the rest of the diagram

Te\Hs	0,75	1,25	1,75	2,25	2,75	3,25	3,75	4,25	4,75	5,5	6,5	7,5	8,5	9,5	11
4,5	61,41	62,69	67,51	71,05	70,65	77,11	79,04	78,64	79,12	81,83	80,14	80,72		83,92	
5,5	57,42	60,85	67,46	60,31	77,02	69,42	79,61	75,76	78,72	75,27	78,46	78,10			
6,5	62,94	63,27	70,53	72,43	73,97	77,17	73,44	57,18	77,29	71,01					
7,5	64,73	73,88	75,71	67,94	53,42	74,25	67,62	54,66	77,86						
8,5	76,97	72,41	72,41	72,97	58,14	67,47	57,06	60,12							
9,5	74,68	74,92	75,05	72,53	74,32	60,43	71,28								
10,5	75,48	75,52	74,37	62,88	61,88	76,19									
11,5	72,26	71,93	75,40	61,41	73,43	63,36	62,80								
12,5	72,96	73,93	71,91	74,27	73,68	74,48	74,32								
13,5	73,48	73,67	74,13	74,58	73,91	69,12									
14,5	71,79	73,57	73,37	73,45	73,76	69,57									
15,5	71,81	72,08	71,77	72,78	73,61	73,28									
16,5	72,30	71,91	73,25	72,47	72,76										
17,5	70,29	72,14	67,96	72,29	72,85	69,79									

Table E.4: Full maximal worst reaction force diagram for the Leixões location. Hs in meters, Te in seconds, forces in kilo newton. According angles in table E.5. Sea state 9.5m, 4.5s is ignored because it is isolated from the rest of the diagram

Te\Hs	0,75	1,25	1,75	2,25	2,75	3,25	3,75	4,25	4,75	5,5	6,5	7,5	8,5	9,5	11
4,5	0,15	0,24	0,31	0,38	0,52	0,56	0,81	0,79	0,82	1,15	1,70	1,86		2,47	
5,5	0,20	0,33	0,46	0,59	0,75	0,89	0,98	1,46	1,19	1,63	2,23	2,21			
6,5	0,30	0,44	0,52	0,65	0,77	0,92	1,35	1,58	1,94	2,14					
7,5	0,35	0,50	0,59	0,87	1,24	1,11	1,49	2,77	3,07						
8,5	0,40	0,56	0,72	0,84	1,37	1,45	1,78	1,66							
9,5	0,35	0,62	0,75	0,89	0,95	1,57	1,61								
10,5	0,33	0,67	0,82	1,21	1,62	1,54									
11,5	0,38	0,63	0,77	1,22	1,05	1,60	1,84								
12,5	0,46	0,62	0,86	1,13	1,59	1,33	1,47								
13,5	0,51	0,65	0,81	1,03	1,45	1,55									
14,5	0,44	0,90	0,87	1,42	1,27	1,61									
15,5	0,49	0,72	1,12	1,36	1,87	1,91									
16,5	0,51	0,81	1,07	1,49	1,51	0,00									
17,5	0,59	0,85	1,25	1,39	1,71	1,87									

Table E.5: Full maximal worst reaction force diagram for the Leixões location. Hs in meters, Te in seconds, angles in degrees. According forces in table E.4. Sea state 9.5m, 4.5s is ignored because it is isolated from the rest of the diagram

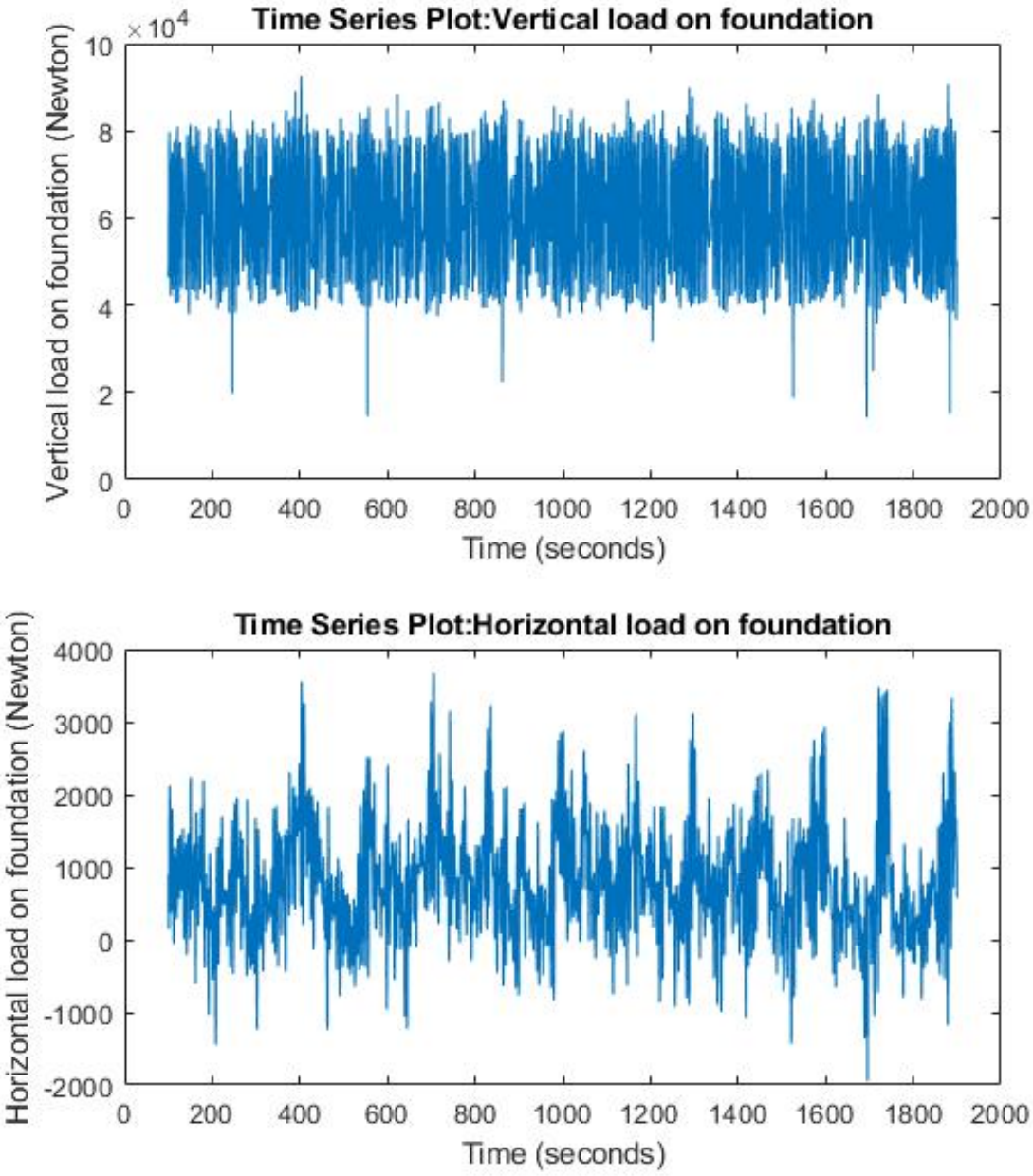

Figure E.1: Horizontal and vertical loads on the foundation for a single wave seed in the Leixões cut out sea state

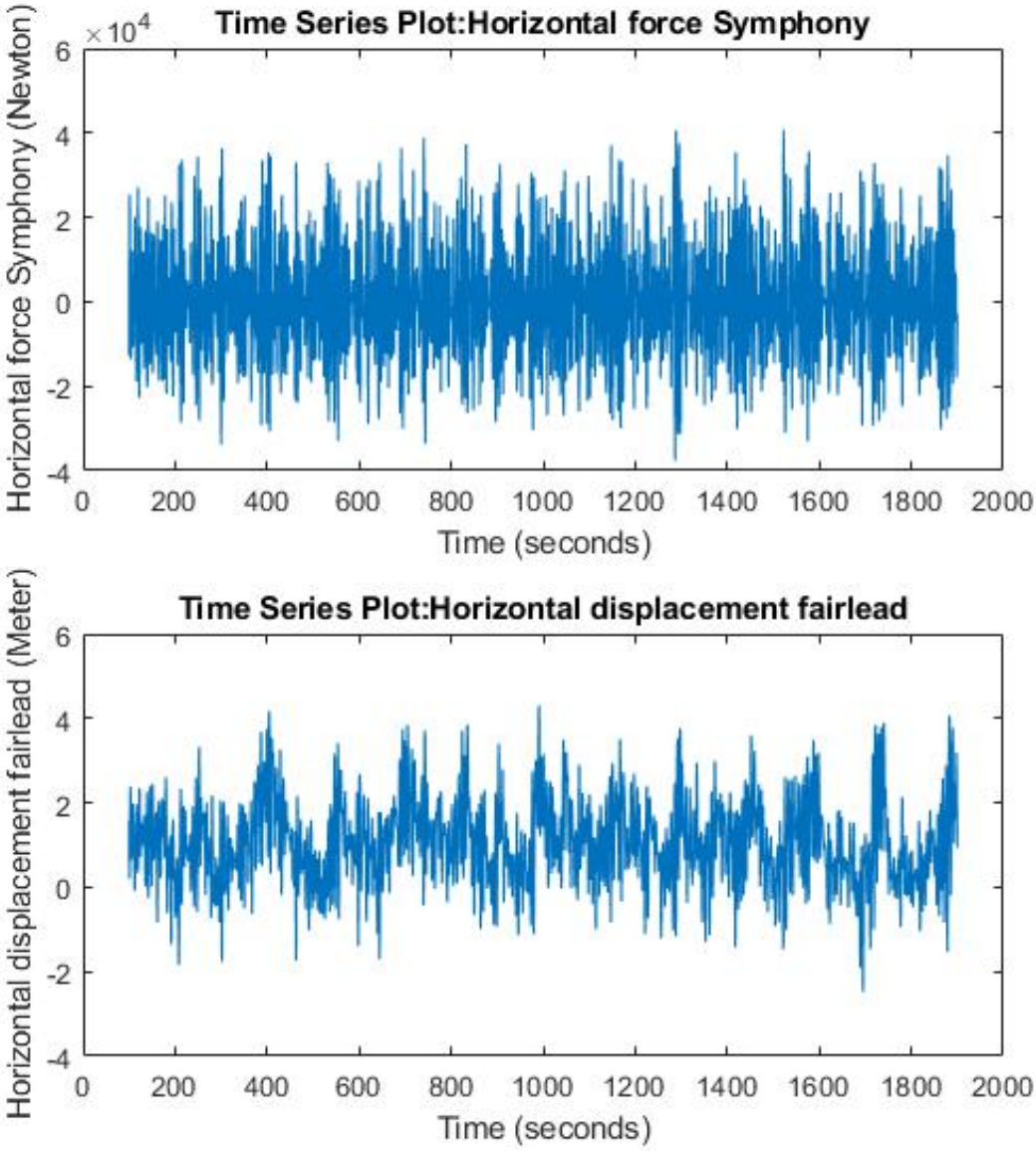

Figure E.2: time traces of the horizontal force acting on the Symphony and the Symphony horizontal motion for a single wave seed in the Leixões cut out sea state

F

FULL OUTPUTS DEN HELDER

.

Te\Hs	0,5	0,75	1	1,25	1,5	1,75	2	2,25	2,5	2,75
1,5	0	0	0	0	0	0	0	0	0	0
1,75	0	0	0	0	0	0	0	0	0	0
2	0	0	0	0	0	0	0	0	0	0
2,25	0	0	0	0	0	0	0	0	1	1
2,5	0	0	0	0	1	1	3	5	8	12
2,75	0	0	1	2	5	9	14	20	27	35
3	0	1	3	8	15	23	33	44	56	69
3,25	0	3	9	18	29	42	57	73	91	109
3,5	1	6	16	30	45	64	83	108	133	158
3,75	2	11	25	44	64	88	114	141	174	208
4	4	17	35	58	83	111	143	178	218	258
4,25	6	23	45	72	101	136	175	215	263	311
4,5	9	28	55	86	122	162	206	257	327	435
4,75	12	35	65	99	140	184	240	300	451	648
5	14	41	74	114	159	208	291	407	577	912
5,25	16	47	85	129	177	237	383	522	897	1361
5,5	19	52	93	140	196	320	476	954	1387	1857
5,75	22	58	102	157	215	384	708	1192	1607	2072
6	25	64	109	178	271	515	941	1343	1871	2193

Table F.1: Full power diagram for the Den Helder location. Hs in meters, Te in seconds, power in watts. Sea state 9.5m, 4.5s is ignored because it is isolated from the rest of the diagram

Te\Hs	0,5	0,75	1	1,25	1,5	1,75	2	2,25	2,5	2,75
1,5	1	1	2	2	3	3	3	3	4	4
1,75	5	7	11	12	16	18	18	21	23	28
2	84	108	136	153	172	190	161	68	73	84
2,25	61	164	216	260	298	345	391	421	460	506
2,5	218	296	385	432	535	587	624	683	767	794
2,75	280	399	490	610	684	779	856	957	1038	1097
3	352	513	628	752	894	977	1054	1150	1301	1387
3,25	380	537	674	783	940	1044	1164	1289	1341	1510
3,5	390	534	664	781	912	1109	1142	1253	1323	1411
3,75	306	434	584	704	771	874	1025	1163	1327	1358
4	313	428	529	638	741	931	980	1063	1266	1351
4,25	274	365	508	613	751	788	1059	1219	1235	1474
4,5	322	399	497	592	725	925	1013	1261	1471	2008
4,75	318	393	559	737	821	1022	1207	1378	1670	1861
5	301	483	685	837	1196	1327	1598	1709	1829	2010
5,25	343	585	711	1039	1451	1645	1829	1938	2262	2391
5,5	403	685	1012	1319	1686	1793	2029	2221	2368	2444
5,75	483	881	1207	1637	1758	1927	2246	2385	2643	2895
6	554	856	1387	1621	1803	2052	2313	2747	3080	3619

Table F.2: Full maximal horizontal reaction force diagram for the Den Helder location. Hs in meters, Te in seconds, forces in newton. Sea state 9.5m, 4.5s is ignored because it is isolated from the rest of the diagram

Te\Hs	0,75	1,25	1,75	2,25	2,75	3,25	3,75	4,25	4,75	5,5	6,5	7,5	8,5	9,5	11
4,5	63,75	68,23	73,02	79,18	81,47	81,65	83,34	85,46	85,12	87,48	89,67	95,17		100,36	
5,5	67,21	72,47	79,61	79,83	80,95	81,63	82,98	84,51	85,25	86,79	90,64	91,99			
6,5	70,14	77,96	79,02	79,24	80,02	81,11	80,99	81,85	81,88	84,67					
7,5	72,59	77,85	77,96	78,38	78,49	78,94	79,76	79,78	80,46						
8,5	75,88	77,03	77,40	78,12	78,25	78,89	78,69	79,27							
9,5	76,20	76,74	76,99	77,30	77,54	77,80	78,38								
10,5	75,65	76,06	76,20	76,24	76,46	76,89									
11,5	74,99	75,24	75,45	75,71	75,72	76,06	76,41								
12,5	74,34	74,56	74,86	74,90	75,38	75,91	75,83								
13,5	73,81	74,20	74,29	74,68	75,04	75,18									
14,5	73,36	73,91	74,07	74,49	74,67	74,78									
15,5	72,99	73,53	73,81	74,16	74,44	74,64									
16,5	72,54	73,20	73,79	74,08	74,16										
17,5	72,13	73,34	73,71	74,06	74,26	74,56									

Table F.3: Full maximal vertical reaction force diagram for the Den Helder location. Hs in meters, Te in seconds, forces in kilo newton. Sea state 9.5m, 4.5s is ignored because it is isolated from the rest of the diagram

Te\Hs	0,5	0,75	1	1,25	1,5	1,75	2	2,25	2,5	2,75
1,5	59,5	59,5	59,0	59,0	59,5	59,5	59,5	59,5	59,5	59,5
1,75	59,5	59,0	59,5	59,5	59,5	59,5	59,5	59,5	59,5	59,6
2	59,5	59,6	59,5	59,5	59,5	59,5	63,7	63,6	63,6	63,6
2,25	64,7	59,5	59,4	59,4	59,4	59,3	59,3	59,3	59,5	59,4
2,5	59,4	59,4	59,4	59,2	59,2	59,1	59,1	59,1	59,0	58,8
2,75	59,4	59,3	59,2	58,9	58,8	58,5	57,9	59,1	58,3	58,0
3	59,4	59,0	58,8	58,5	58,5	58,1	58,3	57,6	57,1	58,1
3,25	59,2	59,0	58,8	58,4	58,4	58,2	56,7	61,5	59,9	59,7
3,5	59,0	59,0	59,5	58,5	60,3	60,6	59,9	60,0	64,7	60,1
3,75	59,3	59,7	59,1	60,4	62,1	60,3	59,0	61,4	67,8	62,5
4	59,3	59,4	60,4	60,2	61,7	63,1	61,7	63,1	71,6	64,9
4,25	59,5	61,3	60,7	61,7	60,9	63,3	65,4	65,3	70,8	74,8
4,5	59,2	60,4	60,4	60,6	59,3	58,2	60,2	73,5	76,2	76,9
4,75	59,1	60,6	58,4	59,3	58,3	59,0	71,1	75,2	77,2	77,7
5	59,4	57,8	57,7	57,6	60,3	61,1	57,5	76,3	61,5	77,8
5,25	58,6	59,0	59,5	61,5	61,0	61,8	62,1	62,4	76,1	76,3
5,5	58,2	59,2	59,4	61,8	61,8	60,3	62,5	62,6	59,0	75,6
5,75	58,6	62,0	63,1	61,4	63,4	59,2	55,9	53,6	76,5	70,2
6	58,3	60,1	66,0	62,7	63,1	75,3	55,7	59,3	55,1	51,9

Table F.4: Full maximal worst reaction force diagram for the Den Helder location. Hs in meters, Te in seconds, forces in kilo newton. According angles in table F.5. Sea state 9.5m, 4.5s is ignored because it is isolated from the rest of the diagram

Te\Hs	0,5	0,75	1	1,25	1,5	1,75	2	2,25	2,5	2,75
1,5	0,00	0,00	0,00	0,00	0,00	0,00	0,00	0,00	0,00	0,00
1,75	0,00	-0,01	0,01	-0,01	-0,02	-0,02	0,02	0,02	-0,02	0,02
2	-0,08	0,10	0,13	-0,14	-0,16	-0,19	0,06	-0,06	0,06	-0,06
2,25	-0,03	-0,16	-0,22	-0,25	-0,29	-0,33	-0,37	-0,41	-0,44	-0,48
2,5	-0,21	-0,28	-0,39	-0,40	-0,52	-0,55	-0,59	-0,69	-0,72	-0,74
2,75	-0,27	-0,39	-0,48	-0,58	-0,68	-0,77	-0,86	-0,84	-1,01	-1,10
3	-0,33	-0,50	-0,62	-0,74	-0,85	-0,97	-1,09	-1,10	-1,35	-1,29
3,25	-0,37	-0,51	-0,63	-0,78	-0,93	-1,05	-1,26	-1,27	-1,29	-1,50
3,5	-0,37	-0,54	-0,64	-0,74	-0,82	-1,02	-1,10	-1,12	-1,23	-1,37
3,75	-0,30	-0,42	-0,61	-0,64	-0,74	-0,79	-1,00	-1,06	1,10	-1,20
4	-0,31	-0,44	-0,48	-0,58	0,72	0,85	-0,83	0,96	1,06	1,22
4,25	-0,24	-0,34	-0,45	-0,57	0,69	-0,74	-0,86	1,06	1,03	1,19
4,5	-0,35	-0,38	-0,46	0,55	0,67	-0,89	1,04	1,12	1,02	1,71
4,75	0,31	-0,36	0,55	-0,63	0,91	1,00	1,15	1,11	1,25	1,36
5	-0,27	0,47	0,69	0,90	1,08	1,06	1,63	1,49	1,58	1,54
5,25	0,35	0,49	0,61	1,08	1,44	1,64	1,78	1,76	1,76	1,74
5,5	0,36	0,70	0,98	1,12	1,37	1,55	2,03	1,89	2,30	1,84
5,75	0,52	0,88	1,03	1,49	1,51	1,98	2,37	2,56	2,10	-2,21
6	0,58	0,73	1,28	1,56	1,54	-1,60	2,36	2,60	3,50	3,71

Table F.5: Full maximal worst reaction force diagram for the Den Helder location. Hs in meters, Te in seconds, angles in degrees. According forces in table F.4. Sea state 9.5m, 4.5s is ignored because it is isolated from the rest of the diagram

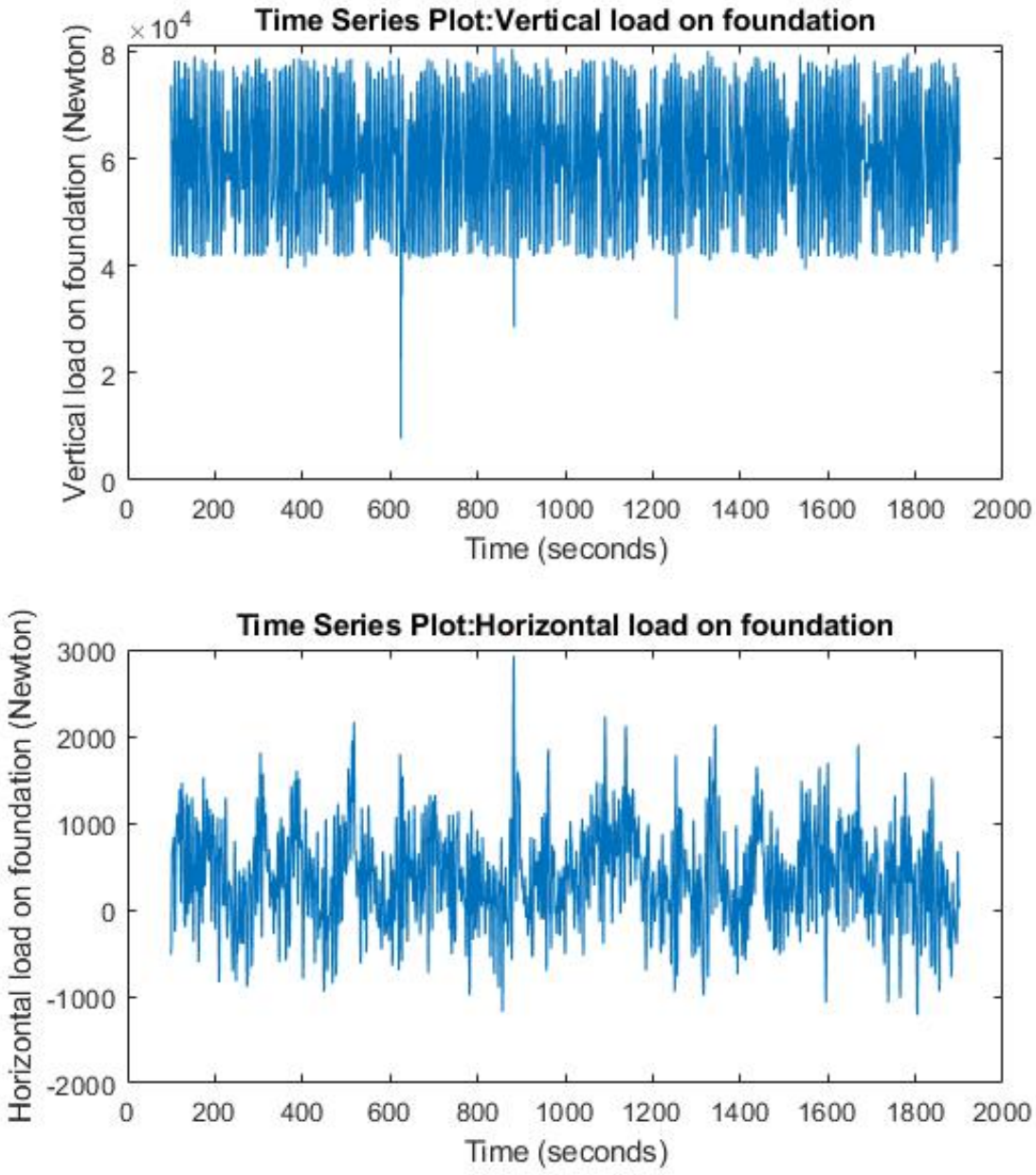

Figure F.1: Horizontal and vertical loads on the foundation for a single wave seed in the Den Helder cut out sea state

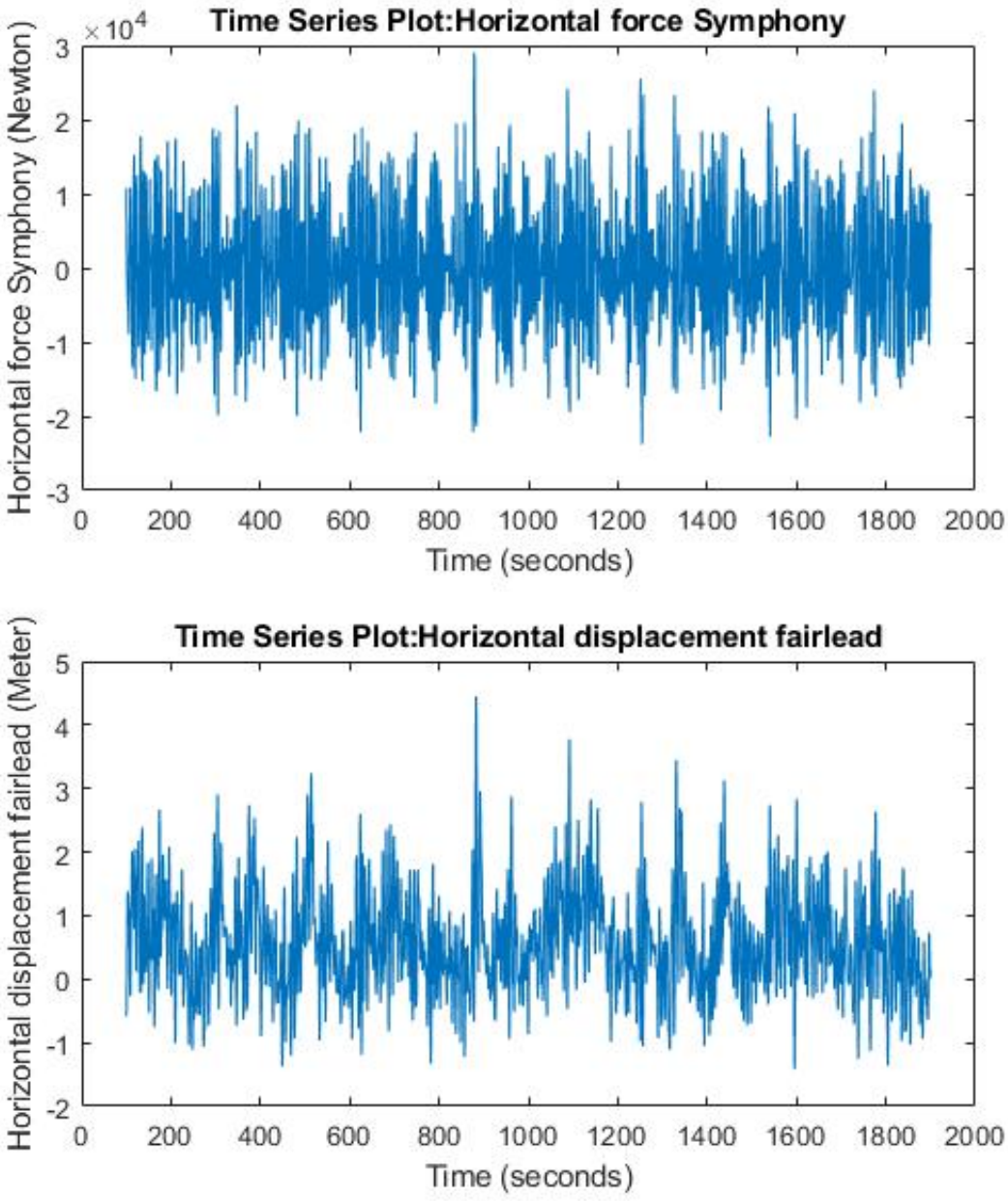

Figure F.2: time traces of the horizontal force acting on the Symphony and the Symphony horizontal motion for a single wave seed in the Den Helder cut out sea state

G

EXTRA OUTPUTS DEN HELDER

.

Te\Hs	3,25	3,5	3,75	4	4,25	4,5	4,75
7	3312	3762	4191	4677	5097	5454	5946
7,25	3270	3673	4161	4489	4925	5435	5876
7,5	3183	3671	3967	4519	4861	5315	0
7,75	3250	3583	4029	4296	4669	5208	0
8	3141	3477	3951	4356	4611	5071	0
8,25	3101	3532	3895	4239	0	0	0
8,5	3145	3529	3889	4045	0	0	0

Table G.1: Extra power diagram for the Den Helder location. Hs in meters, Te in seconds, power in watts. Sea state 9.5m, 4.5s is ignored because it is isolated from the rest of the diagram

Te\Hs	3,25	3,5	3,75	4	4,25	4,5	4,75
7	5425	5453	6160	6263	8795	6415	9252
7,25	5171	5614	7039	6732	7523	7117	9513
7,5	5357	6572	6699	6763	7437	9139	0
7,75	5510	6474	6721	7689	7171	9151	0
8	6039	6273	6378	6602	8452	7848	0
8,25	5399	6428	6069	7801	0	0	0
8,5	5928	6525	7770	8343	0	0	0

Table G.2: Extra maximal horizontal reaction force diagram for the Den Helder location. Hs in meters, Te in seconds, forces in newton. Sea state 9.5m, 4.5s is ignored because it is isolated from the rest of the diagram

Te\Hs	3,25	3,5	3,75	4	4,25	4,5	4,75
7	80,92	80,62	80,99	81,17	85,72	81,45	92,50
7,25	79,46	79,46	80,31	80,90	82,08	82,38	82,57
7,5	79,02	79,60	79,97	80,51	80,83	83,98	0
7,75	78,55	78,97	80,02	79,94	80,45	81,30	0
8	78,36	78,86	79,38	80,15	80,23	80,63	0
8,25	77,79	78,54	78,23	78,82	0	0	0
8,5	77,90	78,41	78,33	80,24	0	0	0

Table G.3: Extra maximal vertical reaction force diagram for the Den Helder location. Hs in meters, Te in seconds, forces in kilo newton. Sea state 9.5m, 4.5s is ignored because it is isolated from the rest of the diagram

H

HORIZONTAL MOTION PLOTS LEIXÕES

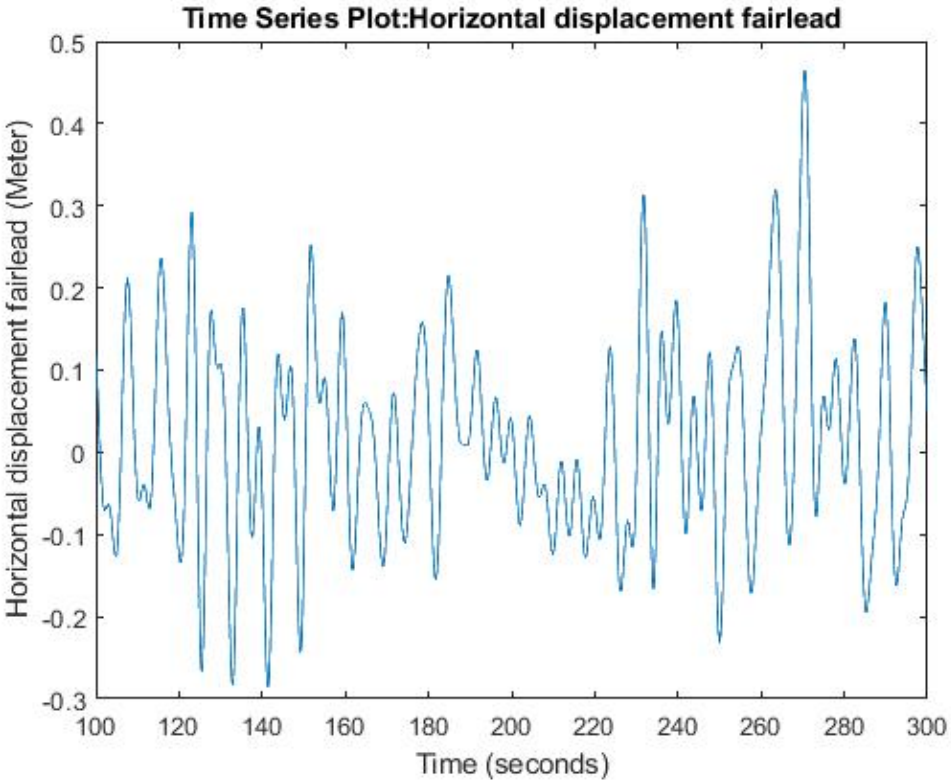

Figure H.1: time trace for the horizontal fairlead motion for Leixões, Hs = 1.0m, Te = 6.0s

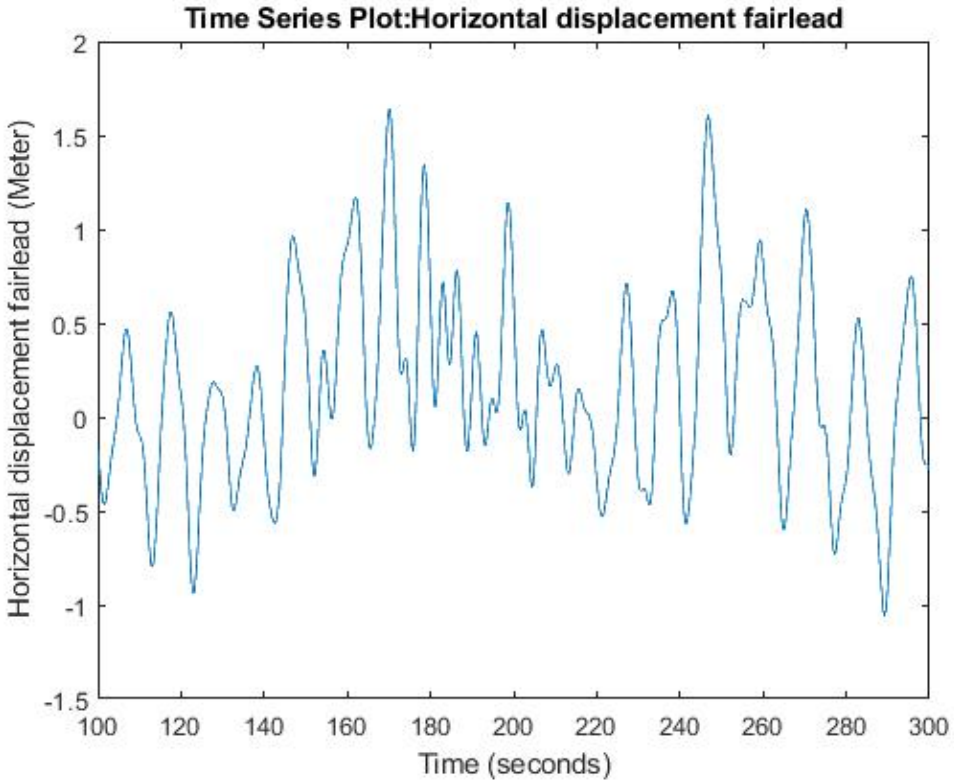

Figure H.2: time trace for the horizontal fairlead motion for Leixões, Hs = 2.25m, Te = 9.0s

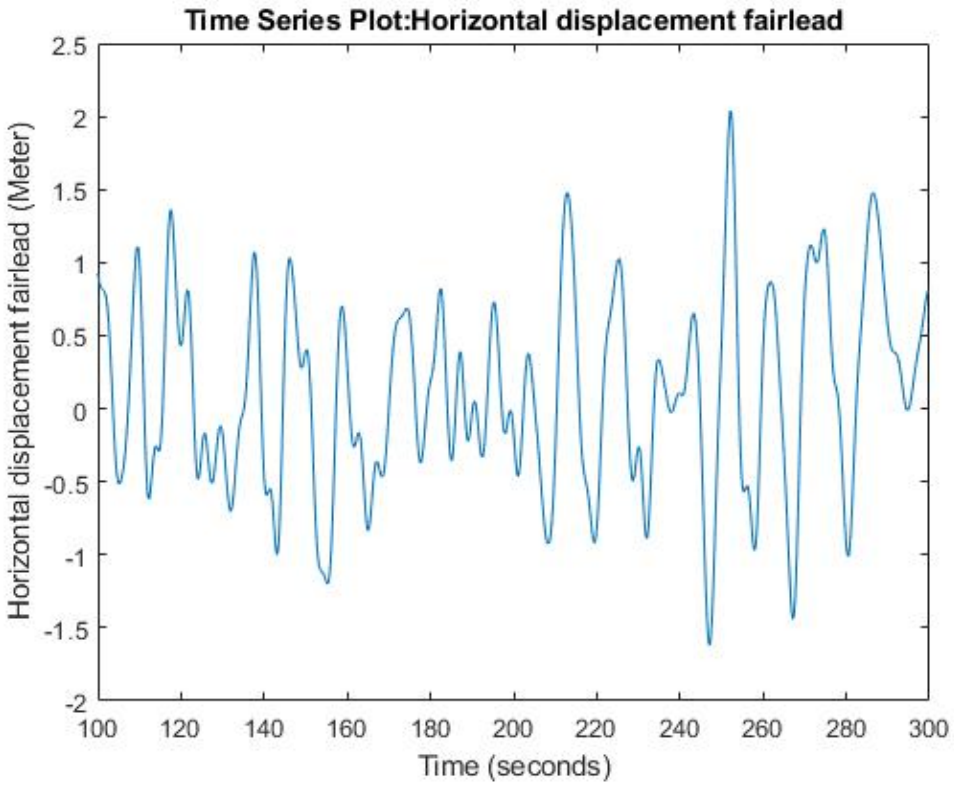

Figure H.3: time trace for the horizontal fairlead motion for Leixões, Hs = 3.5m, Te = 10.0s

I

HORIZONTAL MOTION PLOTS DEN HELDER

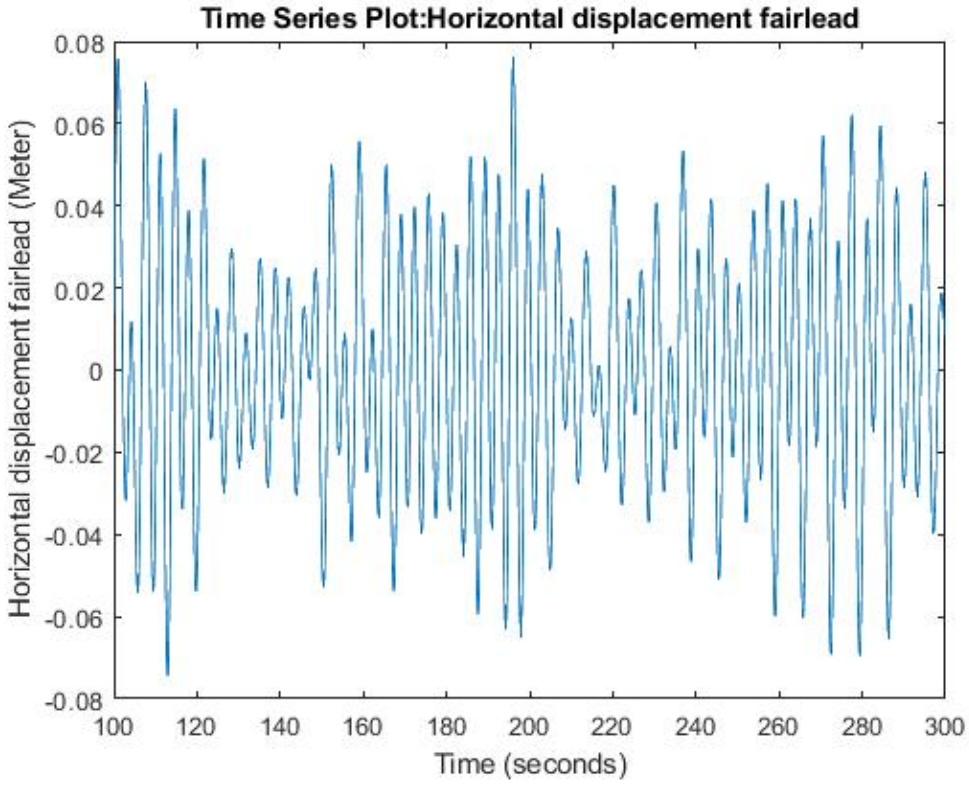

Figure I.1: time trace for the horizontal fairlead motion for Den Helder, Hs = 0.5m, Te = 4.72s

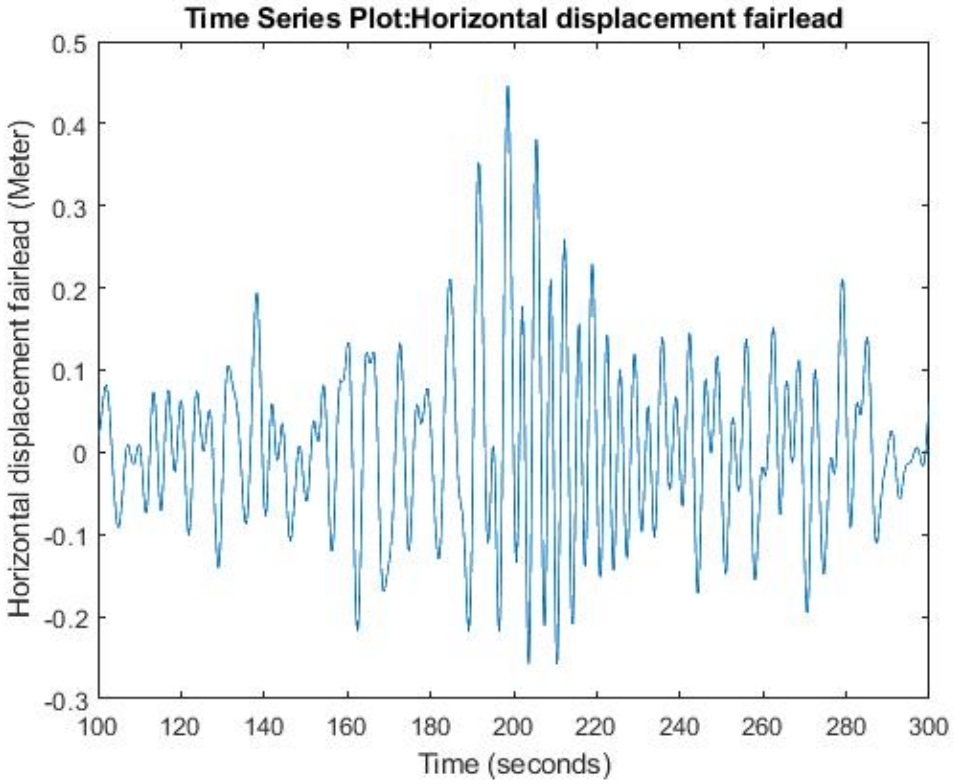

Figure I.2: time trace for the horizontal fairlead motion for Den Helder, Hs = 1.5m, Te = 5.58s

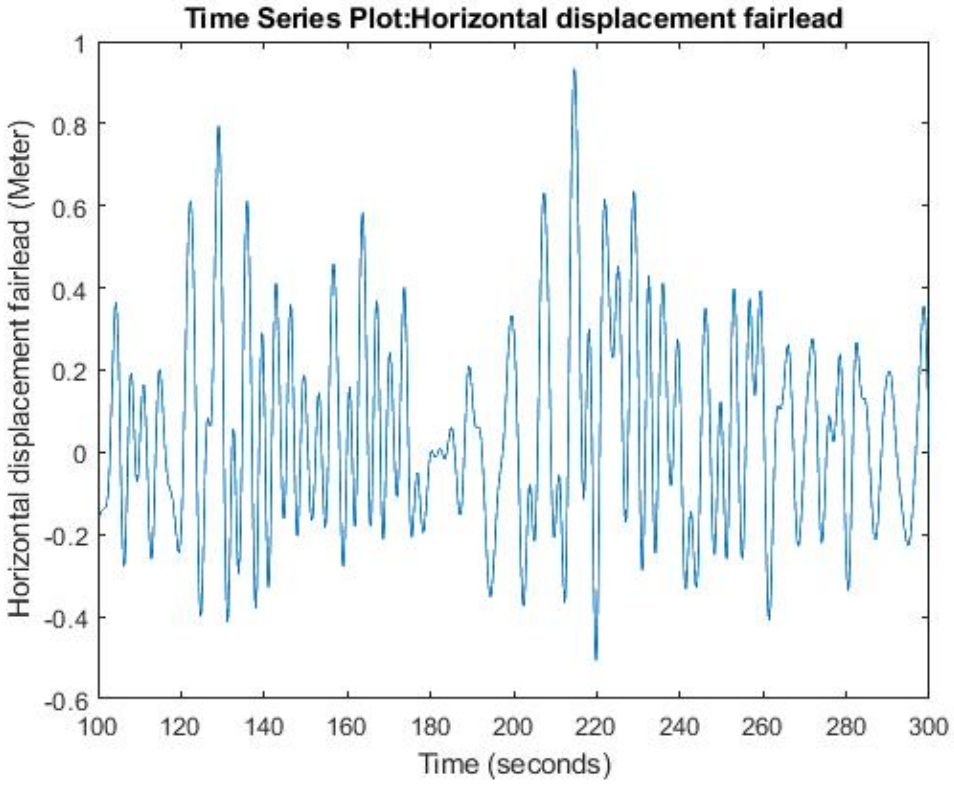

Figure I.3: time trace for the horizontal fairlead motion for Den Helder, Hs = 2.5m, Te = 6.44s

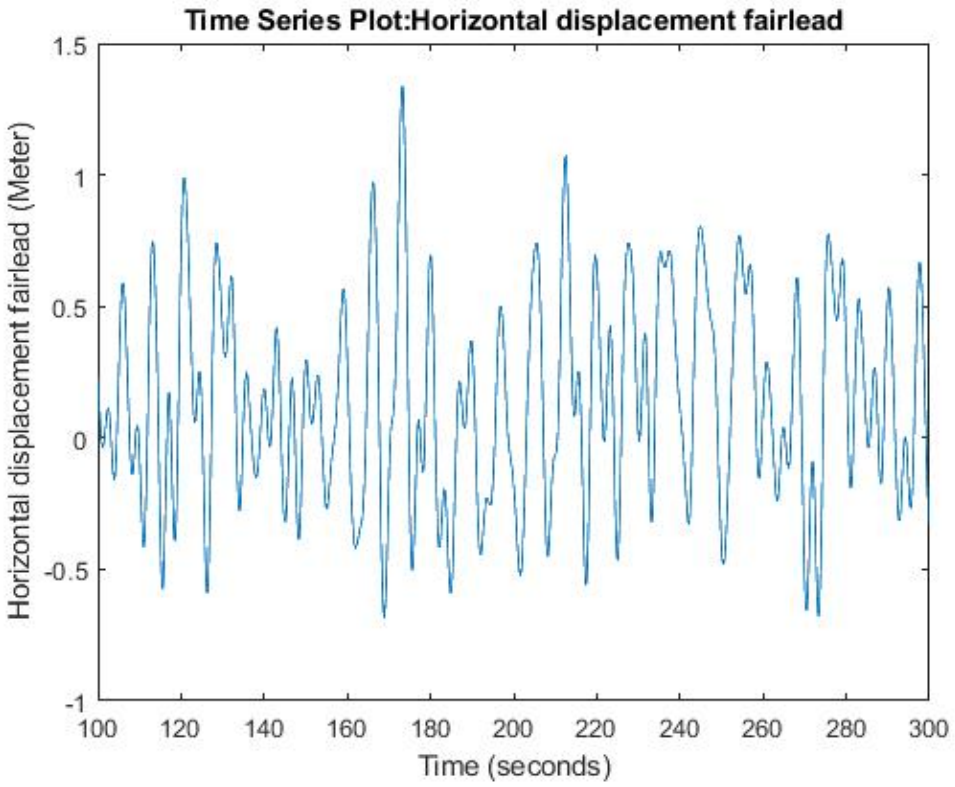

Figure I.4: time trace for the horizontal fairlead motion for Den Helder, Hs = 3.5m, Te = 7.29s

BIBLIOGRAPHY

[1] G. Bruschi, T. Niskioka, K. Tsang, and R. Wang, *Drag coefficient of a cylinder,* (2003).

[2] G. H. Keulegan and L. H. Carpenter, *Forces on cylinders and plates in an oscillating fluid,* Journal of Research of the National Bureau of Standards **60**, 423 (1958).

[3] *BP statistical review of world energy 2018,* https://www.bp.com/en/global/corporate/energy-economics/statistical-review-of-world-energy.html (2018).

[4] *Global Warming of 1.5°C. An IPCC Special Report on the impacts of global warming of 1.5°C above pre-industrial levels and related global greenhouse gas emission pathways, in the context of strengthening the global response to the threat of climate change, sustainable development, and efforts to eradicate poverty* (Interngovernmental Panel on Climate Change, 2018).

[5] E. T. Shahriar Shafiee, *When will fossil fuel reserves be diminished?* Energy Policy **37**, 181 (2009).

[6] F. Parra, *Oil Politics: A Modern History of Petroleum* (WI.B. Tauris, 2009).

[7] *Transitie naar Duurzaam*, Ministerie van Economische zaken (2016).

[8] J. Falnes, *A review of wave-energy extraction,* Marine Structures **20**, 16 (2007).

[9] F. De O. Falcão, *Wave energy utilization : A review of the technologies,* Renewable and Sustainable Energy Reviews **14**, 899 (2010).

[10] P. Girard, *Brevet d'invitation de quinze ans pour diver moyens démployer les vagues de la mer comme mouteurs,* (1799).

[11] A. Pecher and J. P. Kofoed, *Handbook of Ocean Wave Energy* (Springer, 2017).

[12] J. van der Jagt, *A methodology for assessing power performance of Wave Energy Converters, applied to a quasi-rigid submerged pressure differential device,* Master's thesis, Delft University of Technology (2018).

[13] N. Y. Sergiienko, B. S. Cazzolato, B. Ding, P. Hardy, and M. Arjomandi, *Performance comparison of the floating and fully submerged quasi-point absorber wave energy converters,* Renewable Energy **108**, 425 (2017).

[14] Images courtesy of Teamwork Technology BV.

[15] L. Johanning, R. E. Harris, and J. Wolfram, *Mooring systems for wave energy converters: A review of design issues and choices,* 3rd International Conference on Marine Renewable Energy , 899 (2004).

[16] T. Aderinto and H. Li, *Ocean Wave Energy Converters: Status and Challenges,* Energies **11**, 1250 (2018).

[17] N. Y. Sergiienko, B. S. Cazzolato, B. Ding, and M. Arjomandi, *An optimal arrangement of mooring lines for the three-tether submerged point-absorbing wave energy converter,* Renewable Energy **93**, 27 (2016).

[18] M. Jaya Muliawan, Z. Gao, T. Moan, and A. Babarit, *Analysis of a Two-Body Floating Wave Energy Converter With Particular Focus on the Effects of Power Take-Off and Mooring Systems on Energy Capture,* Journal of Offshore Mechanics and Arctic Engineering **135**, 31902 (2013).

[19] N. Leijtens, *Optimal buffer design for the Symphony Wave Power System*, Master's thesis, University of Twente (2016).

[20] L. Holthuijsen, *Waves in oceanic and coastal waters* (Cambridge University Press, 2007).

[21] A. Combourieu, *Preliminary motion analysis of the symphony device*, Tech. Rep. 2 (InnoSea, 2016).

[22] Hasselman et. al., *Measurements of wind-wave growth and swell decay during the joint north sea wave project (jonswap),* Ergnzungsheft zur Deutschen Hydrographischen Zeitschrift Reihe **12** (1973).

[23] Image courtesy of George Lavidas.

[24] C. Beels, J. C. C. Henriques, J. D. Rouck, M. T. Pontes, G. D. Backer, and H. Verhaeghe, *Wave energy resource in the North Sea,* (2009).

[25] G. Lavidas and H. Polinder, *A 38 year north sea wave database (nswd): The need of reliable data for metocean and wave energy assessments,* Energies (2019), under review.

[26] A. M. Davies and G. K. Furnes, *Observed and computed m2 tidal currents in the north sea,* Journal of Physical Oceanography **10**, 237 (1980), https://doi.org/10.1175/1520-0485(1980)010<0237:OACMTC>2.0.CO;2 .

[27] C. Gautier and S. Caires, *Operational wave forecasts in the southern north sea,* E-proceedings of the 36th IAHR World Congress (2016).

[28] A. Kooiman, *Adjustment of the gas spring in the Symphony Wave Power Device*, Master's thesis, University of Twente (2016).

[29] J. R. Morison, M. P. O'Brien, J. W. Johnson, and S. A. Schaaf, *The forces exerted by surface waves on piles,* Petroleum Trans **189**, 149 (1950).

[30] T. Sarpkaya, *Force on a circular cylinder in viscous oscillatory flow at low Keulegan-Carpenter numbers,* Journal of Fluid Mechanics , 61 (1986).

[31] MIT, *Wave forces on a body,* (2005).

[32] D. Wikkerink, *Generator design for the Symphony Wave Power Device*, Master's thesis, Delft University of Technology (2017).

[33] I. Sfikas, *Evaluation and optimization of the control system of the Symphony wave power device*, Master's thesis, Delft University of Technology (2018).

[34] Y.-H. Yu, M. Lawson, K. Ruehl, and C. Michelen, *Development and Demonstration of the WEC-Sim Wave Energy Converter Simulation Tool,* in Proceedings of the 2nd Marine Energy Technology Symposium, METS 2014 (2014).

[35] William D. Callister and David G. Rethwisch, *Materials Science and Engineering* (Wiley, 2011).

[36] Vryhof Anchors B.V., *Vryhof manual* (2015).

[37] STP Offshore, *Suction Piles and Suction Embedded Anchors for Moorings* (2018).

[38] A. Owen, *Chapter 16 - tidal current energy: Origins and challenges*, in *Future Energy (Second Edition)*, edited by T. M. Letcher (Elsevier, Boston, 2014) second edition ed., pp. 335 – 356.